UNIVERSITY OF THE
WITWATERSRAND,
JOHANNESBURG

FACULTY OF
HEALTH SCIENCES

An evaluation of the effects of metal complexes on lung cancer cell lines

Zanele Mangena

A dissertation submitted to the Faculty of Health Sciences, University of the Witwatersrand,
in fulfilment of the requirements for the degree of
Master of Science in Medicine

Johannesburg

05 June 2024

Declaration

I, Zanele Mangena, declare that this dissertation is my own, unaided work. It is being submitted for the Degree of Master of Science in Medicine at the University of the Witwatersrand, Johannesburg. It has not been submitted before for any degree or examination at any other University.

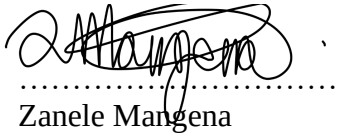

……

Zanele Mangena

On this……5th……...day of……June……2024

Dedication

I dedicate this dissertation to my Lord and Saviour, Jesus Christ whom against all odds, gave me the strength to complete this research.

Isaiah 40:31

"But those who wait upon the LORD will renew their strength;
they will mount up with wings like eagles."

Abstract

Lung cancer remains a predominant global health concern, accounting for approximately 18% of cancer-related deaths. In South Africa, it imposes a significant burden due to high rates of late-stage diagnoses, resulting in compromised survival outcomes. Despite available targeted therapies, treatment efficacy is hindered by drug resistance and severe side effects, highlighting the need for alternative agents. This study aimed to investigate a series of complexes in an *in vitro* setting to assess their potential as alternative agents for lung cancer therapy.

This study evaluated 20 compounds, encompassing novel epidermal growth factor receptor kinase inhibitors, AD and OM copper complexes, and copper-imidazo[1,2-*a*]pyridines *in vitro*. Their cytotoxicity against A549 lung cancer cells was determined by the MTT assay, and the most potent compounds were chosen for further investigation. The mode of cell death for these compounds was assessed through cell morphology, Annexin-V, caspase-3/7, mitochondrial membrane potential, and caspase-8 assays. The capacity of the active compounds to induce reactive oxygen species was measured through the CellROX™ Deep Red assay kit. Immunohistochemistry techniques were employed to analyze the expression and distribution of p21 and p53. Furthermore, changes in the expression levels of apoptosis-related proteins post-treatment with the most effective compound were assessed using the Proteome Profiler Human Apoptosis Array kit.

Four copper-imidazo[1,2-*a*]pyridines, namely JD35, JD46, JD47, and JD88, were the most active, with IC_{50} values in A549 cells between 1.67 μM and 3.37 μM. These compounds induced apoptotic cell death, characterized by chromatin condensation, fragmented nuclei, Annexin-V binding, and activation of caspase-3/7. They also caused a decline in mitochondrial membrane potential, indicating activation of the intrinsic apoptotic pathway, while also inducing late caspase-8 activation. Furthermore, these compounds enhanced reactive oxygen species and upregulated nuclear p21 and p53 expression, suggesting DNA damage leading to apoptosis initiation.

Analysis of apoptotic proteome array data showed that JD88 treatment significantly upregulated the wild-type tumour suppressor protein, p53 in A549 cells while significantly downregulating anti-apoptotic proteins such as Bcl-2, Bcl-xL, XIAP, cIAP-2, survivin, and heat shock proteins (HSP27, HSP60, and HSP70). These findings suggest a reduced threshold for apoptosis and a potential promotion of apoptosis, possibly through p53 activation.

Copper-imidazo[1,2-*a*]pyridines have demonstrated effectiveness in inducing apoptotic cell death in A549 cells, impacting both intrinsic and extrinsic apoptotic pathways and influencing critical proteins for cellular survival and apoptosis. This study contributes to a better comprehension of apoptotic mechanisms in A549 cells, stimulating inquiries into the activation of extrinsic apoptotic pathways especially by copper complexes. These findings support further pre-clinical evaluations of copper-imidazo[1,2-*a*]pyridines, including efficacy assessments in lung cancer animal models, toxicity studies, and determination of pharmacokinetic properties.

Acknowledgments

I would like to acknowledge the following people who have been instrumental in my journey towards completing this dissertation:

• To my supervisor, Dr. Leonie Harmse, thank you for your support, patience, and guidance throughout this journey. It is through your advice and unwavering efforts that I am able to submit this work

• To my co-supervisors, Dr. Carla Martins-Furness and Dr. Armorel Van Eyk, thank you for your insight and assistance with this research work. You have shown me a great deal of patience and kindness in completing this challenging journey.

• Professor Charles de Koning, from the WITS School of Chemistry, thank you for your continuous financial support throughout this study.

• To all the funding bodies that contributed to this research project, I am truly grateful for your contribution: - The National Research Foundation, Blue Skies Grant - The McGill Bequest to Wits Pharmacology Department - The University of the Witwatersrand Faculty Research Committee and Tiso Foundation

• To my fellow colleagues at the Department of Pharmacology, thank you for all the assistance, advice, and discussions over the years. Walking this journey with you was a blessing.

• To Niyanta Jade Rooplal, in you I found not only a lab partner but a sister for life. Thank you for walking this journey with me. Your support, guidance, encouragement, and advice significantly impacted this research and I am forever grateful.

• To my dear friends who have stayed up with me, reviewed my work, and encouraged me to keep going, I wouldn't have done it without you. You have been instrumental in this process. Thank you.

• To my mother, thank you for the sacrifices you have made for me to be able to complete this journey. It was your love, your prayers, and your faith that held me together. May God continue to bless you.

• To my brother and sisters, thank you for your kindness, support, and assistance. You made sure I never lacked anything and pushed me to accomplish this goal. Thank you.

• Above all, I thank the Almighty God for enabling the completion of this project. Father, it is by Your strength and will that this was possible. Thank You for Your everlasting hand on my life.

Research Outputs

Conference Proceedings

Mangena, Z., Martins-Furness, C., de Koning, C., Dam, J., & Harmse, L., 2021. Copper complexes alter the proteome profile of A549 lung cancer cells towards apoptosis. Live poster presentation at the 54th SASBCP Annual Conference, October 22, 2021. Available at: http://tinyurl.com/SASBCP.

Mangena, Z., Martins-Furness, C., de Koning, C., Dam, J., & Harmse, L., 2021. Copper complexes induce apoptosis in A549 lung cancer cells. Oral presentation at the WITS Faculty of Health Sciences, School of Therapeutic Science Biennial Research Day, September 14, 2021.

Mangena, Z., Martins-Furness, C., de Koning, C., Dam, J., & Harmse, L., 2020. Copper complexes inhibit the growth of A549 lung cancer cells. Poster presentation at WITS Faculty of Health Sciences Research Day, September 30, 2020.

Publications

- A journal article based on the findings of this research is currently being prepared for publication.

Table of Contents

List of figures

List of Tables

Abbreviations, Acronyms and Symbols

AD Compounds - Theophylline Conjugates

ADP - Adenosine Diphosphate

ALK - Anaplastic Lymphoma Kinase

AMBRA1 - Activating Molecule in Beclin 1-Regulated Autophagy Protein 1

APC - Adenomatous Polyposis Coli

ASR - Age-Standardised Incidence Rate

Atg - Autophagy-Related

ATM - Ataxia Telangiectasia Mutated

ATP - Adenosine Triphosphate

BAD - Bcl-2-Associated Death Promoter

BCL-2 - B-cell lymphoma-2

BH3 - Bcl-2-homology 3

BIM - Bcl-2-like Protein 11

BSA - Bovine Serum Albumin

CDK - Cyclin-Dependent Kinase

CDKN2A - Cyclin-Dependent Kinase Inhibitor 2A

Chk 1- Checkpoint kinase 1

cIAP1 - Cellular Inhibitor of Apoptosis Protein 1

cIAP2 - Cellular Inhibitor of Apoptosis Protein 2

CTNNB1 - Catenin-Beta 1

DD - Death Domain

DdH2O - Double distilled water

Diablo - Direct IAP-Binding Protein with Low pI

DISC - Death-Inducing Signaling Complex

DMSO - Dimethyl Sulfoxide

DNA - Deoxyribonucleic acid

DYRK2 - Dual-Specificity Tyrosine Phosphorylation-Regulated Kinase 2

EDTA - Ethylenediaminetetraacetic Acid

EGFR - Epidermal Growth Factor Receptor

EKIs - Epidermal Growth Factor Receptor Kinase Inhibitors

EML4-ALK - Echinoderm Microtubule-Associated Protein-Like 4-Anaplastic Lymphoma Kinase

EMT - Epithelial-to-Mesenchymal Transition

EPHA/B - Ephrin Type-A/B Receptor

ER - Endoplasmic Reticulum

Fas - First Apoptotic Signal

FGFR - Fibroblast Growth Factor Receptor

FIP200 - Focal Adhesion Kinase Family Interacting Protein Of 200 Kda

GWAS - Genome-Wide Association Studies

HIK2 - Homeodomain-Interacting Protein Kinase 2

HMOX1 - Heme Oxygenase 1

HMOX2 - Heme Oxygenase 2

HO - Hydroxyl radicals

HRP - Horseradish Peroxidase

HTRA2/Omi - High-Temperature Requirement A2/Omi

IAPs - Inhibitor of Apoptosis Proteins

IC_{50} - Half-maximal inhibitory concentration

IGF - Insulin-Like Growth Factor

JC-1 - 5,5',6,6'-Tetrachloro-1,1',3,3'-tetraethylbenzimidazol-carbocyanine Iodide

JDs - Copper-Imidazo[1,2-a]pyridine Complexes

KCl - Potassium chloride

KH2PO4 - Potassium dihydrogen phosphate

KRAS - Kirsten Rat Sarcoma Viral Oncogene Homolog

LC3 - Microtubule-associated Proteins 1A/1B Light Chain 3

LCLC - Large-cell Lung Carcinoma

MDM2 - Mouse Double Minute 2 Homolog

ml - Milliliter

mM – Millimolar

MMP - Mitochondrial Membrane Potential

MOM - Mitochondrial Outer Membrane

MOMP - Mitochondrial Outer Membrane Permeabilisation

MPT - Mitochondrial Permeability Transition

mTOR - Mammalian Target of Rapamycin

mTOR - Mammalian Target of Rapamycin

MTT - 3-(4,5-Dimethylthiazol-2-yl)-2,5-diphenyltetrazolium Bromide

NAD+ - Nicotinamide Adenine Dinucleotide

NF-kB - Nuclear Factor Kappa B

NLRs - NOD-like Receptors

nM - Nanomolar

NMR - Nuclear Magnetic Resonance

NOXA - Phorbol-12-Myristate-13-Acetate-Induced Protein

NSCLC - Non-Small Cell Lung Carcinoma

O_2 - Superoxide radicals

OM Compounds - Copper-Complexed OM Compounds

p21 - Cyclin-dependent kinase inhibitor 1

p53 - Tumor Protein 53

PAMPs - Pathogen-Associated Molecular Patterns

PARP-1 - Poly-(ADP-ribose) Polymerase-1

PBS - Phosphate buffered saline

PBS - Phosphate-Buffered Saline

PD-L1 - Programmed Death-Ligand 1

PD-L2 - Programmed Death-Ligand 2

PI - Propidium iodide

PI3KC3 - Class III Phosphatidylinositol 3-Kinase Complex

PI3KC3 - Phosphatidylinositol 3-Kinase Catalytic Subunit Type 3

PI3P - Phosphatidylinositol 3-Phosphate

PON2 - Paraoxonase 2

PS – Phosphatidylserine

PTEN - Phosphatase and Tensin Homolog

RB - Retinoblastoma Protein

RIP1- Receptor Interacting Protein 1

RIP3- Receptor Interacting Protein 3

RLRs - RIG-I-like Receptors

ROS - Reactive Oxygen Species

rpm - Rotations per minute

SAR - Structural Activity Relationship

SCLC - Small Cell Lung Carcinoma

SMAC - Second Mitochondria-derived Activator of Caspase

TLRs - Toll-like Receptors

TNF RI - Tumour Necrosis Factor Receptor I

TP53 - Tumour Protein 53

TRAF2 - TNFR-Associated Factor 2

TRAIL R1/DR4 - Tumour Necrosis Factor-Related Apoptosis-Inducing Ligand Receptor 1/Death Receptor 4

TRAIL R2/DR5 - Tumour Necrosis Factor-Related Apoptosis-Inducing Ligand Receptor 2/Death Receptor 5

ULK - Unc-51 Like Autophagy Activating Kinase

ULK1 - Unc-51-Like Autophagy Activating Kinase 1

v/v - Volume per volume

VEGFR - Vascular Endothelial Growth Factor Receptor

Vps34 - Vacuolar Protein Sorting 34

w/v - Weight per volume

WHO - World Health Organization

XIAP - X-Linked Inhibitor of Apoptosis Protein

µl - Microliter

µM – Micromolar

% - Percent

°C - Degrees Celsius

5-FU - 5-fluorouracil

Chapter I: Introduction

1.1 Incidence and prevalence of cancer

Cancer is a significant global health challenge, ranking as the second most common cause of death among non-communicable diseases, which account for 71% of all global mortalities (WHO, 2022). Notably, it emerged as the primary cause of death before the age of 70 in 112 out of 183 countries and ranked third or fourth in an additional 23 countries (WHO, 2022).

In 2020, approximately 19.3 million new cancer diagnoses were reported globally, coupled with an estimated 10 million cancer-related deaths (Sung *et al*., 2021). Projections indicate a significant increase in the global cancer burden, potentially reaching up to 28.4 million cases by 2040 – an increase of 47% from 2020 (WHO, 2022). This increase is anticipated to be greater in developing countries, primarily driven by demographic shifts, ageing populations, and changes in the prevalence and distribution of cancer risk factors linked to socioeconomic development (Sandström *et al*., 2023).

The most common cancer types vary in their incidence and mortality rates. Female breast cancer is the most prevalent, accounting for 2.3 million new cases annually (11.7%), followed by lung (11.4%), colorectal (10%), prostate (7.3%), stomach (5.6%) and pancreatic (3.3%) cancers. Despite the varying prevalence, lung cancer remains the leading cause of cancer-related mortality, resulting in 1.8 million deaths (18%) annually (Sung *et al*., 2021).

This growing global cancer burden underscores the urgent need for effective prevention strategies and novel therapeutic approaches.

1.2 Molecular and Genetic Mechanisms of Cancer

Cancer, comprising approximately 100 distinct types, is characterised by the formation of abnormal cells that proliferate uncontrollably (Hesketh, 2013). Tumours, classified by their origin—carcinomas from epithelial cells, sarcomas from mesodermal cells, and adenocarcinomas from glandular tissues—highlight cancer's diversity (Pecorino, 2016). These abnormal cells are distinguished by their ability to evade normal growth control, division restrictions, and territorial boundaries, thus posing significant health risks. The descendants of these abnormal cells outpace and outlive neighbouring cells, forming a tumour composed of billions of cancer cells before detection (Hesketh, 2013). This underscores cancer's nature as a

disease of the cellular genome propelled by mutation accumulation fostering cancer growth (Fiala and Diamandis, 2020).

1.2.1 Genetic Alterations in Cancer Progression

Unlike diseases triggered by single gene mutations, cancer development primarily stems from multiple aberrant genes or altered expression (Xiong *et al*., 2020). Genetic mutations such as nucleotide substitutions, insertions and deletions, chromosomal rearrangements, and copy number variations, particularly in oncogenes and tumour suppressor genes, are fundamental to cancer progression (Xiong *et al*., 2020). These genes encode proteins regulating cell growth, division, differentiation, and death (Alberts *et al*., 2015).

Mutated proto-oncogenes (oncogenes) promote excessive cell division, while inactivation of tumour suppressor genes propels tumour development due to the loss of suppressive protein products (Li *et al*., 2021). Loss-of-function mutations in tumour suppressor genes, known as genome maintenance genes, lead to unregulated growth and tumour formation (Alberts *et al*., 2015). According to Knudson's two-hit theory, both alleles of a tumour suppressor gene must be mutated to initiate cancer, thereby increasing cancer risk in patients with one mutated allele (Knudson, 1971).

Furthermore, genomic instability, a trait observed in many cancer cells, along with inflammation that supports tumour growth, significantly contributes to the development of cancer hallmarks. These hallmarks encompass sustained proliferative signalling, bypassing mechanisms that restrict growth, resisting cell death, achieving replicative immortality, triggering angiogenesis, promoting invasion and metastasis, reprogramming cellular metabolism, and evading immune system surveillance (Hanahan and Weinberg, 2011)

1.2.2 The Hallmarks of Cancer Progression

Beyond genetic alterations, a comprehensive understanding of cancer biology has been framed around the concept of the hallmarks of cancer, a set of biological capabilities acquired during the development of human tumours (Hanahan and Weinberg, 2000, 2011). These ten hallmarks mentioned below act together to facilitate malignant growth and metastasis, enabling survival in diverse microenvironments and interacting with host immune responses. These features have been illustrated in Figure 1.1.

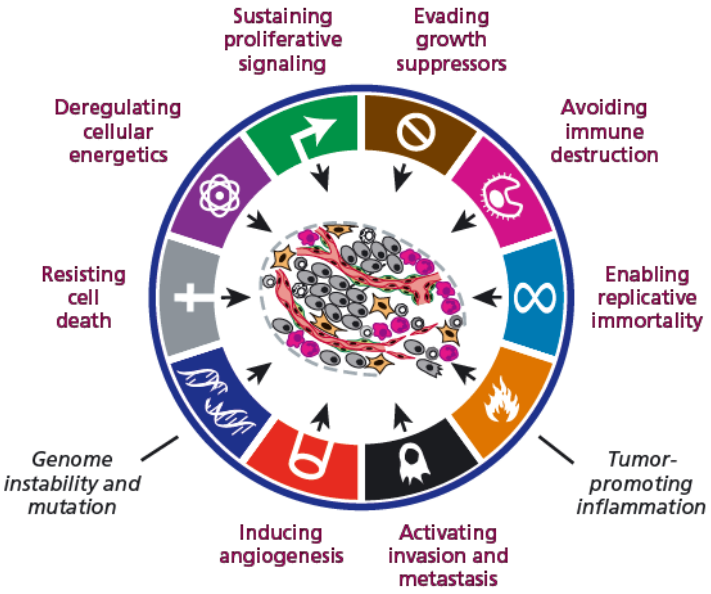

Figure 1.1 The hallmarks of cancer. (Hanahan and Weinberg, 2011) The hallmarks of cancer—comprising ten separate and complimentary functional components.

1.2.2.1 Sustaining Proliferative Signalling and Evading Growth Suppressors

Cancer cells can sustain chronic proliferation, partly by increasing the production of growth factor ligands or their corresponding receptors or activating signalling pathways that stimulate cell growth (Hanahan and Weinberg, 2011). They also develop mechanisms to evade growth suppressors, such as TP53 and RB proteins, which act as molecular brakes preventing unwarranted cell proliferation (Hanahan and Weinberg, 2011).

1.2.2.2 Resisting Cell Death and Enabling Replicative Immortality

Cancer cells resist cell death by inhibiting programmed cell death pathways or acquiring resistance to death signals. They also attain replicative immortality, typically by reactivating telomerase, thus bypassing the barrier of telomere shortening and enabling unlimited cell divisions (Hanahan and Weinberg, 2011; Tutton and Lieberman, 2017; Shay, 2016).

1.2.2.3 Inducing Angiogenesis

To supply nutrients and oxygen to rapidly proliferating cancer cells and to remove waste, tumours trigger the growth of new blood vessels, a process known as angiogenesis. This complex process often leads to abnormal, leaky vessels and varied vascularity across different tumours (Ribatti *et al*., 2015; Forster *et al*., 2017).

1.2.2.4 Activating Invasion and Metastasis

Metastasis, the dissemination of cancer cells to distant body sites, is the primary cause of most cancer-related deaths. This process involves complex changes in cell behaviour, including activating the Mesenchymal-Epithelial Transition Factor (c-MET) and remodelling the extracellular matrix (Pecorino, 2016; Hanahan and Weinberg, 2011; Weinberg, 2013).

1.2.2.5 Deregulating Cellular Energetics and Metabolism

Cancer cells demonstrate a shift in their metabolic programming to facilitate rapid proliferation, commonly known as the Warburg effect. They predominantly utilise glucose and glutamine as fuel sources, occasionally employing lactate, showcasing their metabolic adaptability (Warburg *et al*., 1927; Daye and Wellen, 2012; Dhup *et al*., 2012).

1.2.2.6 Avoiding Immune Destruction

Finally, cancer cells develop strategies to evade immune surveillance, either by impairing the effector function of immune cells or by creating an immunosuppressive microenvironment. Understanding this hallmark has led to the development of novel immunotherapies targeting these evasion strategies (Burnet, 1957; Vajdic and van Leeuwen, 2009; Schreiber, 2016).

These hallmark features of cancer are not acquired sequentially or independently; instead, they often develop synergistically due to the complex interplay between cancer cells and their microenvironment, leading to genetic instability, persistent inflammation, and the evasion of anti-tumour immune responses (Schreiber, 2016). Comprehensive knowledge of these hallmarks is crucial for developing effective therapeutic strategies.

Expanding upon the fundamental hallmarks of cancer that define the cellular transformation leading to the development of malignant tumours, it is imperative to analyse these principles within the context of distinct cancers. For instance, the focus shifts towards lung cancer, which demonstrates these hallmarks and represents a considerable global health issue due to its elevated incidence and mortality rates (Sung *et al*., 2021)

1.3 Lung Cancer Incidence and Impact

Lung cancer is a major global health concern and remains one of the primary causes of cancer-related deaths, with distinct impacts in different regions and populations due to lifestyle factors, particularly tobacco use.

In 2020, lung cancer ranked as the second most frequently diagnosed cancer on a global scale, accounting for about 11.4% of all diagnoses and contributing to approximately 18% of cancer-

related deaths. It holds the primary position for both incidence and mortality among males, while among females, it stands third in incidence and second in mortality after breast cancer (Sung *et al*., 2021).

The global distribution of lung cancer incidence shows the highest rates in the USA and Europe, where smoking has been historically more prevalent, particularly among men in high-income countries. In contrast, rates in Africa, China, and Indonesia have generally been lower but are increasing, particularly in several African countries where smoking has recently peaked (Sung *et al*., 2021; Parkin *et al*., 2012).

In South Africa, lung cancer is a recognized health burden, with 8 950 new cases and 7 730 deaths reported in 2020, making it the leading cause of cancer-related deaths in the country (International Agency for Research on Cancer, 2020). The age-standardised incidence rate (ASR) is 3.22/100 000 in females and 8.06/100 000 in males (International Agency for Research on Cancer, 2020). However, these figures likely underrepresent the actual disease burden due to the lack of formal screening programs, potentially leading to underreporting of lung cancer cases (Van Eeden *et al*., 2020). Moreover, the data regarding smoking prevalence, a major risk factor for lung cancer, are outdated and possibly underestimated, with estimations indicating that 29.2% of adult males and 7.3% of adult females in South Africa smoke (Reddy *et al*., 2015; Van Eeden *et al*., 2020). Therefore, the actual impact of lung cancer and its correlation with smoking prevalence may be more significant than currently estimated.

Continuing in this trend, and without implementing effective smoking cessation initiatives or interventions to reduce smoking initiation, it is predicted that lung cancer rates in South Africa will continue to rise over the next few decades.

1.4 Lung Cancer Classification and Histopathology

Lung cancer is a complex disease with several pathological and clinically significant subtypes (Travis *et al*., 2013). Primary lung cancers, which originate in the lung, are predominantly carcinomas arising from epithelial cells, primarily classified as Small Cell Lung Carcinoma (SCLC) and Non-Small Cell Lung Carcinoma (NSCLC) (Herbst *et al*., 2008).

SCLC constitutes about 15% of lung cancer cases and is characterised by its aggressive nature, rapid doubling time, and early metastasis development. Despite its initially high responsiveness to chemotherapy and radiation, recurrence is prevalent, contributing to its unfavourable

prognosis, with only 4.6% of patients surviving two years post-diagnosis (Woodard *et al*., 2016).

NSCLC, accounting for the remaining 85% of lung cancer cases, remains the primary cause of cancer-related mortality, displaying a 5-year survival rate of 19.3% (Howlader *et al*., 2013). NSCLC is subdivided into three primary pathological subtypes: adenocarcinoma, squamous cell carcinoma (SqCC), and large cell carcinoma (LCLC).

Adenocarcinoma, the most prevalent subtype of NSCLC in lung cancer, constitutes approximately 50% of all NSCLC cases and 38% of all newly diagnosed lung cancers (Cruz *et al*., 2011). It is identified as a malignant epithelial tumour exhibiting glandular differentiation and mucin production, often found in the lung periphery. It displays various histological patterns, where the lepidic pattern suggests a better prognosis, while micropapillary and solid patterns indicate aggressive behaviour (Travis *et al*., 2013).

SqCC comprises nearly 20% of all lung cancers (Cruz *et al*., 2011). It typically presents centrally, originating from a primary or lobar bronchus. According to the World Health Organization (WHO), it is identified as a malignant epithelial tumour demonstrating keratinisation or intercellular bridges or expressing markers of squamous cell differentiation (Travis *et al*., 2015).

LCLC, constituting 2.9% of lung cancers, is identified as an undifferentiated NSCLC lacking specific histological or immunohistochemical differentiation (Travis *et al*., 2015; Cruz *et al*., 2011).

Furthermore, lung cancers are classified based on molecular subtypes and genetic alterations, including mutations in genes such as epidermal growth factor receptor (EGFR), Kirsten rat sarcoma viral oncogene homolog (K-ras), and echinoderm microtubule-associated protein-like 4-anaplastic lymphoma kinase (EML4-ALK) oncogene, as well as secondary alterations such as c-MET (mesenchymal-epithelial transition factor) overexpression, phosphatidylinositol-4,5-bisphosphate 3-kinase catalytic subunit alpha (PI3KCA) amplification, phosphatase and tensin homolog (PTEN) deletions or methylation, vascular endothelial growth factor receptor (VEGFR) overexpression, c-ros oncogene 1 receptor tyrosine kinase (ROS1) translocation, epigenetic changes, and insulin-like growth factor (IGF) alterations (West *et al*., 2012).

This comprehensive classification emphasizes the complexity of the disease and the necessity for targeted therapeutic strategies that consider specific subtypes and their molecular mechanisms.

1.5 Risk Factors and Carcinogenesis in Lung Cancer

Several risk factors contribute to lung cancer development, including smoking, occupational carcinogen exposure (e.g., asbestos, arsenic, aromatic hydrocarbons), air pollution, underlying respiratory disorders, family history, dietary influences, and substance misuse. These factors vary with ethnicity, nationality, region, and socioeconomic status (Akhtar and Bansal, 2017).

1.5.1 Genetic Factors in Lung Cancer

Emerging evidence supports a genetic predisposition to lung cancer, highlighted by its occurrence in non-smokers and those with a family history. A positive family history increases the risk 1.5-fold in non-smoking families (Akhtar and Bansal, 2017). Furthermore, several genetic variations linked to the risk of lung cancer have been detected through Genome-Wide Association Studies (GWAS), particularly identifying key susceptibility regions at 15q25, 5p15, and 6p21 (Amos *et al*., 2008; Landi and Chatterjee, 2009; Truong *et al*., 2010).

1.5.2 Smoking and Carcinogenesis

Smoking accounts for approximately 80% of lung cancer cases (Akhtar and Bansal, 2017). Lung cancer varies molecularly and epigenetically in smokers and non-smokers, with adenocarcinoma predominantly affecting non-smokers and women, while squamous cell carcinoma is more common in male smokers (Subramanian and Govindan, 2013).

Tobacco smoke comprises about 4000 compounds, including at least 69 known carcinogens (Schabath and Cote, 2019). Tar, produced when tobacco is burnt, constitutes the majority of carcinogenic and hazardous substances. Carcinogens in tar include polycyclic aromatic hydrocarbons, aza-arenes, N-nitrosamines, aromatic amines, heterocyclic aromatic amines, and aldehydes (Schabath and Cote, 2019).

Upon oxidation by cytochrome P450 enzymes, these carcinogens become metabolically active, forming DNA adducts predominantly repaired by direct repair and nucleotide excision repair mechanisms. Unresolved DNA adducts may interact with essential genes like p53 and KRAS, leading to mutations and, subsequently, cancer (Schabath and Cote, 2019).

1.5.3 Molecular Aberrations in Lung Cancer

Lung cancer tissues exhibit genomic instability marked by acquired mutations and amplifications affecting regulatory steps in cellular processes. Key oncogenic mutations occur in signalling pathways, such as in the ErbB family that comprises EGFR and the Human epidermal growth factor receptors (HER) and the c-MET gene (Herbst *et al*., 2008; Kristeleit *et al*., 2011). Other mutations, deletions, or epigenetic changes lead to the inactivation of tumour suppressor genes like p53, p16, and PTEN (Herbst *et al*., 2008). Some of these mutations are associated with specific lung cancer subtypes, e.g., EGFR and Liver Kinase B1 (LKB1) mutations with adenocarcinomas, as shown in Figure 1.2, and Fibroblast Growth Factor Receptor 1 (FGFR1) amplification with squamous cell carcinomas. Mutations in the same signalling pathway often appear to be mutually exclusive, such as HER2, EGFR, and KRAS (Cooper *et al*., 2013).

Overall, understanding the complex interplay between genetic, lifestyle, and environmental risk factors, along with the molecular mechanisms of carcinogenesis, is critical to developing targeted therapies and prevention strategies for lung cancer.

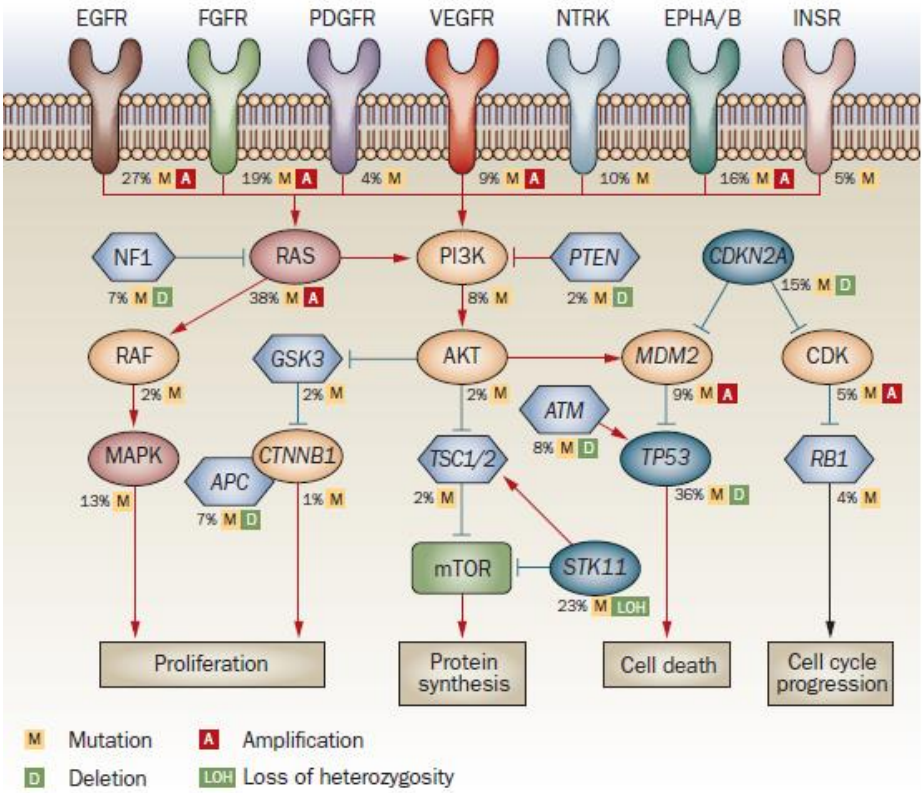

Figure 1.2 Lung adenocarcinoma mutations. (Ding, L. *et al*., 2008; Harris and McCormick, 2010) Lung cancer typically alters MAPK, p53, Wnt, cell cycle, and mTOR genes. Pink to red indicates oncoproteins, while light to dark blue indicates tumour suppressor proteins. Darker hues indicate more genetically altered tumours. Each pathway member's frequency of genetic changes in 188 cancers is shown. Genes exhibiting localised amplification (EGFR, FGFR, VEGFR, EPHA/B, MDM2 and CDK6) were examined for copy number amplification. Legend: ATM, ataxia telangiectasia mutated; APC, adenomatous polyposis coli protein; CDK, cyclin-dependent kinase; CDKN2A, cyclin-dependent kinase inhibitor 2A; CTNNB1, catenin-beta 1; EGFR, epidermal growth factor receptor; EPHA/B, ephrin type-A/B receptor; FGFR, fibro.

1.6 Lung Cancer Therapies and Treatment Resistance

Therapeutic strategies in lung cancer primarily operate through inducing programmed cell death. This includes chemotherapy, radiation, and immunotherapy, among other treatments. However, malignancies often develop resistance to these treatments, in part by evading cell death pathway activation. A comprehensive understanding of cell death and survival mechanisms in cancers and their responses to therapies is thereby crucial for devising more efficient, personalised treatment plans to improve patient outcomes.

1.6.1 Common cell death pathways

1.6.1.1 Apoptosis

Apoptosis, a term first used in 1972 (Kerr *et al*., 1972), describes a well-studied, intrinsically regulated cellular suicide process leading to the formation of apoptotic bodies, subsequently consumed by phagocytic cells. Morphologically, apoptosis is marked by cellular shrinkage, membrane blebbing, and chromatin condensation (Hassan *et al.*, 2014).

At the molecular level, apoptosis is classified into two main pathways: intrinsic and extrinsic, differing mainly by their initial triggers. In addition to this, apoptosis is also regulated by two evolutionarily conserved protein families: the B-cell lymphoma-2 (BCL-2) family, which regulates mitochondrial integrity (Youle, 2008), and caspases, cysteine proteases, managing the execution phase of apoptosis (Shalini *et al*., 2015). Twelve apoptotic and inflammatory caspases exist in humans, consisting of initiator caspases (caspase-2, -8, -9, -10) and executioner caspases (caspase-3, -6, -7). These caspases are synthesized as inactive proenzymes and require proteolytic activation by upstream effectors (Shalini *et al*., 2015). Figure 1.3 depicts the activation of these caspases in mammalian cells. Initiator caspases are further divided into those implicated in the extrinsic (caspase-8 and caspase-10) and intrinsic (caspase-9) apoptotic pathways. Upon the initiation of apoptotic signals, the activation of initiator caspases triggers the cleavage and subsequent activation of downstream executioner caspases such as caspase-3, -6, and -7. These activated caspases further cleave essential substrates crucial for the characteristic features of apoptosis (Crowley *et al*., 2016a; Pistritto *et al*., 2016)

The intrinsic, or mitochondria-mediated apoptotic pathway, is stimulated by cytotoxic insults or DNA damage that disrupts the mitochondrial equilibrium (Pistritto *et al*., 2016). Normally, the mitochondria are safeguarded by anti-apoptotic BCL-2 family members that restrain the pro-apoptotic proteins, Bax (BCL-2-associated X protein) and Bak (BCL-2 antagonist or killer), from altering the mitochondrial membrane's permeability. These proteins transition between the cytosol and the mitochondrial outer membrane (MOM) under normal conditions. However, cellular stress activates Bcl-2-homology 3 (BH3)-only proteins like BIM (Bcl-2-like protein 11), BAD (Bcl-2-associated death promoter), and NOXA (Phorbol-12-myristate-13-acetate-induced protein 1), inhibiting anti-apoptotic BCL-2 family members, thereby releasing Bax and Bak (Hata *et al*., 2015).

The result is a conformational shift in Bax, which exposes the BH3 domain and allows it to insert into the MOM. Consequently, Bax and Bak accumulate at the MOM, oligomerise, and form pores in the mitochondrial membrane, causing mitochondrial outer membrane permeabilisation (MOMP), often regarded as the irreversible stage in apoptosis (Hata *et al*., 2015). This oligomerisation process can be disrupted by Bcl-2, which forms a heterodimer with Bax to prevent mitochondrial pore formation (O'Neill *et al*., 2016).

MOMP triggers the release of cytochrome c and additional pro-apoptotic mitochondrial proteins, namely second mitochondria-derived activator of caspase/direct IAP binding protein with low pI (-SMAC/Diablo) and High-Temperature Requirement A2/Omi (HTRA2/Omi) into the cytoplasm. The alteration of mitochondrial membrane potential (MMP) in response to apoptotic stimuli modifies the permeability of the MOM, facilitating the liberation of the pro-apoptotic protein cytochrome c (Estaquier *et al*., 2012; Lopez and Tait, 2015). Subsequently, cytochrome c forms a complex with apoptotic protease activating factor 1 (Apaf-1) and ATP, resulting in the assembly of the Apaf-1 apoptosome. This assembly promotes the recruitment and activation of procaspase-9, initiating the caspase cascade responsible for activating executioner caspases-3, -6, and -7. These executioner caspases play a vital role in cleaving cellular components, ultimately leading to apoptosis (Pistritto *et al*., 2016; Bao *et al*., 2018).

Simultaneously, SMAC/Diablo and HTRA2/Omi bind to and antagonise Inhibitor of Apoptosis Proteins (IAPs) such as X-linked Inhibitor of Apoptosis Protein (XIAP), cellular Inhibitor of Apoptosis Protein 1 (cIAP1), and cellular Inhibitor of Apoptosis Protein 2 (cIAP2), thus facilitating caspase activation (Obexer and Ausserlechner, 2014). This interaction negates XIAP's inhibitory effect on caspase-9, -3, and -7, enabling these caspases to initiate apoptosis. The cIAP1 and cIAP2 proteins interact with TNFR-associated factor 2 (TRAF2), which assists in activating the NF-kB pathway and promotes the production of anti-apoptotic genes (LaCasse *et al*., 2008).

The extrinsic, or death receptor-mediated apoptotic pathway, involves the activation of the TNF-related apoptosis-inducing ligand receptors (TRAIL-R1 and TRAIL-R2), first apoptotic signal (Fas), and tumour necrosis factor receptor 1 (TNF-R1), which share a conserved region known as the death domain (DD) (Park *et al*., 2016). This pathway's initiation depends on the interaction between TRAIL and its receptors, where decoy receptors compete with death receptors for ligand binding, disrupting the apoptotic signal (Naimi *et al*., 2018; Micheau, 2018).

The activation of this pathway commences with the binding of specific ligands to these receptors. In the case of TRAIL receptors, the interaction between TRAIL and its receptors is crucial, and the presence of decoy receptors that compete for ligand binding can disrupt the apoptotic signal (Naimi *et al.*, 2018; Micheau, 2018). Following ligand binding, a multimeric protein complex known as the death-inducing signalling complex (DISC) is formed, triggering the activation of caspase-8.

Once activated, caspase-8 can propagate the apoptotic signal directly by cleaving other caspases, such as caspase-3, or indirectly through mediators, such as the cleaved form of the Bcl-2 family member Bid, which contains a BH3-only domain ((Huang *et al.*, 2016).). Once cleaved by caspase-8, Bid translocates to the mitochondrial membranes, promoting outer membrane permeabilization (Pfeffer and Singh, 2018). This action effectively links the extrinsic and intrinsic apoptosis pathways, clearly demonstrating the interconnected nature of these cell death pathways.

The elucidation of these apoptosis pathways, particularly the protein cascades and their interplay, is crucial for understanding the mechanism of action of many cancer therapeutics and the development of resistance, providing important insights for developing more effective strategies for lung cancer treatment.

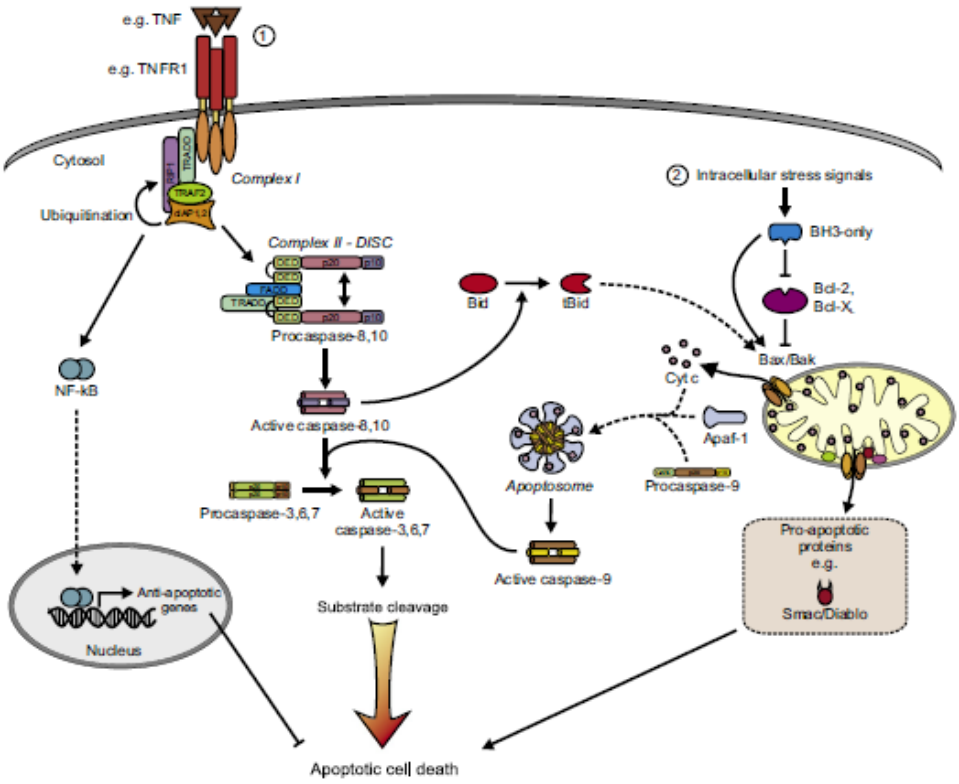

Figure 1.3 Intrinsic and Extrinsic apoptotic signalling (Duprez *et al.*, 2009). Intrinsic apoptosis is triggered by mitochondrial stress. Bax and Bak activate mitochondrial apoptotic mediators to form an apoptosome, which triggers caspase-9 and activates caspases 3, 6 and 7, leading to apoptosis. TNFR1 stimulation causes extrinsic apoptosis directly. TNF stimulates complex I, which activates NF-kB and promotes anti-apoptotic gene transcription. TNFR1 endocytosis activates caspase-8 in complex II. Bid cleavage by caspase-8 activates the mitochondrial pathway, amplifying extrinsic apoptosis. Activating executioner caspases causes substrate breakage and cell death.

1.6.1.2 Necrosis

Historically considered an uncontrolled, chaotic form of cell death, necrosis is now recognised to be a regulated event with defined signalling mechanisms triggered by diverse stimuli (Cai *et al.*, 2014). While death receptor ligands typically promote apoptosis over necrosis in most cell lines, necrotic cell death may be a backup mechanism if caspase activation is inhibited within these pathways (Vandenabeele *et al.*, 2006). Necrosis is characterised by the swelling of the cytoplasm and organelles, formation of irregular clumps of chromatin, rapid loss of plasma membrane integrity, and an uncontrolled release of cytoplasmic contents, ultimately activating an immune response (Baig *et al.*, 2016). Though the resultant local inflammation from programmed necrosis might stimulate tumour growth, it can also be harnessed for cancer cell eradication (Chan *et al.*, 2015).

Multiple factors can trigger necrosis, including pathogen recognition receptors such as transmembrane toll-like receptors (TLRs), cytosolic nucleotide-binding oligomerization domain-like receptors (NLRs), and retinoic acid-inducible gene-I-like receptors (RLRs). These receptors detect pathogen-associated molecular patterns (PAMPs) and initiate inflammation and cell death by necrosis (Figure 1.4) (Galluzzi *et al*., 2018). Among these pathways, the death receptor-mediated pathway, which depends on the TNFR1-induced stimulation of Receptor Interacting Protein 1 (RIP1) to form a complex with Receptor Interacting Protein 3 (RIP3), is most prevalent in necrosis. This RIP1/RIP3 complex—also known as the necrosome—initiates death receptor-triggered necrotic signalling (Xie *et al*., 2013). This RIP1-dependent cell death mechanism has been designated necroptosis (Cai *et al*., 2014), a process delineated in Figure 1.4.

The necrosome complex, consisting of RIP1 and RIP3, facilitates the implementation phase of necrosis by engaging various oxidative agents such as reactive oxygen species (ROS), ceramide, calpains, cathepsins, phospholipases, and calcium ions (Ca^{2+}) (Cai *et al.*, 2014). These agents are known to induce oxidative damage to DNA, proteins, and lipids. When DNA damage surpasses a critical threshold, it activates poly-(ADP-ribose) polymerase-1 (PARP-1), subsequently causing nicotinamide adenine dinucleotide (NAD+) hydrolysis, adenosine triphosphate (ATP) depletion, and ultimately leading to irreversible cellular energy failure and necrotic cell death (Chan *et al*., 2015).

Proteins that undergo oxidation by ROS not only lose their inherent functionality but also become targets for degradation. Moreover, the oxidation of polyunsaturated fatty acid residues in membrane phospholipids by ROS results in the leakage of Ca^{2+} and lysosomal proteases, as well as mitochondrial disruption (Galluzzi *et al.*, 2018). Elevated Ca^{2+} levels initiate mitochondrial permeability transition (MPT) by generating large, non-specific pores between the cytosol and mitochondrial matrix. This MPT causes inner membrane depolarization, oxidative phosphorylation uncoupling, matrix swelling, and outer membrane rupture, ultimately leading to mitochondrial respiration failure and necrotic cell death (Galluzzi *et al.*, 2018).

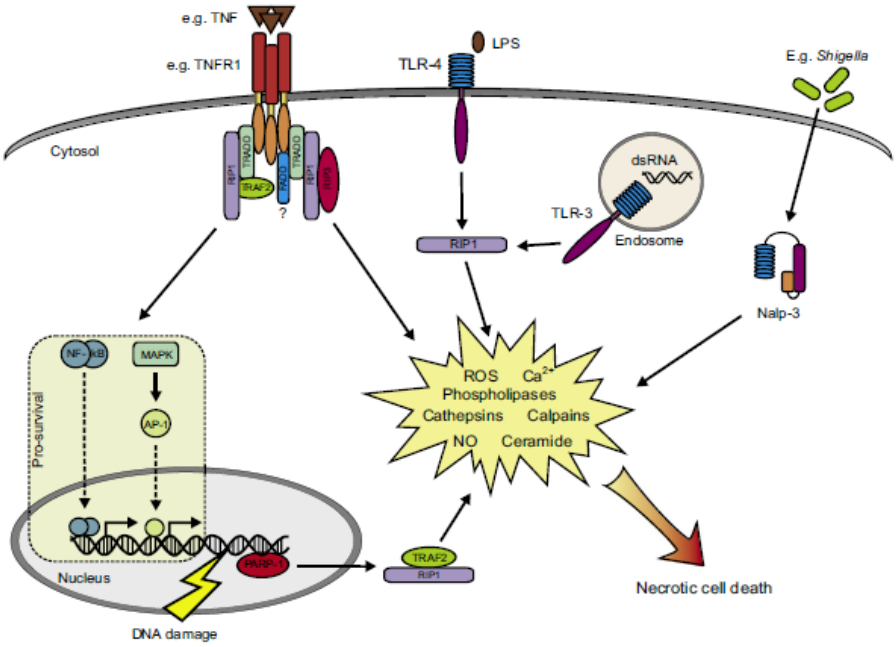

Figure 1.4 Necrotic signalling. (Duprez *et al.*, 2009) Stimulating TNFR1 activates RIP1, which activates transcription factors, including NF-kB and AP-1. RIP1 and RIP3 both initiate death receptor-induced necrotic signalling. ROS, calcium, calpains, cathepsins, phospholipases, NO, and ceramide are activated by RIP1 kinase. DNA damage or TLR-3, TLR-4, and Nalp-3 trigger the same mediators.

1.6.1.3 Autophagy

Autophagy is a catabolic process in eukaryotic cells that degrades and recycles cellular components, employing double-membrane vesicles known as autophagosomes. Primarily, autophagy supports intracellular homeostasis and is vital in stress adaptation, differentiation, and growth (Nencioni *et al.*, 2013). Paradoxically, cells under extreme stress may undergo autophagic cell death, hinting at a self-destructive aspect of autophagy (Bialik *et al.*, 2018). Consistent with this, decreased autophagy has been linked to tumorigenesis, with specific tumour suppressor genes found to be involved in the process (Galluzzi *et al.*, 2018).

Autophagic cell death originates from the self-consumption of cellular organelles through the autophagy process (Bialik *et al.*, 2018). This involves autophagosome formation, which envelopes portions of the cytoplasm, encompassing organelles like mitochondria and the endoplasmic reticulum (ER) (Bialik *et al.*, 2018). These autophagosomes eventually fuse with lysosomes to form autolysosomes, where lysosomal enzymes degrade the sequestered components. Although membrane blebbing and partial chromatin condensation may occur

during autophagic cell death, it is noteworthy that DNA fragmentation and caspase activation are not inherent to this process (Helgason *et al.*, 2013; Crowley *et al.*, 2016b).

The critical autophagic signaling pathway is regulated by the mammalian target of rapamycin (mTOR), a protein kinase involved in managing translation, cell cycle progression, and autophagy. Under conditions of nutrient and growth stimulus abundance, mTOR is active, thereby suppressing autophagy. Conversely, in situations of nutrient or growth factor scarcity, mTOR inhibition occurs, triggering the unc-51-like autophagy activating kinase 1 (ULK1)–autophagy-related protein 13 (Atg13)–focal adhesion kinase family interacting protein of 200 kDa (FIP200) complex to initiate the formation of autophagosomes (Jung *et al*., 2009; Cai *et al*., 2022). The assembly of the class III phosphatidylinositol 3-kinase complex (PI3KC3) involving vacuolar protein sorting 34 (Vps34) is essential for vesicle formation. This complex includes Beclin 1, autophagy-related protein 14 (Atg14), an activating molecule in Beclin 1-regulated autophagy protein 1 (AMBRA1), and general vesicular transport factor (p115) (Morris *et al*., 2013). Activation of PI3KC3 generates phosphatidylinositol 3-phosphate (PI3P), which in turn recruits other autophagy-related (Atg) proteins, facilitating the elongation of the vesicle membrane. This process results in the generation of an Atg12–Atg5–Atg16-like (Atg16L) multimer complex and the lipidation of microtubule-associated proteins 1A/1B light chain 3B (LC3), converting the soluble LC3-I into the vesicle-associated form LC3-II, widely acknowledged as an autophagy marker (Martens and Fracchiolla, 2020; Morris *et al*., 2013). Ultimately, the autophagosome merges with a lysosome, facilitating the degradation of its contents by lysosomal hydrolases (Jung *et al*., 2009). Figure 1.5 illustrates this pathway.

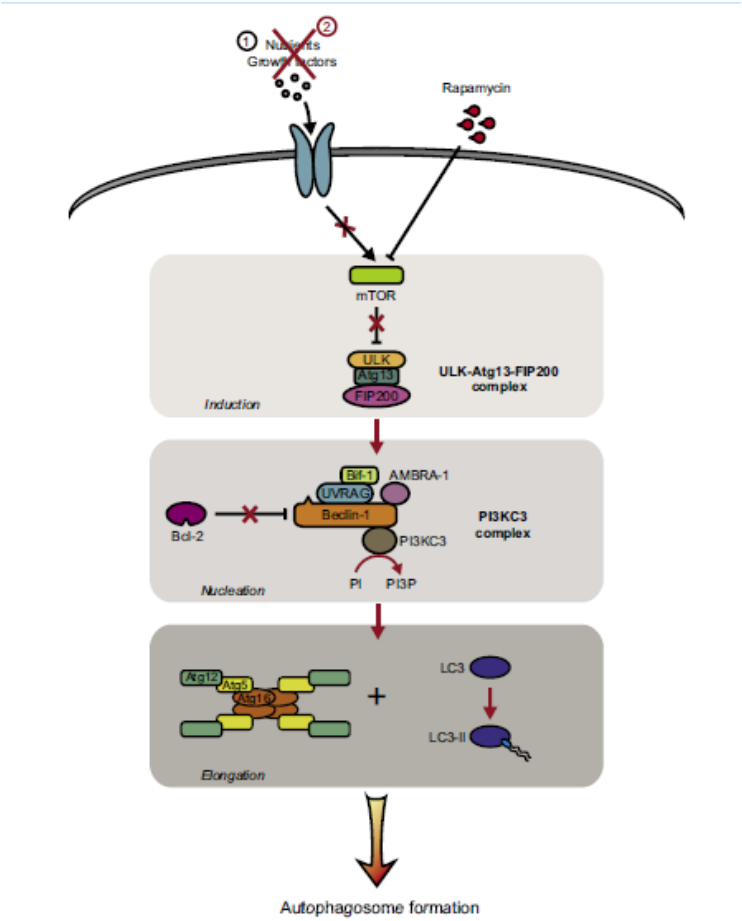

Figure 1.5 Autophagy signalling. (Duprez *et al*., 2009) Nutrients and growth factors activate mTOR, inhibiting autophagy. Deprivation of nutrients or growth factors or therapy with rapamycin inhibits mTOR and activates ULK-|Atg13-FIP200, inducing autophagosome formation. PI3KC3 is needed for vesicle nucleation. PI3P production recruits Atg proteins and elongates vesicle membranes. This forms an Atg12-Atg5-Atg16(L) multimer complex and lipidates LC3 (LC3-II).

1.6.1.4 Pyroptosis

Pyroptosis is a regulated form of cell death characterized by unique morphological and biochemical features, sharing similarities with both apoptotic and necrotic cells (Wang *et al*, 2022). This type of cell death is triggered by proinflammatory signals and is associated with inflammation (Tan *et al*., 2021). The notable features of pyroptosis include the loss of plasma membrane integrity and the release of cellular contents into the extracellular space (Gao *et al*., 2018). Some similarities with apoptosis include DNA fragmentation and nuclear condensation, but pyroptosis displays distinct differences, such as caspase-1-dependent nuclease-mediated DNA cleavage without the oligonucleosomal fragmentation pattern typical of apoptosis (Wang *et al*., 2022)

Initially identified in monocytes and macrophages infected with intracellular bacteria, pyroptosis has also been observed in non-macrophage cells in response to non-infectious stimuli, such as damage-associated molecular patterns (Tan *et al*., 2021). Pyroptosis is dependent on caspase-1, an inactive zymogen found in the cytosol, which is activated within the inflammasome in a manner analogous to caspase-9 activation in the apoptosome (Gao *et al*., 2018).

The inflammasome, a complex molecular platform, consists of various components, including Nucleotide-binding Oligomerization Domain (NOD)-like Receptor (NLR) family members, which recruit caspase-1 through adaptor molecules such as Apoptosis-associated Speck-like Protein Containing a Caspase Activation and Recruitment Domain (ASC/Pycard). Four distinct inflammasomes have been identified and named after their corresponding NLR proteins, such as NLRP1, NLRP3, and NLRC4, or the HIN-200 protein AIM2. Upon detection of intracellular bacterial, viral, or host danger signals by these NLRs, the inflammasome assembles and activates caspase-1, resulting in pyroptotic cell death, as illustrated in Figure 1.6 (Wang *et al*., 2022).

In pyroptosis, caspase-1 generates ion-permeable pores of specific sizes in the plasma membrane (Vande Walle and Lamkanfi, 2016). This action leads to increased osmotic pressure, resulting in cell swelling, lysis, and subsequent cell death. Caspase-1 also activates executor caspases-3 and -7, contributing further to cell death (Vande Walle and Lamkanfi, 2016). Moreover, caspase-1 triggers inflammation by cleaving proinflammatory cytokines pro-IL-1 and pro-IL-18 (Crowley *et al*., 2016b)

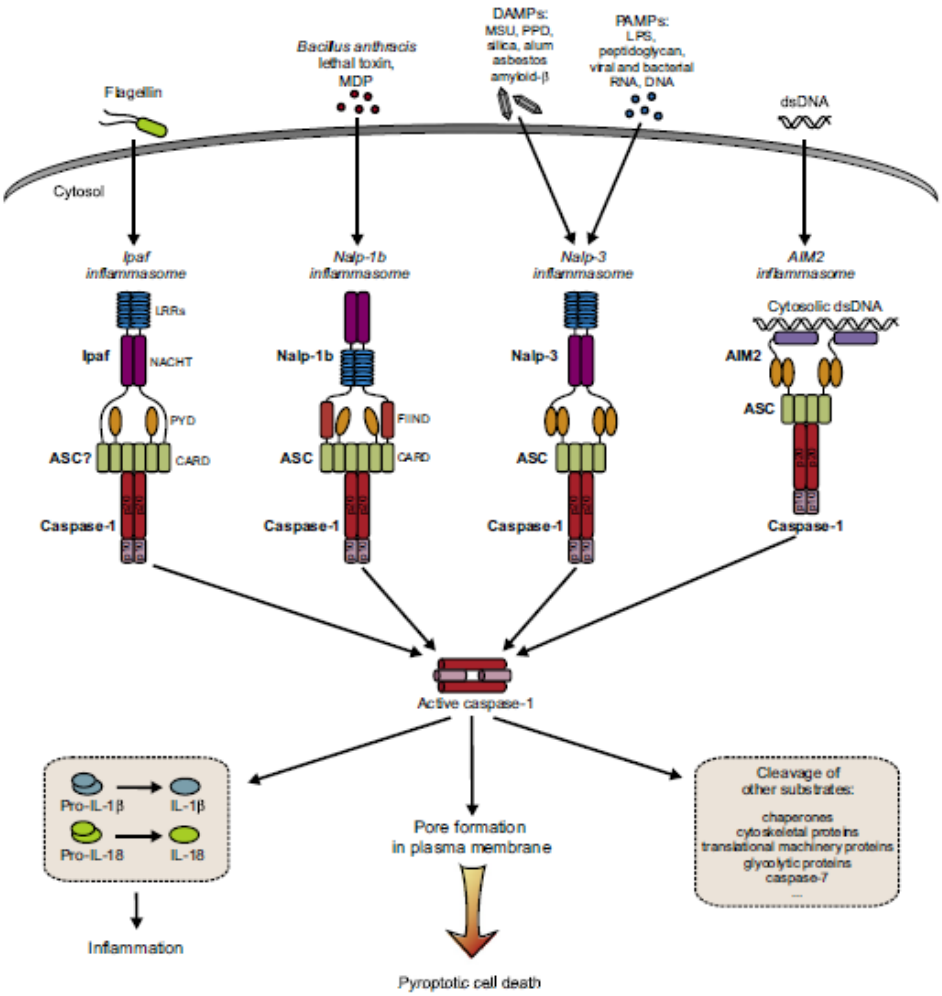

Figure 1.6 Pyroptosis signalling. (Duprez *et al*., 2009) During pyroptosis, bacterial, viral, or host danger signals drive oligomerisation of Nalp-1b, Nalp-3, Ipaf, or AIM2. Caspase-1 is triggered by the adaptor ASC, causing plasma membrane pore development and pyroptotic cell death. Caspase-1-mediated maturation of IL-1b and IL-18 causes inflammation. Activating caspase-1 cleaves additional substrates, causing cell death.

1.6.2 Current Lung Cancer Treatment Strategies

1.6.2.1 Surgical Resection

Surgical resection remains the cornerstone of treatment for early-stage lung cancer in patients of good health, particularly for those with early-stage NSCLC where the tumour is confined to the lung, and no lymph node metastases have been detected (Gadgeel *et al*., 2012). In such cases, the primary treatment objective is curative. The surgical resection procedures adopted include pneumonectomy (complete lung removal), lobectomy (excision of the entire lobe housing the tumour), segmentectomy or wedge resection (removal of a lobe segment, typically for patients with insufficient lung function for lobectomy), and sleeve resection (employed for primary airway malignancies, preserving greater lung function) (Al-Shahrabani *et al*., 2014).

A 53-97% 5-year survival rate has been observed in these patients (Hirsh *et al*., 2017), however, only 10-20% of NSCLC patients qualify for this treatment. It is primarily restricted by tumour quantity and size, the patient's respiratory condition, operability, and risk assessment (Mangal *et al*., 2017).

While this treatment is an optimal first-line approach for early-stage lung cancers, it is unsuitable for managing later-stage lung cancer patients (NCCN, 2022). It carries considerable side effects, which vary based on surgical complexity and the patient's overall health. Potential complications include excessive bleeding, blood clots, wound infections, pneumonia, and a potential risk of operation-related mortality (Mangal *et al*., 2017).

1.6.2.2 Radiotherapy

Radiotherapy uses high-energy ionising radiation to damage the DNA of tumorigenic cells and associated lymph nodes. It is often applied in cases of advanced-stage SCLC and NSCLC or when surgical resection is unfeasible due to medical complications (Gadgeel *et al*., 2012). Different radiotherapy treatment modalities for lung cancer include conventional radiotherapy, stereotactic ablative therapy, and radiofrequency ablation (Hirsh *et al*., 2017).

For medically inoperable stage I NSCLC patients treated with standard radiotherapy, 5-year survival rates range between 15% and 48%, and a 50% local failure rate has been observed (Hirsh *et al*., 2017). These outcomes are less desirable than those of surgical resection. High-dose radiotherapy can potentially damage normal lung tissue. Severe side effects, such as fatigue, weight loss, breathing difficulties, shortness of breath, and skin changes at the radiation site, further limit the suitability of this treatment (Evans, 2013; Gadgeel *et al*., 2012). Furthermore, to achieve optimal efficacy, this therapy often necessitates a combination with chemotherapy (Timmerman *et al*., 2010).

1.6.2.3 Chemotherapy

Chemotherapy refers to the use of drugs to destroy cancer cells, applicable for advanced non-small-cell lung cancer stages and all small-cell cancer stages, unlike surgical resection and radiation therapy limited to early-stage carcinoma (NCCN, 2022). The treatment can involve single or combination drug administration, usually intravenously, with the latter proving superior in response rates and overall survival. In NSCLC, first-line combination chemotherapy often employs a platinum-based compound (cisplatin or carboplatin) with a secondary agent such as gemcitabine, docetaxel, vinorelbine, paclitaxel, or pemetrexed (Azzoli *et al*., 2009; Evans, 2013). Modern platinum-based regimens result in objective response rates

of up to 40%, median overall survival of 8-10 months, and 2-year survival rates of up to 25% (Hirsh *et al*., 2017).

For SCLC patients, therapy-less median survival hovers around 7-14 weeks, contingent on stage. Treatment with combination chemotherapy regimens like cyclophosphamide, doxorubicin, vincristine, or etoposide and cisplatin substantially enhances this outcome, delivering complete response rates from 15% to 25%, and median survival times extending from 7 to 10 months (Gadgeel *et al*., 2012). Trials indicate that the best first-line treatment involves four rounds of combination chemotherapy, as an extension beyond this often culminates in significant toxicity with little survival benefit. Despite its applicability, side effects such as nausea, immunosuppression, and platinum-drug resistance often limit the use and efficacy of chemotherapy (Douillard *et al*., 2008).

1.6.2.4 Targeted Therapy

Advancements in molecular knowledge and comprehension of lung cancer pathophysiology have facilitated the development of targeted therapies. These drugs interact with specific molecular targets to improve patient outcomes, especially those with predominant NSCLC (Yuan *et al*., 2019). These targeted therapies function differently from traditional chemotherapy, focusing on overexpressed and constitutively activated proteins like EGFR, ALK, and KRAS (Yuan *et al*., 2019).

Approximately 15% of NSCLC patients harbour a gene mutation that promotes uncontrolled growth of the EGFR tyrosine kinase domain. Erlotinib and gefitinib counteract this expression (Pirker and Filipits, 2009). ALK fusion protein is found in 4-5% of advanced NSCLC, and the ALK kinase inhibitor crizotinib has received approval for treatment in ALK mutation-positive NSCLC patients (Gadgeel *et al*., 2012). Although targeted therapies have provided a 60-80% response rate superior to traditional chemotherapy (Jones and Baldwin., 2018), the targeted mutations occur in a low percentage of lung cancer patients, making these treatments ineffective in patients lacking these mutations.

1.6.2.5 Immunotherapy

The recent advent of immunotherapies, or immune checkpoint inhibitors such as pembrolizumab, nivolumab, and atezolizumab, has provided a new class of targeted therapies. These drugs activate the programmed death-ligand 1/2 (PD-L1 and PD-L2) and programmed death 1 (PD-1) receptor pathways. These pathways, when stimulated by tumour antigens,

inhibit the immune system by interacting with the PD-1 receptor on activated T lymphocytes, thereby causing cancer cell death (Jones and Baldwin., 2018).

Some cancer cells express PD-L1 and PD-L2 on their cell membranes, protecting them from immune attack. Immunotherapies disrupt the PD-L1/2 and PD-1 receptor pathways, lifting the brakes on the immune system and allowing cancer cells to be recognised and eliminated by cytotoxic T cells. Patients must be tested for PD-L1-positive cancer cells before administering the therapy. Studies have shown that pembrolizumab at two doses improved overall survival compared to traditional chemotherapy (docetaxel) in previously treated NSCLC patients with 1% PD-L1 tumour cells (Herbst *et al*.,2016). Similar results were observed with nivolumab compared to docetaxel in PD-L1-low patients (Borghaei *et al*., 2016).

Despite their enhanced efficacy, the high costs and narrow specificity of immunotherapies limit their use. These drugs are effective only in patients expressing specific membrane proteins, a small percentage of lung cancer patients. Additionally, immunotherapies can induce severe side effects as they inhibit immune system protection, leading to autoimmune responses and potentially life-threatening disorders in the lungs, intestines, liver, glands, kidneys, and other organs (Steven *et al*., 2016).

1.6.3 The Emergence of Copper as a Potential Chemotherapeutic Agent

Copper, a vital trace element for several metalloenzymes, has emerged as a promising candidate for nonplatinum anticancer metallodrugs. Copper-based compounds are biocompatible and exhibit a multifaceted approach to inhibiting cancer proliferation (Usman *et al*.,2017). Over recent years, various copper complex families have been investigated as potential anticancer agents. These copper coordination complexes show potential as potent anticancer drugs, demonstrating reduced harm to normal cells and presenting an alternative strategy to evade chemoresistance linked to recurrent platinum therapy (Usman *et al*.,2017). Moreover, cancer cells' modification of copper homeostatic systems to resist traditional platinum-based treatments can be mitigated by specific copper coordination complexes, which can re-sensitise the cancer cells (Denoyer *et al*., 2015).

Numerous copper complexes have demonstrated anticancer efficacy in both *in vitro* and *in vivo* studies. The diverse coordination chemistry of copper, enhanced by the dynamic Cu(I/II) redox behaviour, offers significant implications for metallo-nucleases. Sigman *et al*., (1996) discovered the first copper nuclease complex, pioneering novel research avenues. Unlike their platinum counterparts, copper complexes bind non-covalently with DNA through intercalation,

electrostatic forces, and minor or major groove binding. Though this interaction has not yet been definitively proven intracellularly, these complexes are believed to cause DNA cleavage of the sugar-phosphate backbone, nucleobase oxidation, and deoxyribose sugar oxidation (Santini *et al*., 2014). This mechanism potentially results in less toxic side effects and offers an avenue to bypass chemoresistance observed with platinum compounds (McGivern *et al*., 2018).

A broad spectrum of Cu(II) complexes is synthesised using diverse ligand groups, including Schiff bases, amino acids, peptides, five-membered aromatic heterocycles (imidazoles, pyrazoles, triazoles), thiosemicarbazones, and numerous naturally occurring bioactive flavonoids like coumarins (Zehra *et al*., 2021). These ligand groups have facilitated the production and testing of multiple copper complexes, some of which have exhibited promising cytotoxic activity and even progressed to clinical trials. For example, the mixed Cu(II)-phenanthroline complex "Cas-II Gly" [Cu(4,7-diMephen)(Gly)](NO_3), part of the Casiopeinas® (Cas) pharmaceutical series, demonstrated anticancer action through mitochondrial malfunction, DNA damage, and apoptosis induction. However, its cardiotoxic effects restricted application (Ruiz-Azuara and Bravo-Gomez., 2010).

Further studies have elucidated the antitumor activities of copper complexes. Tamaya *et al*., (2017) reported that two synthesised copper (II) complexes in combination with flavonoids - naringenin and hesperetin, inhibited the proliferation of A549 NSCLC lung cancer cells (IC_{50} = 5.82 µM) by inducing apoptosis. Salimi *et al*., (2015) found that two polypyridyl-based copper(II)complexes effectively inhibited MCF7 breast cancer cells (IC_{50}=4.57 µM and IC_{50} = 1.98 µM, respectively), triggering cell death by apoptosis. Mendo *et al*., (2015) also demonstrated cytotoxicity in breast, colorectal, and hepatocellular carcinoma cell lines by a copper compound conjugated to the ligand 4′-phenyl-terpyridine (IC_{50} =0.07 to 7 µM). The compound was found to induce apoptosis and delay cell cycle progression.

These findings are similar to those observed in cells treated with novel copper-imidazo[1,2-*a*]pyridine complexes, showing efficacy against cell lines from breast, leukaemia, and colorectal cancers at low micromolar concentrations below 10 µM (Dam *et al*., 2017). These complexes induced cell death *via* apoptosis, with the activation of intrinsic apoptosis identified in colorectal and leukaemia cell lines (Harmse *et al*., 2019; Ismail *et al*., 2022). The precise mode of action of these copper complexes is yet to be fully elucidated. However, evaluating these copper complexes on lung cancer cell lines, where they have not yet been tested, might provide a potential alternative to current therapies.

Taken together, these studies suggest a significant potential for copper complexes as powerful agents in upcoming cancer treatment regimens.

1.7 A549 Cell Line

An effective *in vitro* model for NSCLC is necessary to examine the effectiveness and to understand the mechanisms of action of these copper complexes when examining the potential of such complexes as a treatment strategy for lung cancer. The A549 cell line is an ideal candidate for this type of investigation.

The A549 cell line, established from lung carcinoma tissue collected from a 58-year-old Caucasian male in 1972, represents a human cell line derived from alveolar basal epithelial cells (Giard *et al*., 1973). It is widely utilised in NSCLC research due to the retention of numerous characteristics of type II alveolar epithelial cells.

Several factors contribute to the suitability of the A549 cell line for lung cancer research. First, it replicates many features of the original tumour, including morphology, growth properties, and tumour antigen production, thus providing a reliable model for investigating lung cancer biology (Lieber *et al*., 1976). Second, the A549 cell line is robust and straightforward to culture, offering practical advantages for researchers (Freshney, 2015). Third, given the extensive research involving A549 cells, a significant amount of comparative data is available, which aids the interpretation of new findings (Langthaler *et al*., 2021). Lastly, the inherent resistance of A549 cells to standard chemotherapeutic agents allows for the examination of drug resistance mechanisms within NSCLC (Gazdar *et al*., 2010).

Including the A549 lung cancer cell line in the study added important information about the possible therapeutic use of these complexes in NSCLC, given the positive results about the effectiveness of copper complexes against other cancer cell lines. Additionally, by concentrating on the A549 cell line, the information gap regarding the impact of copper-imidazo[1,2-*a*]pyridine complexes on NSCLC was covered.

Thus, the A549 cell line remains a fundamental tool in lung cancer research. Its unique characteristics render it an ideal *in vitro* model for exploring novel treatment strategies for NSCLC, including those involving copper complexes. The extensive exploration of copper complexes as potential therapeutics in this review highlights the potential that this area of study holds for advancing the understanding of and approach to treating lung cancer.

1.8. Aims and Objectives

1.8.1 Aim

To evaluate the potential anticancer effect of a small library of copper-imidazo[1,2 a]pyridines on the A549 lung cancer cell line and to determine the mechanism of cell death of the active compounds.

1.8.2 Objectives

1. Identify test compounds that exhibit an 80% reduction in A549 cancer cell growth at a screening concentration of 50 μM using the MTT cytotoxicity assay.
2. Determine the 50% inhibitory concentration (IC_{50} concentration) of the active test compounds identified in the first objective.
3. Evaluate morphological changes in A549 cells exposed to the most active test compound complexes to exclude those inducing necrotic cell death.
4. Evaluate the role of active test compounds in modulating ROS in A549 cells, offering insights into oxidative stress-related anti-cancer mechanisms.
5. Investigate if the active test compounds prompt apoptosis by measuring apoptotic markers such as phosphatidylserine externalisation using Annexin-V binding and the activation of caspase-3/7.
6. Assess whether the apoptosis, if induced, is intrinsic or extrinsic by assessing the mitochondrial membrane potential and the activation levels of caspase-8.
7. Examine the effect of active copper-imidazo[1,2-*a*]pyridine complexes on the regulation of cell cycle proteins by evaluating the expression and distribution of p21 and p53 using immunohistochemistry techniques.
8. Analyse the impact of the active copper-imidazo[1,2-*a*]pyridine complexes on the expression levels of apoptosis-associated proteins to understand the complexes' interaction with the cellular apoptosis pathway

Chapter II. Methodology

An ethics waiver for the use of cell lines was obtained from the Human Research Ethics Committee (Appendix A).

2.1 Cell Culture

The A549 cell line, an NSCLC pulmonary adenocarcinoma human cell line, was cultured (Giard *et al*., 1973) using the standard sterile technique

The cells were propagated in a 1:1 mixture of Dulbecco's Modified Eagles Medium (DMEM)/Ham's F-12 medium, supplemented with 10 % (v/v) heat-inactivated fetal bovine serum (FBS), 1% (v/v) non-essential amino acids, 1% (v/v) sodium pyruvate, 1% L-glutamine, and 0.1 mg/ml of penicillin-streptomycin (Appendix B). The cell culture was maintained in 75 cm^3 flasks at 37 °C in a 5 % CO_2 humidified incubator (Appendix B).

2.1.1 Cell Subculture

The A549 cells were sub-cultured upon reaching approximately 80% confluence. The culture medium was aspirated and discarded, and the cells were washed twice with 1x phosphate-buffered saline (PBS) (Appendix C). Cells were dissociated with 5 ml of a Trypsin-EDTA solution, which typically contains 0.25% Trypsin and 0.53 mM EDTA. The Trypsin-EDTA solution was pre-warmed to 37°C to enhance its activity. After the cells were detached, they were distributed into flasks with fresh culture media and returned to the incubator. The surplus cells collected following trypsinisation were used in experiments or cryopreserved.

2.1.2 Cryopreservation

Cryopreservation was performed on the cells while in the logarithmic growth phase. Cells were centrifuged at 1000 g for 5 minutes. The resultant cell pellet was resuspended in 1.5 ml of freezing media (Appendix C) containing culture-grade dimethyl sulfoxide (DMSO), aliquoted into cryovial tubes and placed in a CoolCell container for 72 hours at -80°C. The CoolCell container allows for a controlled freezing process of approximately -1°C per minute. Long-term storage of cells was conducted in liquid nitrogen vapour at -196 °C.

Upon revival from cryopreservation, cells were quickly thawed in a 37°C water bath and transferred to 25 cm^2 tissue culture flasks. These revived cells were maintained in cell culture media supplemented with 20% FBS until proliferation was observed, at which point the FBS in the culture media was reduced to the standard 10%.

2.1.3 Cell Counting and Viability

The cell count and viability were determined using the trypan blue exclusion assay. A 0.4% (w/v) trypan blue dye (Appendix C) was mixed with the cell suspension in a 1:1 ratio, and 10 µl of this mixture was loaded onto one half of a haemocytometer and 10 µl onto the other half, allowing for live-dead cell counts in duplicate for accuracy.

Viable, unstained cells were counted using the Nikon Optiphot light microscope (Appendix B) at 100x magnification. The total cell count was calculated by counting the number of viable cells in four large corner squares of the haemocytometer, multiplying by the dilution factor, and then multiplying by 10,000 to convert to cells per milliliter.

The percentage of viable cells was calculated by dividing the number of viable cells by the total number of cells (viable and non-viable), and multiplying by 100. The cells were considered suitable for experiments only if their viability exceeded 97%. This rigorous approach ensured the accuracy and reproducibility of the cell counts and viability assessments, which were critical for the success of the subsequent experiments.

2.2 Test Compounds

This study investigated the effects of four categories of compounds, namely copper-imidazo[1,2-*a*]pyridine complexes (JDs), theophylline conjugates (AD compounds), copper-complexed OM compounds, and epidermal growth factor receptor kinase inhibitors (EKIs), on the A549 lung cancer cell line. These compounds were synthesised and characterised at the University of the Witwatersrand's School of Chemistry. For the copper-imidazo[1,2-*a*]pyridines, structural validation was carried out *via* elemental analysis and nuclear magnetic resonance (NMR) spectroscopy. Stock solutions of compounds were prepared at a concentration of 2 mM in 100% culture-grade DMSO. They were freshly prepared for each experiment to maintain consistent efficacy.

2.2.1 Positive Controls

Four established anticancer drugs – 5-Fluorouracil, Temozolomide, Doxorubicin, and Cisplatin– were used as positive controls. The preparation of these control compounds mirrored the test compounds, ensuring identical conditions.

2.2.2 Screening of Test Compounds for Cytotoxic Activity and Apoptosis Induction

Initial screening involved exposing A549 cells to 20 distinct test compounds from the four drug classes, each administered at concentrations of 5 and 50 µM. The MTT cell viability assay was

utilized to assess the compounds' effects over 48 hours, and those causing over 80% cell growth inhibition at the 50 µM concentration were selected for further study. The half-maximal inhibitory concentration (IC_{50}) values were calculated for these compounds to ascertain their relative potency and effectiveness.

2.3 The 3-[4,5-dithylthiazol-2-yl]-2,5 diphenyl tetrazolium bromide (MTT) cell viability assay

The 3-[4,5-dimethylthiazol-2-yl]-2,5 diphenyl tetrazolium bromide (MTT) is a colourimetric method that evaluates metabolic activity to indicate cell viability. It is based on the conversion of the yellow tetrazolium salt, MTT, into a purple formazan crystal by the mitochondrial enzyme succinate dehydrogenase in viable cells (Mosmann, 1983). The colourimetric change is quantitatively correlated with cell viability and is detectable *via* spectrophotometry.

A549 cells were seeded at a density of 8 x 10^3 cells per well in a 96-well plate at a volume of 100 µl. This seeding density was determined based on a linear relationship between cell number and absorbance values from an MTT standardisation experiment (Appendix D). After seeding, cells were incubated at 37 °C under a 5% CO_2 atmosphere for 24 hours to facilitate adherence before being exposed to the test compounds at concentrations ranging from 0.05 µM to 50 µM.

The cells were then incubated with the test compounds for 44 hours. This incubation period was chosen to allow for a total treatment time of 48 hours between the cells and the test compounds. At the 44-hour mark, 40 µl of MTT solution (5 mg/ml in 1x PBS) was added to each well. The plates were then incubated for an additional 4 hours to allow for the reaction with MTT.

After the 4-hour incubation with MTT, the plates were centrifuged at 1 500 g for 5 minutes to precipitate the formazan crystals. The supernatant was then carefully aspirated, ensuring not to disturb the precipitated formazan crystals.

The formazan crystals in the wells were then dissolved in 200 µl of 100% DMSO, and the plates were then shaken on an orbital microplate shaker at 1 000 rpm for 5 minutes to ensure complete solubilisation of the crystals. The absorbance was measured using the Lab Systems Multiskan iEMS plate reader (Appendix B) at a test wavelength of 540 nm and a reference wavelength of 690 nm as per standard MTT assay (Appendix D).

Controls for the assay included untreated cells, media-only wells, and wells with positive control compounds at 10 µM.

All data points were obtained in quadruplicate, and each assay was replicated at least five times to ensure the robustness of the findings. The results were analysed using Microsoft Excel and GraphPad Prism 5 software package (Appendix B), which aided in constructing dose-response curves and calculating IC_{50} values.

IC_{50} values were calculated using non-linear regression analysis for sigmoidal dose-response curves, providing a detailed and quantitative measure of each test compound's potency. Comparisons between the IC_{50} values of the control and test compounds were conducted using the Mann-Whitney U-test on GraphPad Prism with the statistical significance set at $p < 0.05$.

2.4 Evaluation of Cell Morphology using Fluorescence Microscopy

Cellular morphological changes in A549 cells following treatment with the four most potent compounds, JD35, JD46, JD47, and JD88, were evaluated using a range of fluorescent dyes, which included Hoechst 33342, propidium iodide, and acridine orange. These assessments were conducted using an Olympus BX41 epifluorescence microscope (Appendix B).

Hoechst 33342, a nuclear counterstain, was employed to label chromatin DNA, allowing for the visualisation of cellular nuclei. It emits a blue fluorescence upon excitation by ultraviolet light, with peak emission at 461 nm. This dye facilitated the evaluation of cytomorphological characteristics such as nuclear fragmentation and chromatin condensation.

Propidium iodide, a membrane-impermeant dye, was used to discern viable cells through the permeation of compromised cell membranes, forming a complex with nuclear DNA and emitting a red fluorescent signal (535 nm excitation and 617 nm emission).

Owing to its weak basic property, Acridine orange dye accumulates in lysosomes, staining them orange, while staining cell nuclei green. It has a490 nm excitation wavelength and its emission under a green filter (522 nm) allows for the identification of potential apoptosis and autophagy (Pierzynska-Mach *et al.*, 2014; Vermes and Haanen, 1994)

For the staining protocol, Hoechst 33342 (5 μg/ml), propidium iodide (10 μg/ml), and acridine orange (10 μg/ml) were prepared in 1x PBS. Post-preparation, A549 cells were harvested, quantified, and seeded onto sterilised glass coverslips in a six-well culture plate at 1×10^6 cells/ml density. After a 24-hour incubation period at 37 °C with 5% CO_2 to allow for cell adherence, the cells were treated with the test compounds, JD35, JD46, JD47, and JD88, at concentrations corresponding to their IC_{80} values and further incubated for 18 hours. Untreated

cells were prepared as negative controls, while doxorubicin-treated cells were prepared as positive controls.

Post-treatment, the cells were stained with the Hoechst/propidium iodide/acridine orange dye mixture (700 µl/coverslip) for 30 minutes, shielded from light exposure. This was followed by a 1ml 1x PBS wash step, after which the coverslips were mounted, cells-side down, on microscope slides with a drop of Fluoromount (Appendix B).

Subsequent observation was conducted using the aforementioned Olympus BX41 epifluorescence microscope at 400x magnification, employing filter cubes: U-MWU2 (for Hoechst 33342), U-MNIBA3 (for acridine orange), and U-MWIG2 (for ethidium bromide). Images were captured using an Olympus DP72 digital camera (Appendix B) and analysed with the Olympus CellSens software package (Appendix B).

The fluorescent staining patterns provided critical insights into the morphological changes induced by the test compounds, potentially highlighting the onset of apoptosis or other cell death mechanisms such as necrosis or autophagy. All experiments were conducted at least three times.

2.5 Detection of Reactive Oxygen Species (ROS) Accumulation

The study of ROS accumulation is pivotal in understanding cellular stress response to cytotoxic compounds. For this purpose, CellROX® Deep Red Reagent (Appendix B), a ROS-sensitive fluorescence probe was utilised.

A549 cells were seeded at a density of 2.0 x 10^5 cells per coverslip in a six-well plate and subsequently incubated at 37˚C for 24 hours in a 5% CO_2 humidified atmosphere. Post-incubation, the cells were exposed to the test compounds JD35, JD46, JD47, and JD88 at their respective IC_{80} concentrations. Doxorubicin-treated cells were used as positive controls, while untreated cells were maintained as negative controls. After the treatment, two additional incubation periods of 6 and 18 hours were established under the same conditions.

Simultaneously, a 5 µM CellROX® Deep Red Reagent solution was prepared by adding 1.5 µl of the 2.5 mM reagent to 750 µl of cell culture medium. This reagent was stored with heated silica gel beads to ensure desiccation. Upon the incubation periods, the cell culture medium was removed, and each well was rinsed with 2 ml of 1x PBS. Then, 120 µl of the CellROX® Deep Red Reagent mixture was added to each coverslip, followed by a 30-minute dark incubation period.

Post-incubation, coverslips were mounted onto microscope slides and ROS accumulation was visualised using the BX41 Microscope with U-MWG2 filter cube (λex= 520-550 nm, λem= 580 nm) at 400x magnification (Appendix B). Captured images were analysed following the previously mentioned methodology. This entire procedure was replicated three times for each incubation period, with each replication examining three independent fields.

2.6 Detection of apoptosis by the Annexin V Assay

An early event in apoptosis is the disruption of plasma membrane phospholipid asymmetry, which leads to the externalization of phosphatidylserine (PS) on the cell surface. Annexin V, a calcium-dependent phospholipid-binding protein with a high affinity for negatively charged phospholipids such as PS, is employed to detect this shift (Vermes *et al.,* 1995). For this purpose, the ThermoFisher Alexa Fluor® 488 Annexin-V/Dead Cell Apoptosis Kit was used (Appendix B).

To differentiate between viable, early apoptotic, late apoptotic, and necrotic cells, propidium iodide (PI) was incorporated into the assay. PI is a dye that intercalates with the DNA of cells possessing compromised membranes—necrotic and late apoptotic—but is repelled by the intact membranes of viable and early apoptotic cells. Thus, viable cells are identified as Annexin-V and PI negative, early apoptotic cells as Annexin-V positive and PI negative, late apoptotic cells as both Annexin-V and PI positive, and necrotic cells as Annexin-V negative and PI positive.

During this experiment, A549 cells were seeded onto coverslips in six-well plates at $2x10^5$ cells/ml density and incubated for 24 hours. Post-incubation, these cells were exposed to the test compounds JD35, JD46, JD47, and JD88 at their respective IC_{80} concentrations at different exposures of 6 and 18 hours, respectively. Untreated cells were negative controls, while doxorubicin-treated cells were positive controls.

Following this exposure, cells were washed with 1x PBS and then incubated with an Annexin-V binding buffer (50 mM HEPES, 700 mM NaCl, 12.5 mM $CaCl_2$, pH 7.4) containing Alexa Fluor® 488 (6% v/v) and PI (1% v/v) in the dark at room temperature for 15 minutes.

After incubation, cells were visualised under an Olympus BX41 epifluorescence microscope This allowed for the detection of the Alexa Fluor® 488-Annexin-V conjugate with a U-MNIBA3 filter cube (excitation: 470 – 490 nm ± 20; emission: 510 – 550 nm), thus determining cells in varying stages of apoptosis or necrosis. Images were captured with the Olympus DP72

camera and subsequently analysed using the Olympus CellSens Software package to ascertain the proportion of cells in each stage.

2.7 Determination of caspase 3/7 activation

Caspase-3 and Caspase-7, key executioner caspases, play a vital role in the proteolytic degradation of structural and repair proteins during the execution phase of apoptosis. The activation of these caspases was monitored *via* the CellEvent™ Caspase-3/7 Green Detection Reagent (Appendix B), a unique fluorogenic substrate containing a DEVD peptide (Asp-Glu-Val-Asp) linked to a nucleic acid-binding dye. Initially, this substrate is non-fluorescent, given that the DEVD peptide inhibits the dye's ability to bind to DNA. Once caspase-3 or -7 are activated, the DEVD peptide undergoes cleavage, enabling the dye to bind to DNA and emit a bright green fluorescence signal at a maximum emission of 530 nm.

In the experiment, A549 cells were seeded on sterile coverslips within six-well plates at a density of $2x10^5$ cells in a 2 ml volume. They were incubated at 37 ºC, 5% CO_2 in a humidified environment for 24 hours to ensure cellular adherence. Post-incubation, the cells were exposed to JD35, JD46, JD47, and JD88 test compounds, each at their corresponding IC_{80} values, and subsequently incubated for an additional 24 and 48 hours under identical conditions. As experimental controls, untreated cells served as negative controls, while those treated with doxorubicin as positive controls.

After the incubation, the medium was carefully removed, and a 40 µl aliquot of the Caspase-3/7 Green Detection Reagent (prepared to a final concentration of 5 µM in 1x PBS with 5% w/v FBS) was added to each coverslip. This was followed by a 30-minute incubation at 37 ºC in a 5% CO_2 humidified incubator. Apoptotic cells with activated caspase-3/7 displayed bright green nuclei, while cells without activated caspase-3/7 exhibited minimal fluorescence.

The subsequent examination of cells was conducted using an Olympus BX41 epifluorescence microscope. Captured images were subsequently analysed for relative fluorescence intensity, quantitatively measuring caspase-3/7 activation. It should be noted, however, that this methodology does not differentiate between the activities of caspase-3 and caspase-7, as both caspases participate in the DEVD sequence cleavage in proteins. This experiment was repeated at least three times.

2.8 Determination of caspase-8 activation

The activity of caspase-8, a crucial biomarker for extrinsic apoptosis, was evaluated using a selective fluorescent inhibitor, Red-IETD-FMK (Appendix B). This inhibitor binds explicitly to active caspase-8, enabling the visual assessment of its activity.

A549 cells were seeded at a density of 2.0 x 10^5 cells per coverslip in a six-well plate, each with a 2 ml volume. The plate was incubated at 37˚C in a 5% CO_2 humidified atmosphere for 24 hours. Subsequently, cells were treated with the specified test compounds (JD35, JD46, JD47, and JD88) at their respective IC_{80} concentrations. Untreated cells functioned as negative controls, while cells treated with doxorubicin were used as positive controls. These cells were then subjected to two further incubation periods, 24 and 48 hours, under the same conditions (37˚C in a 5% CO_2 humidified atmosphere).

The Red-IETD-FMK reagent was prepared during incubation by combining 3 µl of the reagent with 900 µl of wash buffer. After the incubation, the culture medium was removed, and each well was washed with 2 ml of 1x PBS. Each coverslip was then treated with 150 µl of the prepared Red-IETD-FMK reagent solution, followed by a one-hour incubation.

Post incubation, coverslips were mounted onto microscope slides. Active caspase-8 was identified and examined using fluorescence microscopy with a BX41 microscope (Appendix B), at 400x magnification and utilising the U-MWG2 filter cube (λex= 520-550 nm, λem= 580 nm). Captured images were analysed according to the previously described methodology. The entire experiment was replicated three times for each period, with each replication examining three independent fields.

2.9 Mitochondrial Membrane Potential Assessment

Mitochondrial membrane potential (MMP) disruptions are signature features of apoptosis. MMP is essential for various mitochondrial processes and reflects the functional status of mitochondria (Sakamuru *et al.*, 2016). To assess MMP, an assay using the 5,5',6,6'-tetrachloro-1,1',3,3'-tetraethylbenzimidazol-carbocyanine iodide (JC-1) dye was utilised (Appendix B). This dye is sensitive to changes in mitochondrial function as reflected by changes in the mitochondrial membrane potential. In cells with a healthy (normal) MMP, the dye accumulates within the mitochondria (Smiley *et al.*, 1991), forming aggregates that shift the fluorescence spectrum from green to red. In contrast, cells with low MMP (under apoptotic stress) retain JC-1 in its monomeric form, causing a green fluorescence emission.

A549 cells were seeded onto coverslips in six-well plates at a 4.0 x 10^5 cells/ml density and incubated at 37 ºC for 24 hours. The cells were then treated with the test compounds JD35, JD46, JD47, and JD88 at their respective IC_{80} values and incubated for 12 and 18 hours, respectively. Untreated cells served as negative controls, while doxorubicin-treated cells as positive controls.

Following the two incubation periods, the culture medium was aspirated, and each well was washed twice with 2 ml 1x PBS. A working solution of JC-1 dye (5 µg/ml) was prepared in 1x PBS and centrifuged to remove potential dye aggregates. Each coverslip was subsequently incubated with 500 µl of the prepared JC-1 dye solution in darkness for 20 minutes.

Post-incubation, the coverslips with the stained cells were mounted onto microscope slides for evaluation. Using an Olympus BX41 epifluorescence microscope with the U-MNIBA3 filter cube (λex=470-490 nm, λem=510-550nm), the cells were observed at a 400x magnification. Changes in MMP were discerned by the shift in JC-1 dye fluorescence from green to red. Images were captured using the Olympus DP72 digital camera and analysed using the Olympus CellSens software package. The procedure was conducted in triplicate for each period, with three independent fields observed per experiment for data analysis.

2.10 Immunohistochemistry for p21 and p53

The cellular localisation and expression levels of p21 and p53 proteins were evaluated using immunohistochemistry techniques. Both p21 and p53 are critical regulators of the cell cycle, playing essential roles in cell response to stress, including DNA damage. This procedure comprised multiple steps, as detailed below:

A549 cells were plated at a density of 2.0 x 10^5 cells per coverslip in a six-well plate, followed by a 24-hour incubation at 37˚C. Subsequently, the cells were exposed to the test compounds JD35, JD46, JD47, and JD88 at their respective IC_{80} concentrations, followed by a further 20-hour incubation at 37˚C. Doxorubicin-treated cells were positive controls, while untreated cells functioned as negative controls.

Post-incubation, cells were washed twice with 1x PBS, while ensuring the slides did not dry out. Cells were then fixed with 3% formaldehyde solution in 1x PBS, followed by cell permeabilization with a solution containing 0.25% Triton X and 0.5% bovine serum albumin (BSA)(Appendix B).

Membrane Blocking

After permeabilization, cells were treated with a 0.5% BSA solution in 1x PBS to block non-specific protein binding. The solution was prepared by diluting 600 µl 5% BSA in 5400 µl 1x PBS. The blocking solution was removed, and the cells were washed with PBS.

Primary Antibody Binding

Primary antibodies for p21 and p53 (Appendix B) were each prepared at a 1:200 dilution in 0.5% BSA). A volume of 120 µl of the primary antibody solution was added to each coverslip. The cells were then incubated overnight at 4°C. Negative controls were treated solely with 0.5% BSA to ensure specificity of the primary antibody binding.

Secondary Antibody Binding

Following the primary antibody incubation, coverslips were washed thoroughly with 1x PBS to remove any unbound primary antibodies. Subsequently, 120 µl of a 1:200 dilution of secondary antibodies, prepared in 0.5% BSA, was added to each coverslip.

For p21 detection, an anti-mouse Alexa Fluor 488-conjugated secondary antibody with green fluorescence (Appendix B) was used. For p53 detection, an anti-rabbit Alexa Fluor 568-conjugated secondary antibody with red fluorescence (Appendix B) was used. The coverslips were then incubated in the dark at room temperature for one hour.

Slide Preparation and Imaging

After secondary antibody incubation, coverslips were washed in 1x PBS, mounted onto microscope slides using Fluoromount, and allowed to dry for approximately 30 minutes. Slides were then examined using the BX41 Microscope with U-MWG2 filter cube (λex= 520-550 nm, λem= 580 nm) for p53 and U-MNIBA3 filter cube (λex=470-490 nm, λem=510-550nm) for p21, each at 400x magnification. Images captured were analysed and co-localised using Olympus Cellsense software. This experimental procedure was performed at least twice for each antibody, with five independent fields analysed in each experiment.

2.11 Protein Concentration Estimation

To determine the protein concentration in cell lysates, the Bradford protein assay (BIO-RAD) (Appendix B) was utilized. This dye-binding assay takes advantage of the absorption spectrum shift of the Coomassie Brilliant Blue G-250 dye upon binding to proteins. Specifically, the absorption maximum of the dye changes from 465 nm to 595 nm when it binds to a protein (Bradford, 1976).

For the assay, standardized BSA (1.0 mg/ml) was used to construct a standard curve. The dye reagent was prepared by diluting the concentrated reagent in a 1:4 ratio with double distilled water (ddH_2O).

The procedure involved pipetting 10 µl of each test sample into individual wells of a 96-well microtiter plate in duplicate. Then, 200 µl of the diluted dye reagent was added to each well. To ensure thorough mixing, the plate was shaken at 1000 rpm for 5 minutes using the Thermo Scientific™ Multiskan™ GO Microplate Spectrophotometer (Appendix B).

Absorbance measurements were conducted at 595 nm using the same spectrophotometer. The absorbance data was used to plot a standard curve for protein determination. This curve served as the reference for calculating the protein concentrations in the test samples. The standard curves for protein determination are provided in Appendix D.

Due to the interference of copper with the bicinchoninic acid assay, the Bradford protein assay was specifically chosen for protein quantification in this study, facilitating the support of proteomic profile assays. The assay was conducted in triplicate to ensure the accuracy of the results.

2.12 Apoptotic Regulatory Proteome Array

To investigate the impact of JD88, the most potent copper-imidazo pyridine compound, on apoptotic regulatory proteins, the Proteome Profiler Human Apoptosis Array Kit was used (Appendix B). This kit facilitates the simultaneous detection of 35 apoptosis-related proteins through a membrane-based sandwich immunoassay.

A549 cells were harvested and seeded at $1x10^6$ cells per 75 cm^3 flask in triplicate. Cells were then incubated for 24 hours at 37 ºC in a 5% CO_2 humidified incubator to allow adherence. Subsequently, cells were treated respectively with JD88 and the positive control compound, doxorubicin, at their respective IC_{80} concentrations.

Post-treatment, cells were harvested and lysed with protease inhibitors present. The protein concentration of the lysates was determined *via* the Bradford protein assay, following the previously outlined procedure. The lysates were then prepared with a concentration of 400 µg of protein.

In preparation for incubation, membranes were blocked using array buffer 1, a buffered protein solution with preservatives, for one hour at 4°C on a rocking platform shaker. The cell lysates were then diluted to a final volume containing 400 µg of protein per lysate with array buffer 1.

This diluted lysate was incubated with the membranes overnight at 4°C on a rocking platform shaker in a final volume of 2 ml, allowing specific target proteins to bind to the immobilised antibodies on the four nitrocellulose membranes.

Following this overnight incubation, the membranes were washed three times with 1x washing buffer for 10 minutes each on a rocking platform shaker to remove unbound proteins. Subsequently, the membranes were incubated with a detection biotinylated antibody cocktail diluted in 1x array buffer 2/3 for one hour, followed by incubation with a 1:2000 dilution of streptavidin-horseradish peroxidase (HRP) conjugate (Appendix B) in 1x array buffer 2/3 for 30 minutes.

Post-incubation, membranes underwent further washes, as previously detailed, and were then enclosed in a plastic sheet protector before detection. All array membranes for each cell line were incubated simultaneously to prevent discrepancies. The membranes were exposed for one minute to a chemiluminescent detection reagent mix, where luminol oxidation, catalysed by HRP, led to light emission. As the light emission is concurrent with the enzyme-substrate reaction, chemiluminescence is a sensitive detection method for trace proteins in a single sample. Each captured spot produced a chemiluminescent signal proportional to the bound protein quantity.

Finally, the membranes were analysed for positive chemiluminescent signals using a BIO-RAD ChemiDoc ™ MP Imager (Appendix B). Data was analysed using Image Lab Software Version 6 (Appendix B) and subjected to statistical analysis using Graph Pad Prism v. 5 *via* analysis of variance (ANOVA ($p < 0.05$), followed by a post-hoc Dunnet's test. Significance was allocated as follows: p-values of 0.01 and 0.001 were considered highly significant, 0.05 significant, and 0.1 poorly significant. All data analysis and graph constructions were carried out using GraphPad Prism v.5.

Chapter III. Results

3. Outline

In this chapter, the results obtained from the investigation are presented. Initially, the IC_{50} values of the most active copper complexes are reported. This is followed by a morphological examination of the impact of these complexes on the A549 lung cancer cell line and their capacity to generate ROS species in these cells. Next, the induction of apoptosis is assessed through the study of phosphatidylserine exposure in A549 cells and the activation of caspase-3/7 in these cell lines by the copper complexes. The activation of the extrinsic pathway of apoptosis by the complexes is then explored through the study of caspase-8. Subsequently, intrinsic apoptosis in A549 cells is evaluated by determining the mitochondrial membrane potential. Finally, an immunohistochemistry examination of p21 and p53 in A549 cells is presented, along with the changes in the apoptotic proteome profile of A549 cells affected by one of the most active complexes.

3.1 Evaluating the cytotoxicity of test compounds on the A549 lung cancer cell line

3.1.1 Evaluation of a library of test compounds to identify active compounds

The effects of four groups of test compounds were investigated in the A549 lung cancer cell line. These compounds, comprising of copper-imidazo[1,2-*a*]pyridine complexes (JDs), theophylline conjugates (AD compounds), copper-complexed OM compounds as well as epidermal growth factor receptor kinase inhibitors (EKIs), were synthesised and characterised by the School of Chemistry at the University of the Witwatersrand. The compounds were tested against the A549 lung cancer cell line to determine their cytotoxic activity at 5 and 50 μM concentrations for 48 hours using the MTT cell viability assay. Four cancer chemotherapeutic drugs were evaluated: temozolomide, 5-fluorouracil, cisplatin and doxorubicin to determine the most effective drug to use as a positive control in this study. Figure 3.1 shows the effects of the test compounds on the percentage of cell viability.

At 50 μM, the cells that were treated with the copper complexes- JD35, JD36, JD46, JD47, JD49, JD88, JD253 OM, AD3 and doxorubicin had a cell viability below 20% compared to the untreated cells, which had a cell viability of 100%. The cells treated with the EKI complexes showed cell viability between 50 and 100%, which indicates that the compounds were moderately active. At 5 μM the copper complexes- JD35, JD46, JD47, JD49, JD88, OM and

AD3 showed less than 50% cell viability. These complexes were identified as the most active and selected for further investigation. No additional work was pursued on the EKI complexes and the cancer drugs -cisplatin, 5-fluorouracil and temozolomide.

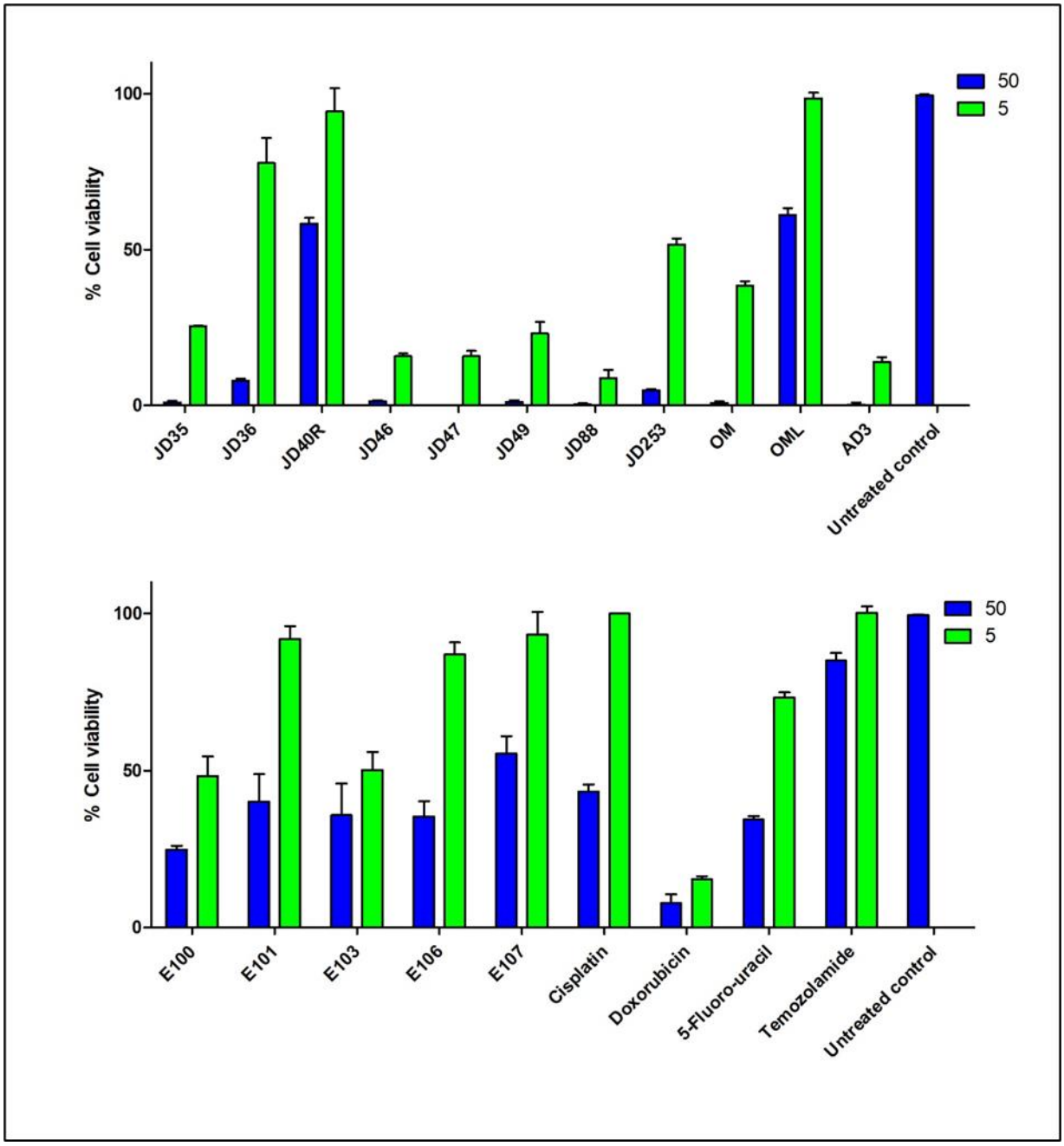

Figure 3.1 Percentage cell viability of A549 cells after treatment with the test compounds and positive control drugs at 5 µM and 50 µM. A549 cells were exposed to test compounds (JDs, ADs, OM and EKIs) and the positive controls (cisplatin, doxorubicin, 5-fluorouracil and temozolomide) for 48 hours and cell *via*bility was determined with the MTT assay. Each bar represents the mean ± SEM of values obtained in quadruplicate from five independent assays.

3.1.2 Determination of IC50 values of the most active complexes in the A549 lung cancer cell line

To determine the IC_{50} values of the active compounds identified in Section 3.1.1, cells were treated with a broad range of concentrations, each data point was obtained in quadruplicate, and the MTT assays were repeated at least five times. The GraphPad Prism Version 5.0 software package was used to construct sigmoidal dose-response curves and calculate the IC_{50} values. These results are presented in Figure 3.2.

The most active copper complexes- JD35, JD46, JD47 and JD88 had IC_{50} values below 5 μM (Figure 3.2), while OM, OML, AD3, and AD7 had IC_{50} values between 6 μM and 25 μM, JD88 was the most active compound with an IC_{50} value of 1.67±0.13 μM. Statistical analysis was performed on these IC_{50} values compared to the positive control doxorubicin (IC_{50}: 6.25 ± 0.28 μM) using the two-sample Mann-Whitney U-test with a p-value <0.05 and a 95% confidence interval. The results are displayed in Appendix E, Table E.1. The IC_{50} values of JD35, JD46, JD47, JD88, and OM were significantly lower than those of doxorubicin ($p<0.05$, $p = 0.02$), indicating that these compounds were more effective than doxorubicin. The IC_{50} values of JD49, AD3, and OML were not significantly different from that of doxorubicin ($p > 0.05$, $0.06< p< 0.62$), indicating a similar efficacy in the A549 cell line.

Based on their low IC_{50} values, the four copper-imidazo[1,2-*a*]pyridine complexes JD35, JD46, JD47 and JD88 were selected for further investigation in this study. Doxorubicin was selected as the positive control.

Table 3.1 shows the chemical structures of the selected copper-imidazo[1,2-*a*]pyridine complexes and doxorubicin and their IC_{50} and IC_{80} values. The IC_{80} values are a meaningful metric since cancer medications are used clinically to achieve 100% cell death. Concentrations at IC_{80} values were thus used in all subsequent experiments to determine the effect of the copper complexes. The positive control, doxorubicin, was used at 10 μM throughout this study to minimize its interference with fluorescence.

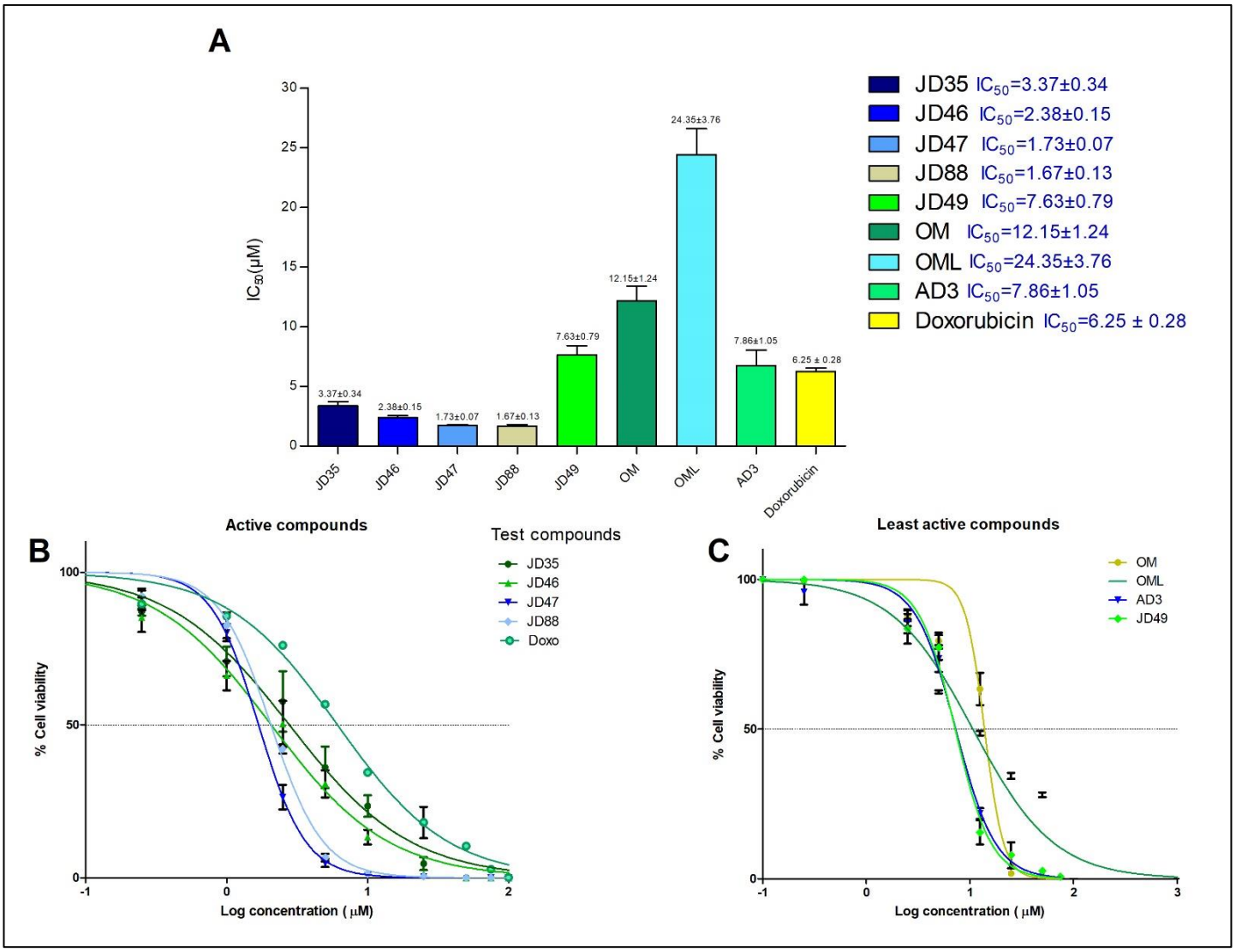

Figure 3.2 IC_{50} values and dose-response curves of active copper complexes and doxorubicin in A549 cells. (A) Summary of IC_{50} values of the selected copper complexes (B) Representative sigmoidal dose-response curves of the most active complexes and doxorubicin (C) Representative sigmoidal dose-response curves of the least active copper complexes. A549 cells were exposed to active copper complexes and doxorubicin concentrations ranging from 0.025 µM to 50 µM for 48 hours using the MTT assay. Each bar represents the mean ± SEM of IC_{50} values obtained from five independent MTT assays.

Table 3.1 Comparison of the structures of the active copper-imidazo[1,2-*a*]pyridine complexes and doxorubicin and their IC_{50} and IC_{80} in A549 cells 48 hours after treatment.

Compound name	Compound structure	IC_{50} (µM)±SEM	IC_{80} (µM)±SEM
Basic Scaffold of copper co-ordination complexes	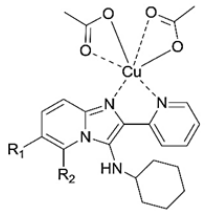		
JD35 Copper 6-bromo-N-cyclohexyl-2-(pyridin-2-yl)imidazo[1,2-a]pyridin-3-amine nitrate	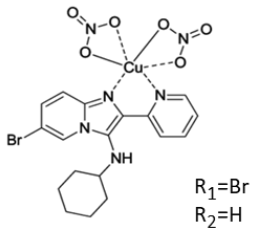 R_1=Br R_2=H	3.37±0.34	11.08±0.36
JD46 Copper N-cyclohexyl-2-(pyridin-2-yl)imidazo[1,2-a]pyridin-3-amine acetate	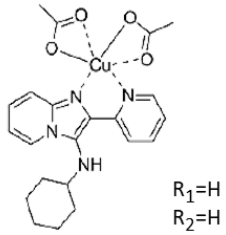 R_1=H R_2=H	2.40±0.15	7.10±1.01
JD47 Copper 5-bromo-N-cyclohexyl-2-(pyridin-2-yl)imidazo[1,2-a]pyridin-3-amine acetate	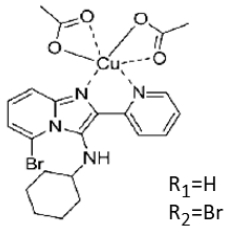 R_1=H R_2=Br	1.72±0.07	4.88±0.41
JD88 Copper 6-bromo-N-cyclohexyl-2-(pyridin-2-yl)imidazo[1,2-a]pyridin-3-amine acetate	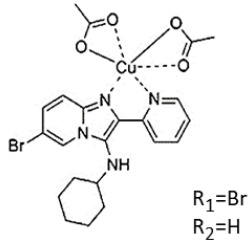 R_1=Br R_2=H	1.67±0,13	4.16±0.30
Doxorubicin (7S,9S)-7-[(2R,4S,5S,6S)-4-Amino-5-hydroxy-6-methyloxan-2-yl]oxy-6,9,11-trihydroxy-9-(2-hydroxyacetyl)-4-methoxy-8,10-dihydro-7H-tetracene-5,12-dione	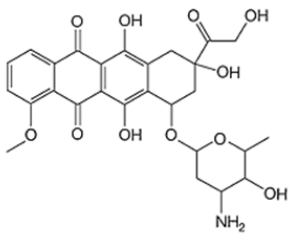	6.25 ± 0,28	16.98 ± 0.81

Based on Table 3.1, the active test compounds used in this investigation were based on a copper imidazo[1,2-*a*]pyridine scaffold. The library of test compounds was created using various substitutions or R groups with a central copper atom added to the scaffold (Dam *et al*., 2017). A qualitative structural activity relationship (SAR) to examine the impact of the different substitutions on cytotoxicity shows that the cyclohexyl amine arm of all the copper compounds in this investigation improved the overall cytotoxicity of all these compounds, as they all have an IC_{50} below 5 μM. JD35 (R_1=Br, R_2=H) differs from all the compounds in that it is an amine nitrate, while the other three test compounds are classified as amine diacetates. Although JD35 has a substitution R group of the halogen bromine at the 6th position, it has the least cytotoxicity on A549 cells compared to the other three test compounds with lower IC_{50} values. The amine diacetate copper coordination complexes have improved cytotoxic activity compared to JD35, which suggests more efficacy with the amine diacetate arm. JD46 (R_1=H, R_2=H), which is an amine diacetate that contains no halogen substitution groups, has an IC_{50} higher than JD47 (R_1=H, R_2=Br) and JD88 (R_1=Br, R_2=H), which each have a bromide group at positions 5 and 6 of the imidazopyridine moiety, respectively. The 6th position of the bromide R group in JD88 boosts the cytotoxic activity of this compound, as it is the most active with the lowest IC_{50} of all. It can, therefore be deduced that the different substitution groups and arms added to the imidazo[1,2-*a*]pyridine scaffold have a sizeable impact on the cytotoxic activity of these copper test compounds, as evidenced by the variation of the IC_{50} values.

3.2 Evaluation of changes to cell morphology induced by the copper-imidazo[1,2-*a*]pyridine complexes and doxorubicin in A549 lung cancer cells

The morphological effects of the active copper-imidazo[1,2-*a*]pyridine complexes and doxorubicin on the A549 lung cancer cells were evaluated by epifluorescence microscopy using the fluorochromes Hoechst 33342 (HO), propidium iodide (PI), and acridine orange (AO) as described in Section 2.4 of the methodology.

The cells were treated with the test compounds at their respective IC_{80} values for a duration of 18 hours. The IC_{80} values enable the visualisation of the cytotoxic effects of the test compounds and the 18-hour treatment interval was chosen based on preliminary experiments that indicated significant morphological changes could be observed after this period of treatment with the test compounds.

Following this treatment, the effect of the complexes on cell morphology was assessed and is shown in Figure 3.3.

The untreated cells (Figure 3.3, panels a-c) displayed the normal cell morphology of A549 cells. In cells treated with doxorubicin, nuclear fragmentation and chromatin condensation were observed (Figure 3.3, panel e), and staining with AO indicated an increase in lysosomal acidic granules (Figure 3.3, panel f). JD35 and JD46 caused extensive cytoplasmic vacuolisation (Figure 3.3 g and j), formed fragmented nuclei, and caused chromatin condensation (Figure 3.3, panels h and k), but not the formation of acidic vesicles (Figure 3.3, panels i and l). Similarly, cells treated with JD47 and JD88, showed vacuole formation (Figure 3.3, panel m and p), nuclear fragmentation (Figure 3.3, panel n and q) as well as lysosomal aggregation (Figure 3.3, panel o and r). These changes, particularly fragmentation of nuclei and chromatin condensation, are consistent with apoptotic cell death. PI staining of the nuclei was absent in all treated cells, indicating the absence of necrotic cell death.

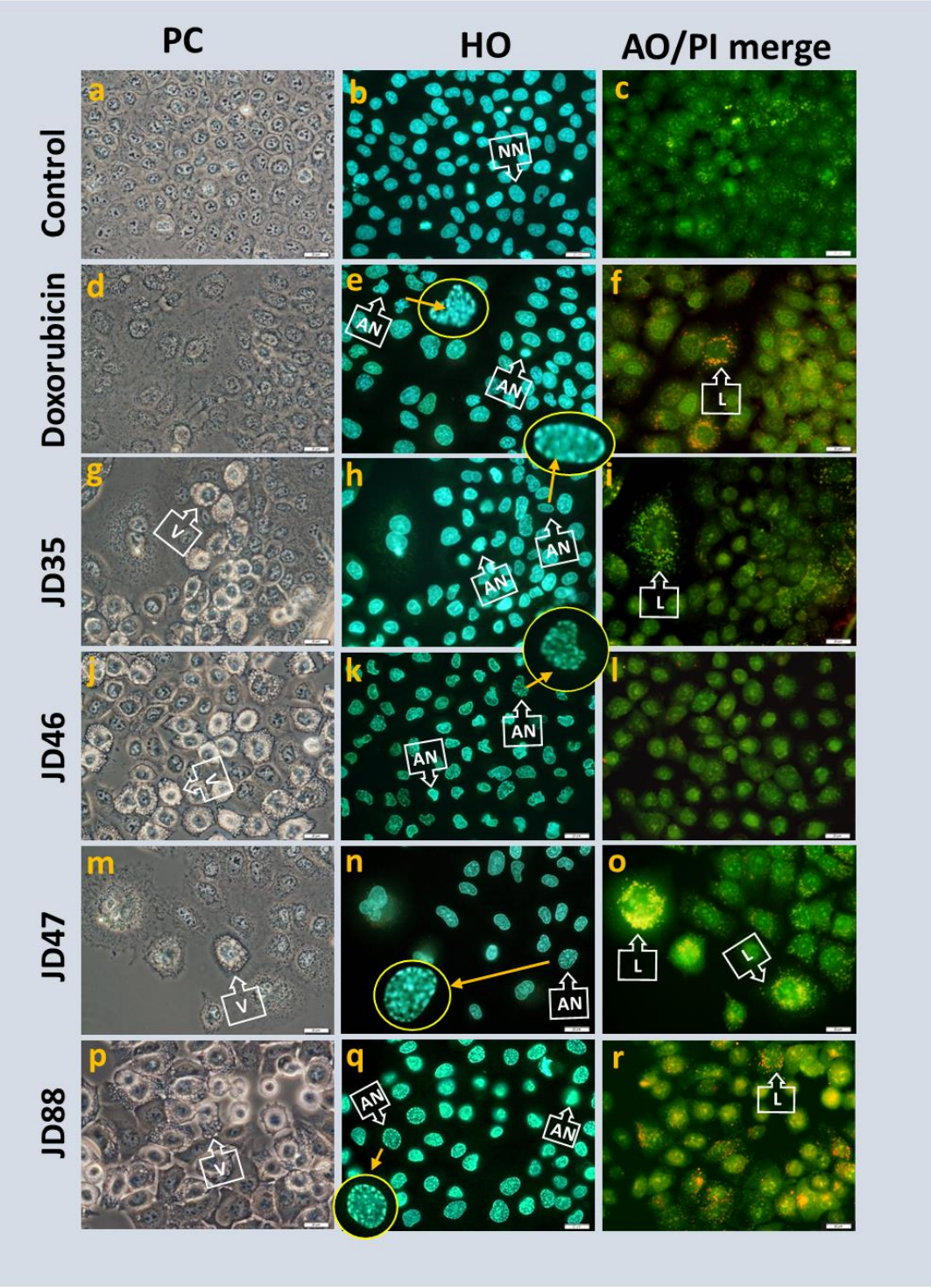

Figure 3.3 Photomicrographs of A549 cells after treatment with copper-imidazo[1,2-*a*]pyridines and doxorubicin using the fluorescent dyes, HO, AO and PI. Cells were treated with 11 µM of JD35, 7 µM of JD46, 4 µM of JD47, 4 µM of JD88 and 10 µM of doxorubicin for 18 hours and thereafter stained with HO, AO and PI. Cells displayed characteristic morphological changes such as nuclei fragmentation, chromatin condensation (apoptotic nuclei), and lysosomal aggregation. Cells were observed with an Olympus BX41 microscope, and images were captured using a DP72 camera Magnification: 400 X, scalebar: 20µm. Legend: AN=Apoptotic nucleus L=lysosomes, NN= normal nucleus V=vacuoles.

3. 3 The effect of the copper-imidazo[1,2-*a*] pyridines on reactive oxygen species in A549 lung cancer cells

ROS induction in A549 cells was measured 6 and 18 hours after treatment with the copper complexes and doxorubicin at their respective IC_{80} concentrations (Section 2.5). The results are presented in Figure 3.4.

ROS was absent in the untreated control cells (Figure 3.4, panels a-d) at 6 and 18 hours, in contrast to doxorubicin-treated cells, where ROS was observed in the perinuclear area at both periods (Figure 3.4, panels e-h). In JD35-treated cells, ROS was observed in several cells at 6 hours (Figure 3.4 , panel j) and in more cells at 18 hours (Figure 3.4, panel l). In cells treated with JD46 and JD47, ROS was observed in a few cells at 6 hours (Figure 3.4, panels n and r) while no detection of ROS was observed at 18 hours for both compounds (Figure 3.4, panel p and t). Cells treated with the JD88 compound showed the highest accumulation of ROS at 6 hours (Figure 3.4, panel v) and minimal observation of ROS at 18 hours (Figure 3.4, panel x). All compounds showed a transient increase in ROS at 6 hours of varying degrees, while only JD35 displayed the highest expression of ROS at 18 hours.

This experiment was repeated at least four times, and the captured photomicrograph data was analysed using the Olympus CellSens software to calculate the percentage of cells showing an increase in ROS at 6 and 18 hours. The data from this analysis is presented in Figure 3.5. The control cells showed a 0% increase in ROS at 6 and 18 hours, while cells treated with the positive control, doxorubicin, showed a 90 and 70% increase in ROS species at 6 and 18 hours, respectively. JD35-treated cells showed an increase of 80% in ROS species at both 6 and 18 hours, while cells treated with JD46 showed a greater increase of 40% in ROS activity at 6 hours than at 18 hours, where there was only a 2% increase in ROS species. Similarly, in JD47-treated cells, 50% of cells showed an increase in ROS species at 6 hours, while less than 10% of the JD47-treated cells showed an increase in ROS species at 18 hours. Cells treated with JD88 showed the highest increase of ROS at 6 hours, with cells showing an increase of 65% of ROS, while a lower increase of 30% was detected in the JD88-treated cells at 18 hours.

The transient increase of ROS at 6 hours shows that it is an early event in the culmination of cell death, likely leading to DNA damage and, therefore, initiating apoptosis. Further investigations of the apoptosis mechanism of cell death will give further insight into the activity

of these copper complexes and the mechanisms employed by these compounds to produce cell death.

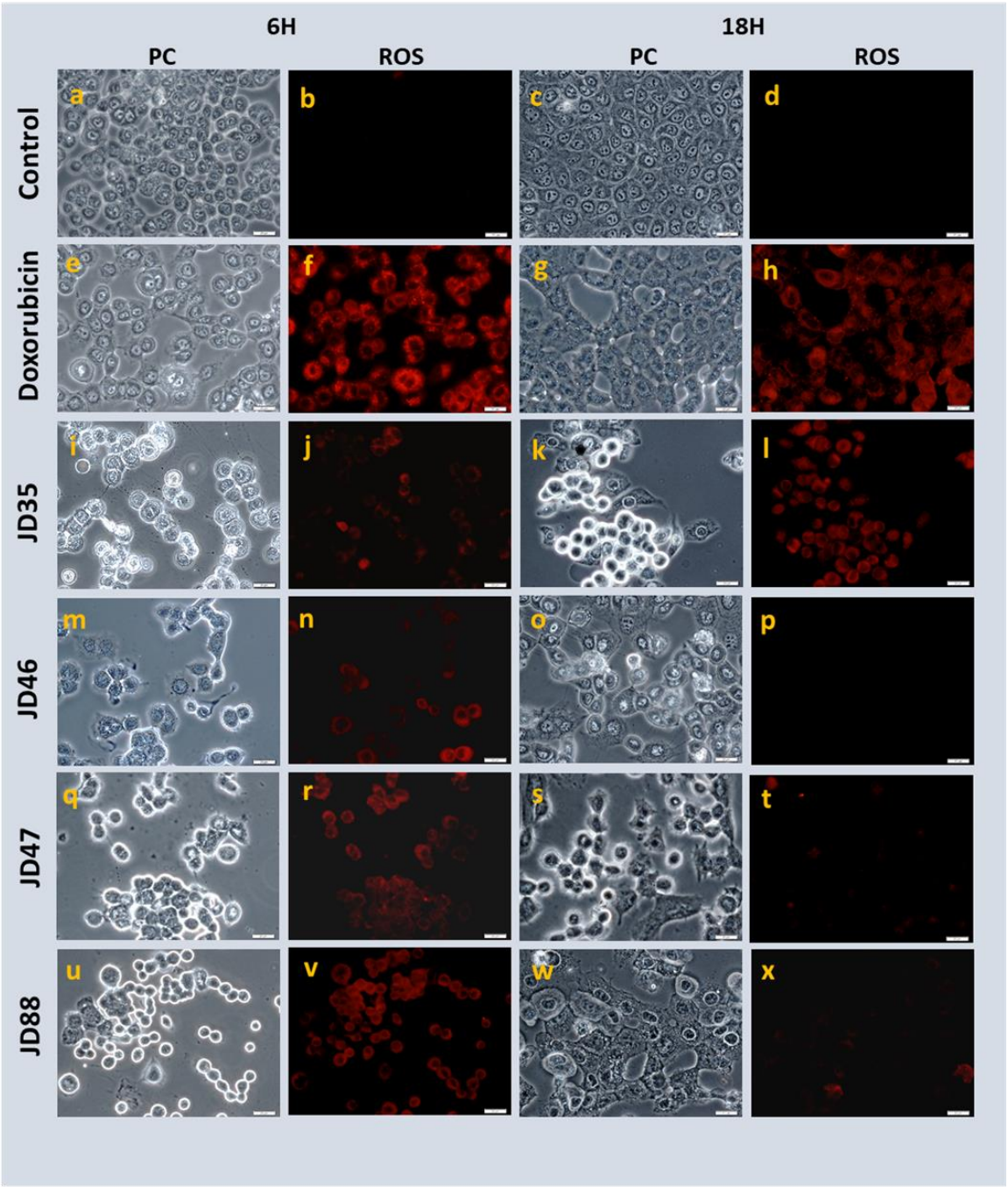

Figure 3.4 Photomicrographs of A549 cells showing the presence or absence of ROS after treatment with copper-imidazo[1,2-*a*]pyridines and doxorubicin. A549 cells were treated with 10 µM of JD35, 7 µM of JD46, 4 µM of JD47, 4 µM of JD88, and 10 µM of doxorubicin for 6 and 18 hours. The cells were observed using the Olympus BX41 microscope with the UMWIG filter cube that detects red fluorescence at 40X magnification. The images were captured using the Olympus DP72 camera. Magnification: 400 X, scalebar: 20µm.

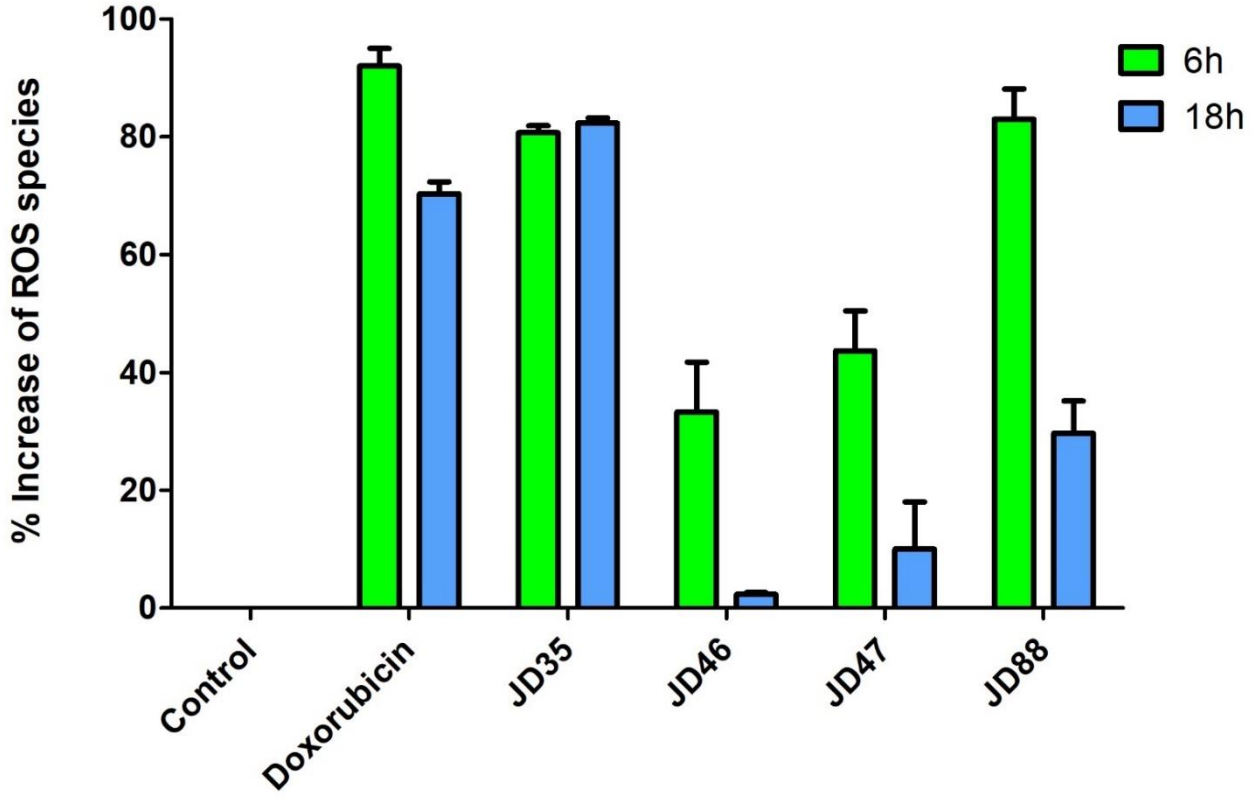

Figure 3.5 Average percentage of ROS produced in A549 cells after 6 and 18 hours of exposure to copper-imidazo[1,2-*a*]pyridines and doxorubicin. A549 cells were exposed to 10 µM of JD35, 7 µM of JD46, 4 µM of JD47, 4 µM of JD88, and 10 µM of doxorubicin. Each bar represents the mean ± SEM of values obtained from three independent experiments.

3.4 The effect of copper-imidazo[1,2-*a*]pyridines and doxorubicin on phosphatidylserine exposure in A549 cells

The exposure of phosphatidylserine at the cell surface is an early biochemical change characteristic of cells undergoing apoptosis and was detected using Annexin-V conjugated to the Alexa-fluor 488 fluorochrome as described in Section 2.6. The results are shown in Figures 3.6 and 3.7.

The cell membranes were intact in the untreated cells, and no Annexin-V binding was observed after 6 and 18 hours (Figure 3.6, panels a-d). Cells treated with doxorubicin showed distressed cells with Annexin-V binding 6 and 18 hours after treatment (Figure 3.6, panel e-h). The nuclei of these cells were stained red. In cells treated with JD35, the cells showed a rounded morphology with fibrils at 6 hours post-treatment (Figure 3.6, panel i) as well as Annexin-V binding on the cell surface (Figure 3.6, panel j). No PI dye was detected in the nucleus of these

cells, indicating early apoptosis at 6 hours, however, at 18 hours, Annexin V with PI staining of the nucleus was detected in the JD35-treated cells, suggesting late apoptosis (Figure 3.6, panel l).

In JD46-treated cells, Annexin-V binding was detected in a small fraction of cells at 6 hours (Figure 3.5, panel n), with a larger fraction of cells showing both Annexin-V binding and PI staining of the nucleus at 18 hours (Figure 3.6, panel p). In cells treated with JD47, distressed cells with intact plasma membranes are displayed at 6 hours (Figure 3.6, panel q) with Annexin-V binding and a small fraction of cells displaying PI staining of the nucleus (Figure 3.6, panel r). At 18 hours, more cells show Annexin-V binding and PI staining of the nucleus (Figure 3.6, panel t). Cells treated with JD88 displayed intact cell membranes at 6 hours, with a large percentage of cells displaying Annexin V (Figure 3.6, panels u and v). At 18 hours post treatment with JD88 the cells showed membrane blebbing as well as Annexin V binding and PI staining (Figure 3.6, panel w and x).

Experiments were conducted in triplicate, and the resulting data were analysed using Olympus CellSens software to ascertain the percentage of cells demonstrating Annexin-V and PI binding. The data are presented in Figure 3.7, depicting the percentage of cells exhibiting Annexin-V binding alone and those showing both Annexin-V and propidium iodide staining at 6 and 18 hour time points.

Untreated control cells showed no signs of Annexin-V binding or propidium iodide (PI) staining. In contrast, 25% of doxorubicin-treated cells had Annexin-V binding at 6 hours post-treatment, and 18% of both Annexin-V binding and PI staining at 18 hours post-treatment. Treatment with JD35, JD46, and JD47 resulted in more than 50% of cells showing Annexin-V binding at 6 hours, with fewer than 5% demonstrating both Annexin-V and PI detection. JD88-treated cells had the most pronounced effect, with over 70% of cells exhibiting Annexin-V binding and no PI staining. These observations suggest the initiation of early apoptosis in the cells 6 hours after treatment. At 18 hours post-treatment, there was a significant increase in cells staining positive for both Annexin-V and PI. This suggests that by 18 hours post-treatment, the cells could be transitioning to late-stage apoptosis.

The data presented in Figures 3.6 and 3.7 collectively provide additional evidence that the copper complexes induced apoptotic cell death. The detection of exposed phosphatidylserine on the cell surface by Annexin-V binding in A549 cells treated with the copper complexes and

doxorubicin suggests apoptosis as the cause of cell death, given that exposed phosphatidylserine is an early marker of apoptotic cells. Notably, PI staining without Annexin-V binding was not observed, indicating that necrotic cell death did not occur.

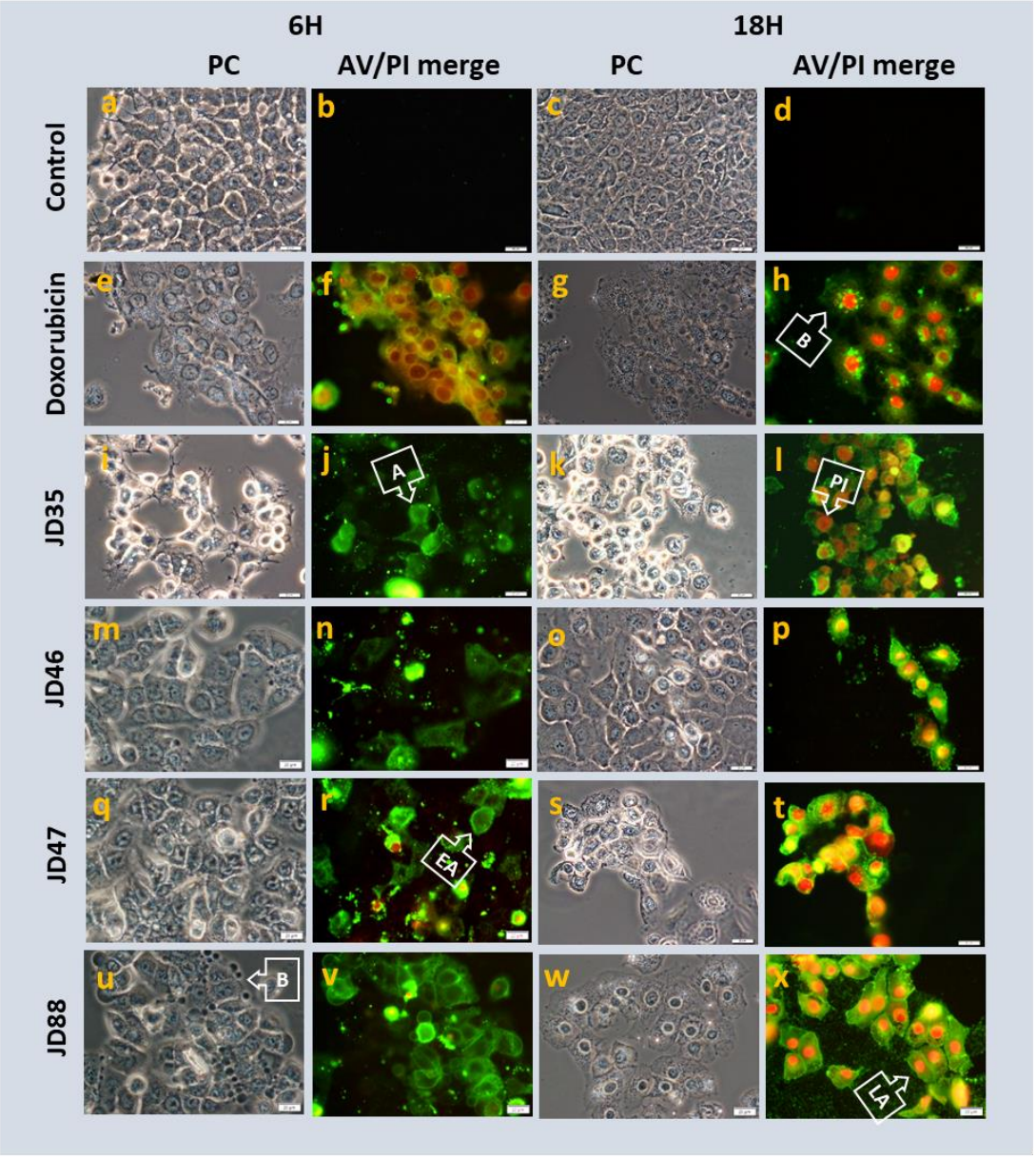

Figure 3.6 Photomicrographs of A549 cells showing Annexin-V binding and propidium iodide staining after treatment with copper-imidazo[1,2-*a*]pyridines and doxorubicin. A549 cells were treated with 11 µM of JD35, 7 µM of JD46, 4 µM of JD47, 4 µM of JD88,. and 10 µM of doxorubicin for 6 and 18 hours. The cells were observed using the Olympus BX41 microscope with the U-MNIBA3 filter cube for Alexa Fluor 488 detection. The images were captured using the Olympus DP72 camera. Magnification: 400 X, scalebar: 20µm. Legend, AV=Annexin-V, B=membrane blebbing, EA= early apoptosis, LA=late apoptosis, PC=phase contrast, PI=propidium iodide.

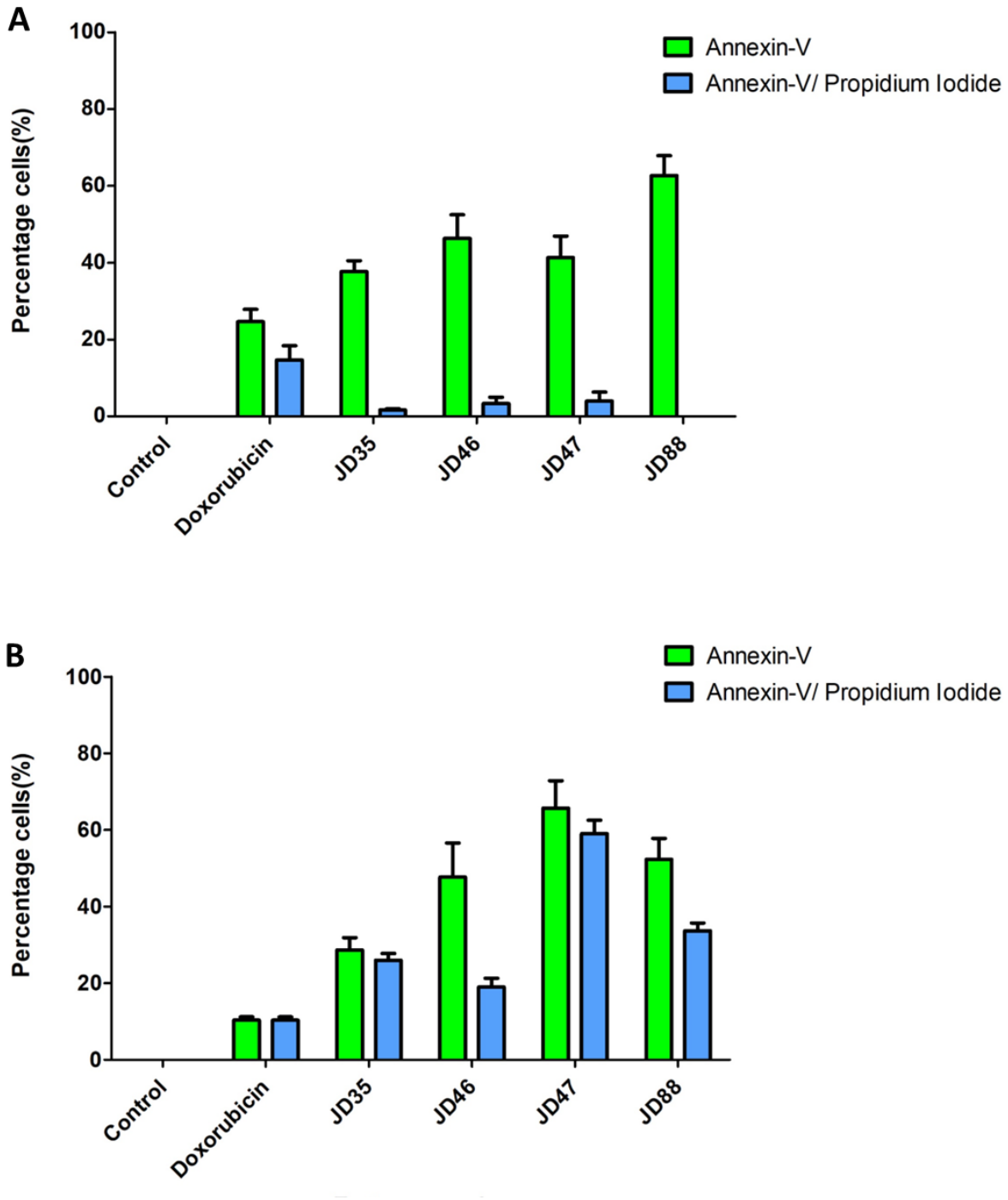

Figure 3.7 Average percentage of A549 cells positive for Annexin-V and PI after a 6 and 18 hours exposure to copper-imidazo[1,2-*a*]pyridines. A) 6 hours post-exposure B) 18 hours post-exposure. A549 cells were exposed to 10 µM of JD35, 7 µM of JD46, 4 µM of JD47, 4 µM of JD88, and 10 µM of doxorubicin. Each bar represents the mean ± SEM of values obtained from three independent experiments.

3.5 The effect of copper-imidazo[1,2-*a*]pyridines and doxorubicin on the activation of caspase-3/7 in A549 cancer cells

The caspases-3 and -7 are effector caspases whose activation is essential for apoptosis. Caspase 3/7 was measured in A549 cells at 24- and 48-hours following treatment with the copper complexes and doxorubicin using the Abcam's Fluorometric Caspase-3/7 Assay Kit (Ab39383) as described in Section 2.7 of the methodology. The results are presented in Figures 3.8 and 3.9.

Active caspase 3/7 was not observed in the untreated control cells at 24 and 48 hours (Figure 3.8, panels a-d). In cells treated with doxorubicin, the presence of active caspase 3/7 was detected after 24 hours and this increased at 48 hours where close to 100% of cells were positive (Figure 3.8, panel f and h). JD35-treated cells showed a similar effect (Figure 3.8, panel j-l). Cells treated with JD46 showed a rounded appearance at 24 hours with accompanying activation of caspase-3/7 (Figure 3.8, panel m-n). At 48 hours after treatment with JD46, the cells were enlarged (Figure 3.8, panel o) with no caspase-3/7 activity in the large cells (Figure 3.8, panel p). JD47 and JD88 treated cells showed rounded cells at 24 hours with accompanying caspase-3/7 activity (Figure 3.8, panel q-r; u-v), at 48 hours there were more damaged cells all showing increased caspase-3/7 activity (Figure 3.8, panel s-t; w-x).

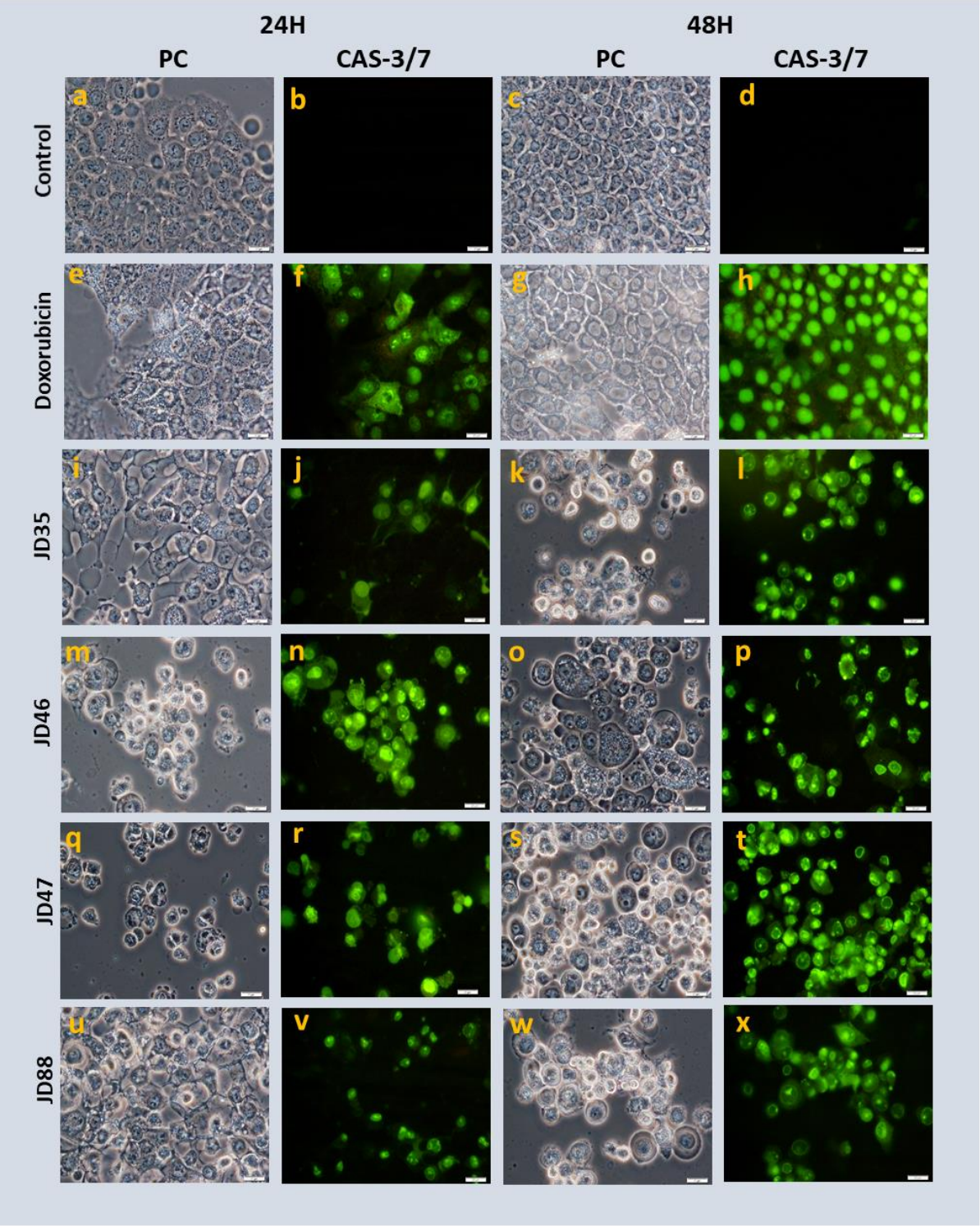

Figure 3.8 Photomicrographs of A549 cells showing active caspase-3/7 after treatment with copper-imidazo[1,2-*a*]pyridines and doxorubicin. A549 cells were treated with 11 µM of JD35, 7 µM of JD46, 4 µM of JD47, 4 µM of JD88 and 10 µM of doxorubicin for 6 and 18 hours observed using the Olympus BX41microscope with the U-MNIBA3 filter cube and images captured with the Olympus DP72 camera. Magnification: 400 X, scalebar: 20µm.

Figure 3.9 shows the average percentage of cells positive for caspase-3/7 activity obtained from three independent experiments 24 and 48 hours after treatment with the copper-imidazo[1,2-*a*] pyridines and doxorubicin. There was no caspase-3/7 activity detected in the untreated control cells at 24 and 48 hours. In cells treated with doxorubicin, 50% of the treated cells displayed an increase in caspase-3/7 activity at 24 hours, increasing to 60% at 48 hours. JD35-treated cells showed 22% of cells positive for caspase-3/7 after 24 hours, increasing to 80% at 48 hours. In cells treated with JD46, 80% were positive at 24 hours and 90% at 48 hours. JD47-treated cells showed a 65% increase at 24 hours and 85% at 48 hours. In cells treated with JD88, 30% of cells indicated caspase-3/7 activity at 24 hours, which increased to 80% at 48 hours. This data indicated the late activation of caspase-3/7 by all the copper-imidazo[1,2-*a*] pyridines and confirmed apoptotic cell death.

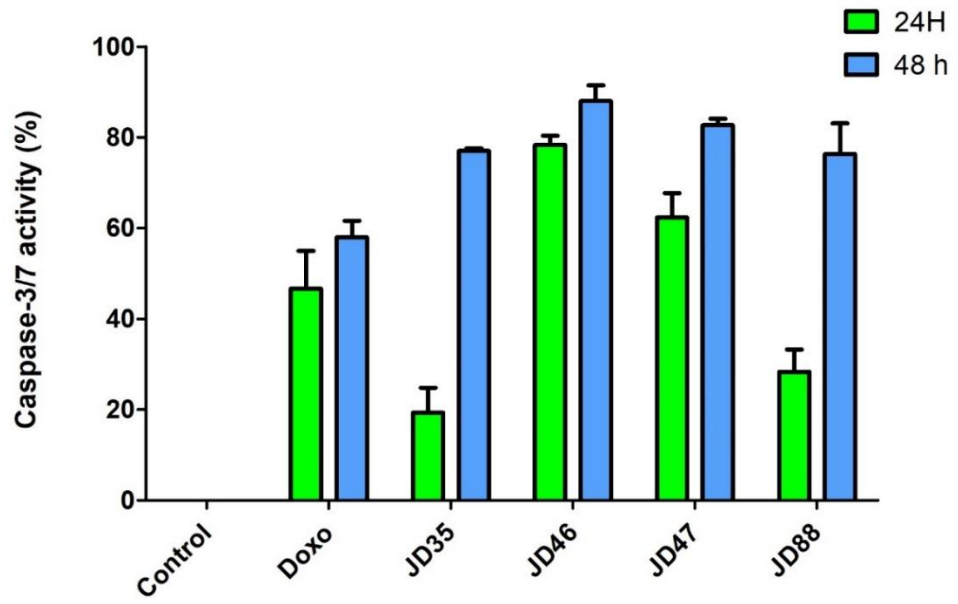

Figure 3.9 Average percentage of A549 cells positive for caspase-3/7 activity after a 24 and 48 hours exposure to copper-imidazo[1,2-*a*]pyridines. A549 cells were treated with 10 µM of JD35, 7 µM of JD46, 4 µM of JD47, 4 µM of JD88 and 10 µM of doxorubicin for 24 and 48 hours.Each bar represents the mean ± SEM of values obtained in duplicate from three independent experiments

3.6 The effect of the copper-imidazo[1,2-a]pyridines and doxorubicin on caspase-8 activity in A549 lung cancer cells

This study investigated activation of the extrinsic apoptosis pathway by evaluating caspase-8 activity using the Abcam Caspase-8 (active) FITC Staining Kit (ab65618) as described in Section 2.8. A549 cells were exposed to the copper complexes and doxorubicin for 24 and 48 hours, and the results of three independent experiments are presented in Figures 3.10 and 3.11

Caspase-8 activity was not detected in the untreated control cells (Figure 3.10, panels a-d). In cells treated with doxorubicin, the red fluorescence indicating caspase-8 activity was detected at 24 and 48 hours respectively (Figure 3.10 panels f and h). Since doxorubicin has an innate red fluorescence and localises to the nucleus, the fluorescence detected can be attributed to caspase-8 detection, as the fluorescence was not localised in the nucleus as regularly observed in cells treated with doxorubicin. For cells treated with JD35, JD47, and JD88 (Figure 3.10, panels j, r, v), caspase-8 activity was evident at 24 hours and displayed a noticeable increase by 48 hours (Figure 3.10, panels l, t, x). Conversely, in JD46-treated cells (Figure 3.10, panels m-p), caspase-8 activity was observed consistently at 24 and 48 hours. The phase-contrast images supported these findings, showing that cells presenting a positive caspase-8 signal appeared compromised. Conversely, cells appearing intact displayed a weaker or no caspase-8 signal.

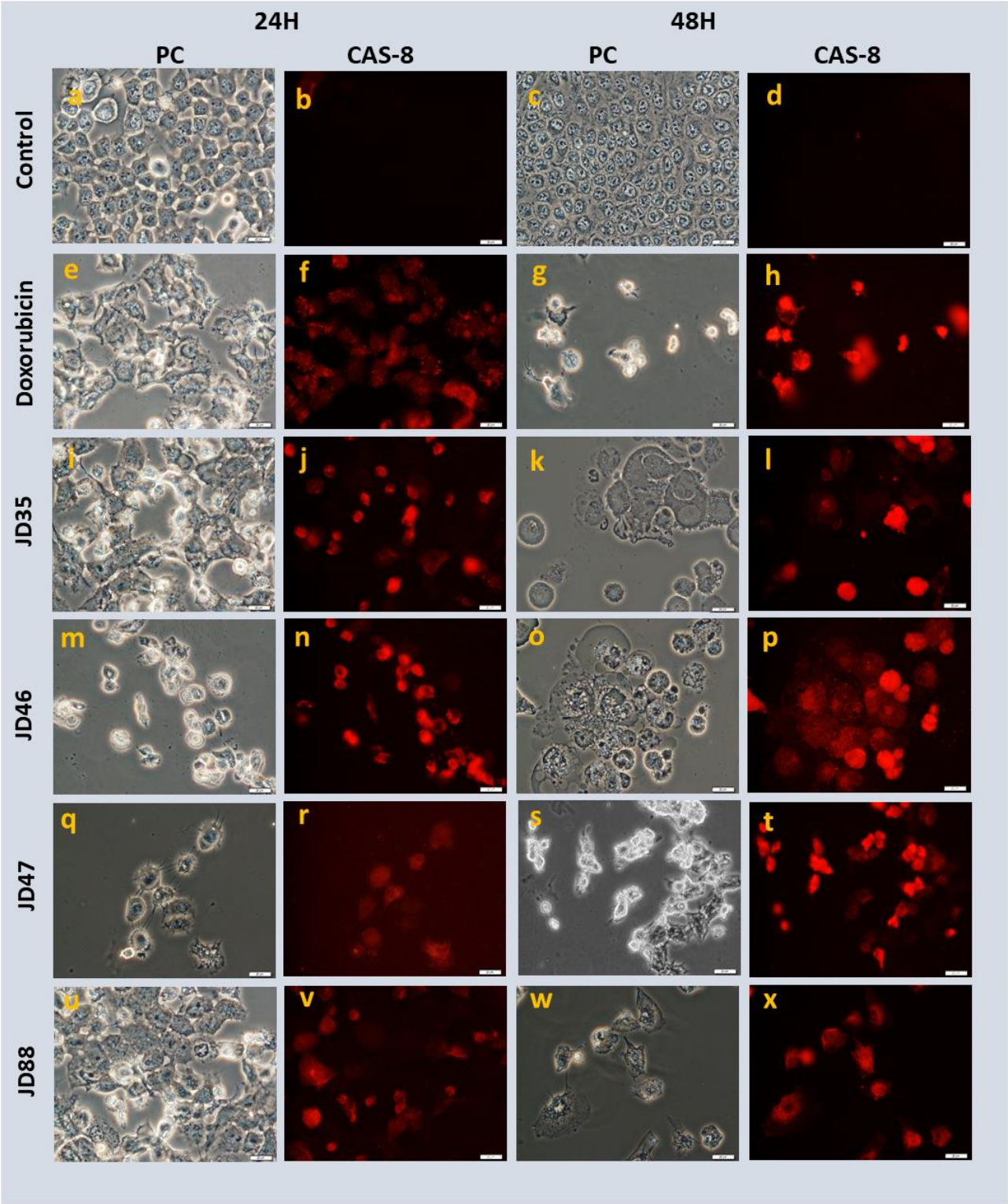

Figure 3.10 Photomicrographs of A549 cells displaying the activity of caspase-8 in A549 cells after treatment with copper-imidazo[1,2-*a*]pyridines and doxorubicin. A549 cells were treated with 11 µM of JD35, 7 µM of JD46, 4 µM of JD47, 4 µM of JD88, and 4 µM of doxorubicin for 24 and 48 hours and were viewed with the Olympus BX41 microscope using the Olympus U-MWIG2 filter cube and imaged with the Olympus DP72 camera. Magnification: 400 X, scalebar: 20µm.

The Olympus CellSens software was used to calculate the percentage of cells showing caspase-8 activity in three independent experiments (Figure 3.11). The untreated control cells did not show any caspase-8 activation. At 24 hours post-treatment, cells exposed to doxorubicin demonstrated caspase-8 activation in 80% of the cell population, which increased to 90% at 48 hours. Caspase-8 activity was seen in 55% of JD35-treated cells at 24 hours and in 65% of these cells at 48 hours. In the JD46-treated group, 65% of cells showed caspase-8 activation at 24 hours, increasing to 75% at 48 hours. For the JD47-treated cells, 57% displayed caspase-8 activation at 24 hours, with the percentage rising to 80% at 48 hours. In the cells treated with JD88, caspase-8 activation was apparent in 35% of cells at 24 hours and 75% at 48 hours.

Thus, at 24 hours, caspase-8 activation was highest in cells treated with doxorubicin, followed by JD35, JD46, and JD47, with the lowest activation in JD88-treated cells. At 48 hours, all test compounds increased caspase-8 activity, with activity levels ranging between 65% and 80%. Doxorubicin was consistently the most potent activator of caspase-8 at both time points, demonstrating over 80% cell positivity for active caspase-8. These results suggest that each test compound can induce caspase-8 activation at 24- and 48-hours post-treatment.

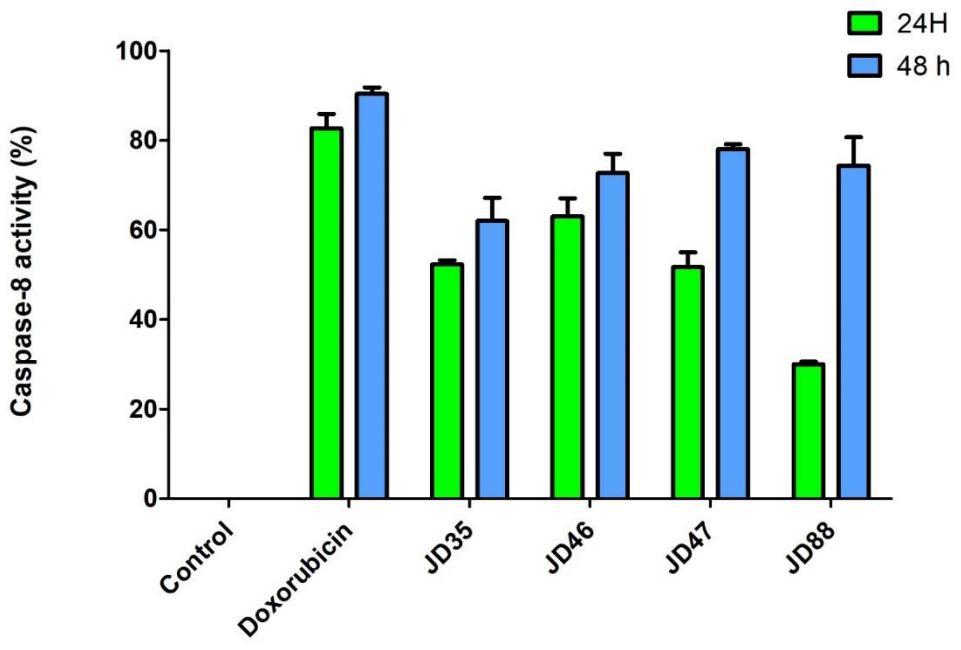

Figure 3.11 Average percentage of A549 cells positive for caspase-3/7 activity after a 24 and 48 hour treatment with copper-imidazo[1,2-*a*]pyridines and doxorubicin. A549 cells were treated with 10 µM of JD35, 7 µM of JD46, 4 µM of JD47, 4 µM of JD88 and 10 µM of doxorubicin for 24 and 48 hours. Each bar represents the mean ± SEM of values obtained in duplicate from three independent experiments.

3.7 The effect of copper-imidazo[1,2-*a*]pyridines on mitochondrial membrane potential in A549 lung cancer cells

Mitochondrial membrane potential (MMP) disruption is associated with the onset of intrinsic apoptosis. The effects of the copper complexes and doxorubicin on the mitochondrial membrane potential were evaluated in A549 cells using the JC1-dye as described in Section 2.9 of the methodology. The results are shown in Figures 3.12 and 3.13.

Figure 3.12 presents photomicrographs of cells subjected to the different test compounds captured at 12- and 18-hours post-treatment. In the untreated control cells (panels a-d), red-orange fluorescence in the perinuclear region indicated the accumulation of JC-1 aggregates in the mitochondria, demonstrating a high mitochondrial membrane potential and undamaged mitochondria. Red-orange and green fluorescence were observed in the doxorubicin-treated cells (panel f and panel h), suggesting a partial loss of MMP. A diffuse green fluorescence (panels j-l) and granular green fluorescence (panels n-r) were seen in the perinuclear region of cells treated with JD35, JD46, JD47, and JD88 at 12 hours, indicating a decrease in MMP. At 18 hours, cells treated with these copper complexes showed predominantly green fluorescence, indicating low membrane potential and disrupted mitochondrial function. Notably, JD88-treated cells had the largest proportion showing predominantly green fluorescence (panels u-x), suggesting a significant loss in MMP.

Figure 3.13 A and B present the calculated percentages of cells with either JC-1 monomers or aggregates following treatment with the compounds. At 12 hours post-treatment, cells treated with JD35 and JD88 showed the greatest loss in MMP, with over 60% of cells having the JC-1 monomers. At 18 hours, all test compounds showed a high percentage of cells (90%) with JC-1 monomers, indicating a significant decrease in MMP and suggesting the activation of the intrinsic apoptotic pathway. The presence of green fluorescence only and the absence of yellow-orange/red fluorescence, confirm a significant loss of MMP for all test compounds.

These results, presented in Figures 3.12 and 3.13, provide further evidence supporting the ability of the copper complexes to induce apoptotic cell death, likely through the intrinsic pathway, by disrupting the mitochondrial membrane potential.

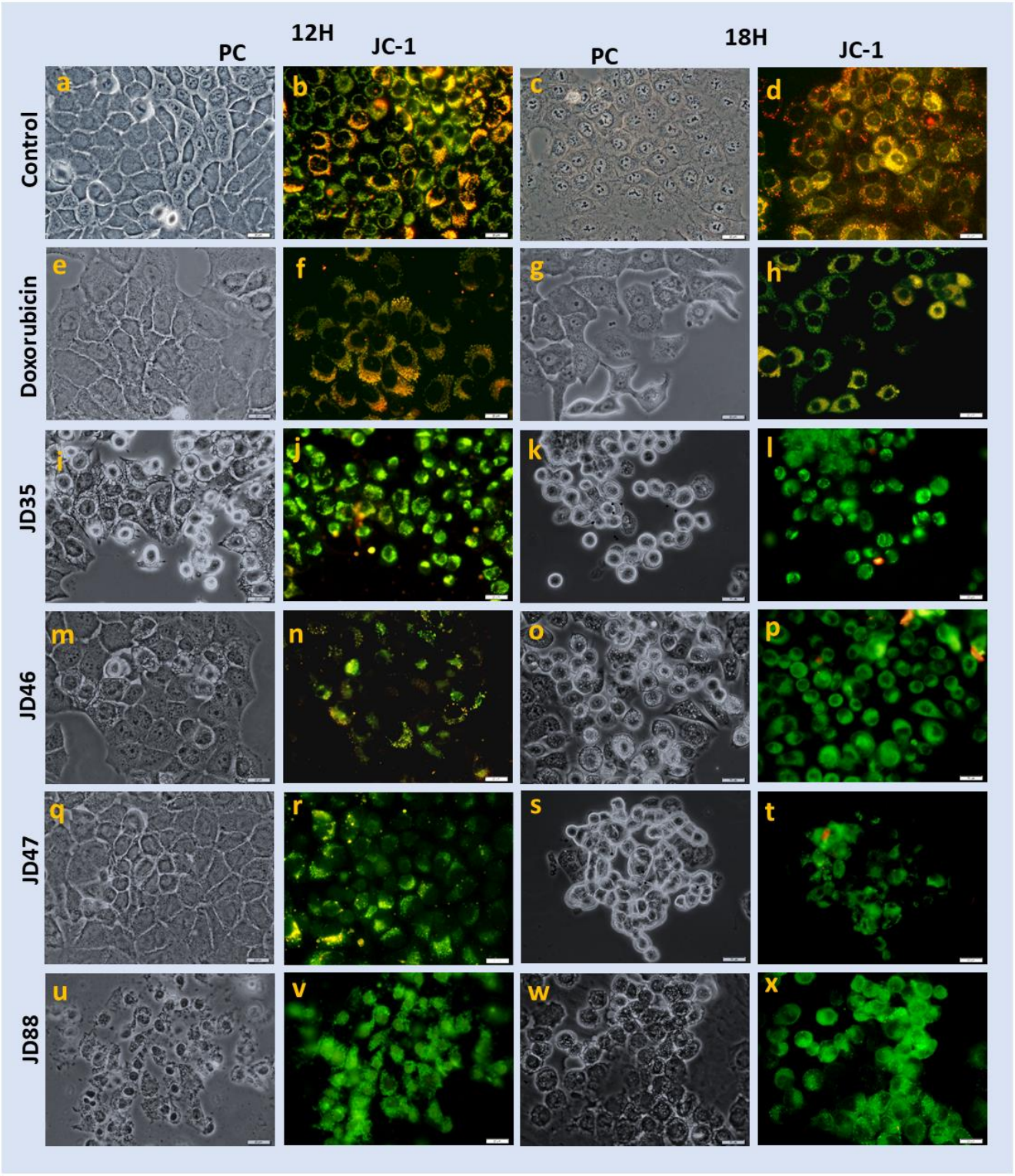

Figure 3.12 Photomicrographs showing the change in mitochondrial membrane potential of A549 cells after treatment with copper-imidazo[1,2-*a*]pyridines and doxorubicin. A549 cells were treated with 10 µM of JD35, 7 µM of JD46, 4 µM of JD47, 4 µM of JD88 and 10 µM of doxorubicin for 12 and 18 hours. Slides were observed with the Olympus BX41microscope with the U-MNIBA3 filter cube, and images captured with the Olympus DP72 camera and analysed using the Olympus CellSens software package. Magnification: 400 X, scalebar: 20µm.

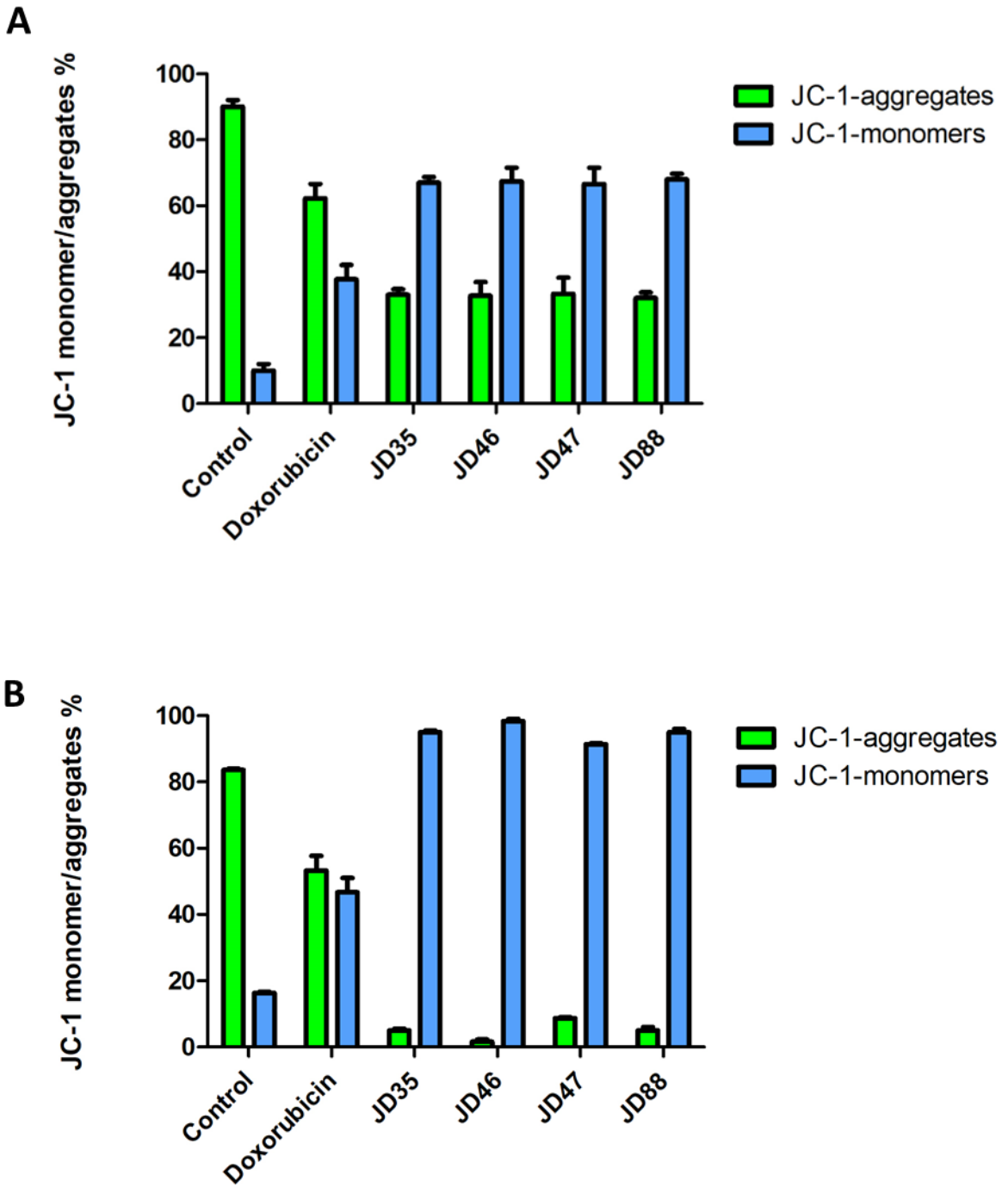

Figure 3.13 The effect of copper-imidazo[1,2-*a*]pyridines on the mitochondrial membrane potential of A549 cells (A)12 hours and (B) 18 hours post treatment. A549 cells were treated with with 10 µM of JD35, 7 µM of JD46, 4 µM of JD47, 4 µM of JD88 and 10 µM of doxorubicin for 12 and 18 hours. Magnification: 400 X, scalebar: 20µm . Each bar represents the mean ± SEM of percentages.

3.8 Immunohistochemistry analysis of p21 and p53 expression in A549 cells post-treatment with copper-imidazo[1,2-a]pyridines and doxorubicin

Following the assessment of apoptotic markers, the impact of copper-imidazo[1,2-a]pyridine complexes on cell cycle regulation was assessed. This assessment centred on the expression levels of the pivotal cell cycle proteins, p21 and p53. These proteins play a significant role in the cell cycle, acting as tumour suppressors by regulating cell cycle progression and mediating the cellular response to DNA damage.

This study segment examined the influence of the active copper-imidazo[1,2-*a*]pyridine complexes on regulating these crucial proteins. The A549 cells, post-treatment with these complexes and doxorubicin at their respective IC_{80} values for a duration of 20 hours. The treatment duration was extended to 20 hours for this set of experiments to ensure that the cells had sufficient exposure to the test compounds to allow for any delayed effects on the expression of p21 and p53 to manifest.

Post-treatment, the cells were examined using immunohistochemistry assays with anti-p21 and anti-p53 antibodies as outlined in Section 2.10. This technique provides a visual and quantitative assessment of p21 and p53 expression and localization within the cells, thereby granting insights into the role of the tested compounds in cell cycle control and their potential mechanisms of action in inducing cell death.

3.8.1 The immunohistochemistry effects of copper-imidazo[1,2-*a*]pyridines and doxorubicin on p21 expression

The nuclear localisation of p21 is often associated with DNA damage, whereas its cytoplasmic presence generally denotes the loss of cell cycle inhibitory effects and prevention of apoptosis (Karimian *et al.*, 2016). The examination of p21 protein expression and distribution in A549 cells after treatment with copper-imidazo[1,2-*a*]pyridines, JD35, JD46, JD47, and JD88, and doxorubicin at their IC_{80} values for 20 hours was conducted using immunofluorescence microscopy. Figure 3.14 and Table 3.2 present these results.

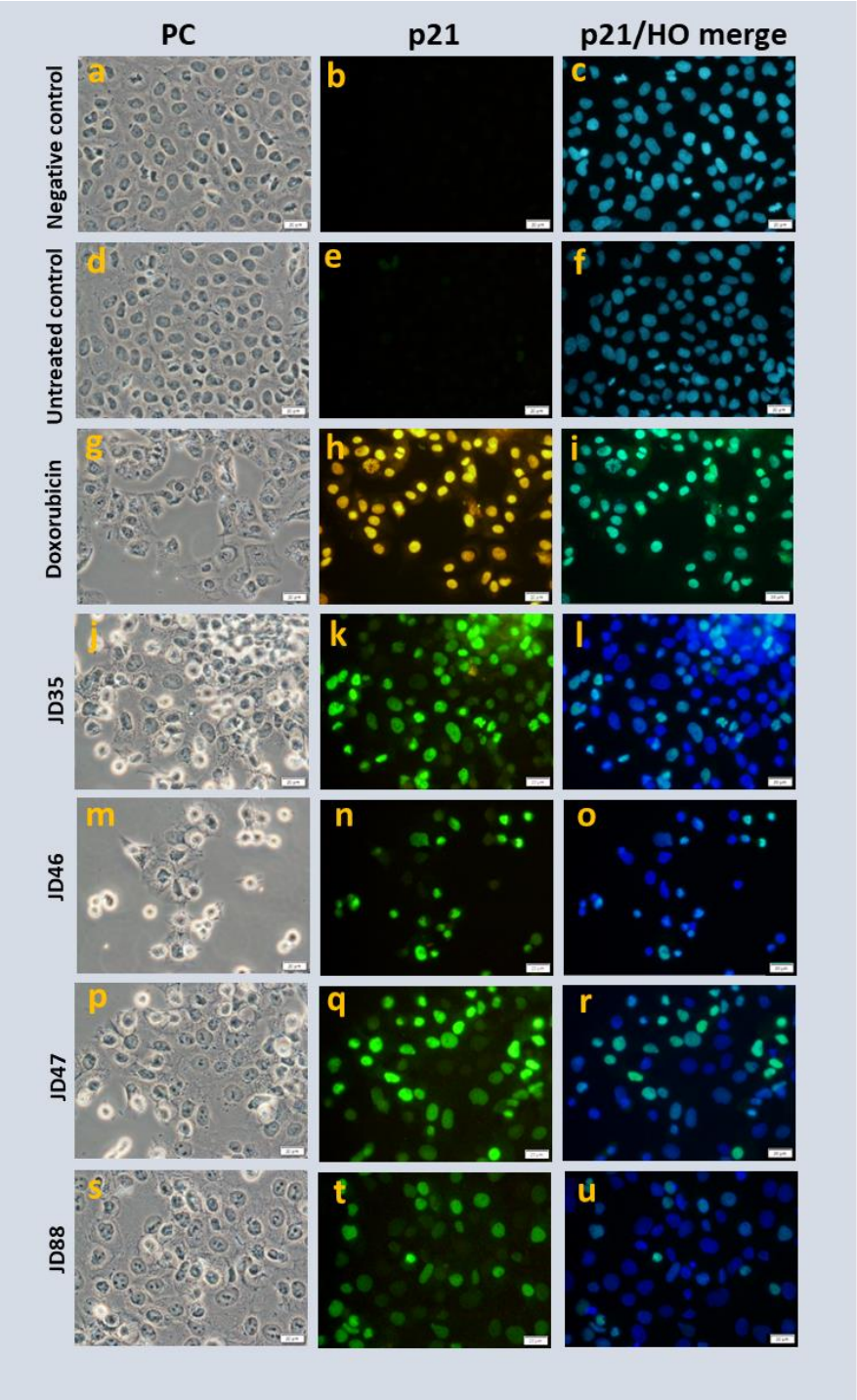

Figure 3.14 Photomicrographs showing p21 expression in A549 lung cancer cells post-treatment with copper-imidazo[1,2-*a*]pyridines and doxorubicin. A549 cells were treated with 10 µM of JD35, 7 µM of JD46, 4 µM of JD47, 4 µM of JD88, and 10 µM of doxorubicin for a duration of 20 hours. The detection of p21 expression was performed employing immunofluorescence. The cellular nuclei were counterstained using HO. Observation of cells was conducted with an Olympus BX41 epifluorescence microscope at a 400× magnification, deploying U-MWU2 and U-MNIB3 filter cubes. and images were captured with an Olympus Dp72 camera. Further processing was achieved using the Olympus CellSens software package. Scale bar: 20 µm.

Table 3.2 Quantitative representation of the percentage of A549 cells exhibiting nuclear p21 expression following a 20-hour exposure to copper-imidazo[1,2-*a*]pyridines and doxorubicin. The table categorises cells based on the intensity of the p21 signal observed. These experiments were performed in duplicate to validate the consistency of the results.

Complexes	**% cells with p21 signal**	**% cells with a high-intensity p21 signal**	**% cells with a low-intensity p21 signal**
Untreated control	2%	0%	2%
Doxorubicin	91%	59%	32%
JD35	58%	33%	25%
JD46	55%	33%	22%
JD47	46%	26%	20%
JD88	35%	20%	15%

Figure 3.14 and Table 3.2 illustrate the copper complexes' induction of nuclear p21 expression, with varying intensities observed across the treated cells. In Figure 3.14, panels b, e, h, k, n, q, and t demonstrate p21 expression, while panels c, f, l, o, r, and u exhibit merged images of p21 expression with HO. In these panels, it is observed that the bright blue stain of the nucleus from the HO stain and the green p21 fluorescence of the cells overlap accurately to produce a darker blue colour. This suggests the nuclear localization of p21. The negative control (panel a-c), lacking the primary antibody, showed no signal, thus validating the results observed, while untreated control cells displayed minimal p21 expression (less than 2%).

Doxorubicin-treated cells (Figure 3.14, panels g-h) showed a pronounced yellow/green p21 signal, likely due to the nuclear co-localization of p21 and doxorubicin, which has an innate red fluorescence. Compared to the untreated control, all test compounds enhanced nuclear p21 expression. Doxorubicin treatment resulted in p21 signals in 91% of the cells, with 59% showcasing high-intensity and 32% showing lower-intensity signals. JD35 treatment showed a 58% p21 signal, with 33% high-intensity and 25% lower-intensity staining. JD46 led to a 55% p21 signal, with 33% high-intensity and 22% lower-intensity. JD47 resulted in p21 signals in 46% of cells, with 26% high-intensity and 20% lower-intensity. JD88 yielded the lowest p21 expression at 35%, with 20% high-intensity and 15% lower-intensity signals.

Moreover, a relationship was identified between cells demonstrating morphological alterations suggestive of cellular distress (e.g., detachment, rounding) and pronounced p21 intensity

(panels j, m, p). Taken together, doxorubicin elicited the highest percentage of high-intensity p21 staining, while JD88 showed the lowest percentage of p21 among the tested compounds.

3.8.2 The immunohistochemistry effects of copper-imidazo[1,2-*a*]pyridines and doxorubicin on p53 expression in A549 cells

In this investigation, the impact of novel copper-imidazo,2-a]pyridines (JD35, JD46, JD47, and JD88) on the expression and localization of the p53 tumour suppressor protein in A549 lung cancer cells was assessed using immunohistochemistry assays with anti-p53 antibody. The p53 protein plays a critical role in regulating cell cycle arrest, DNA repair, and apoptosis in response to various cellular stresses (Ozaki and Nakagawara, 2011). The immunofluorescence images obtained in this study are represented in Figure 3.15 and summarized in Table 3.3.

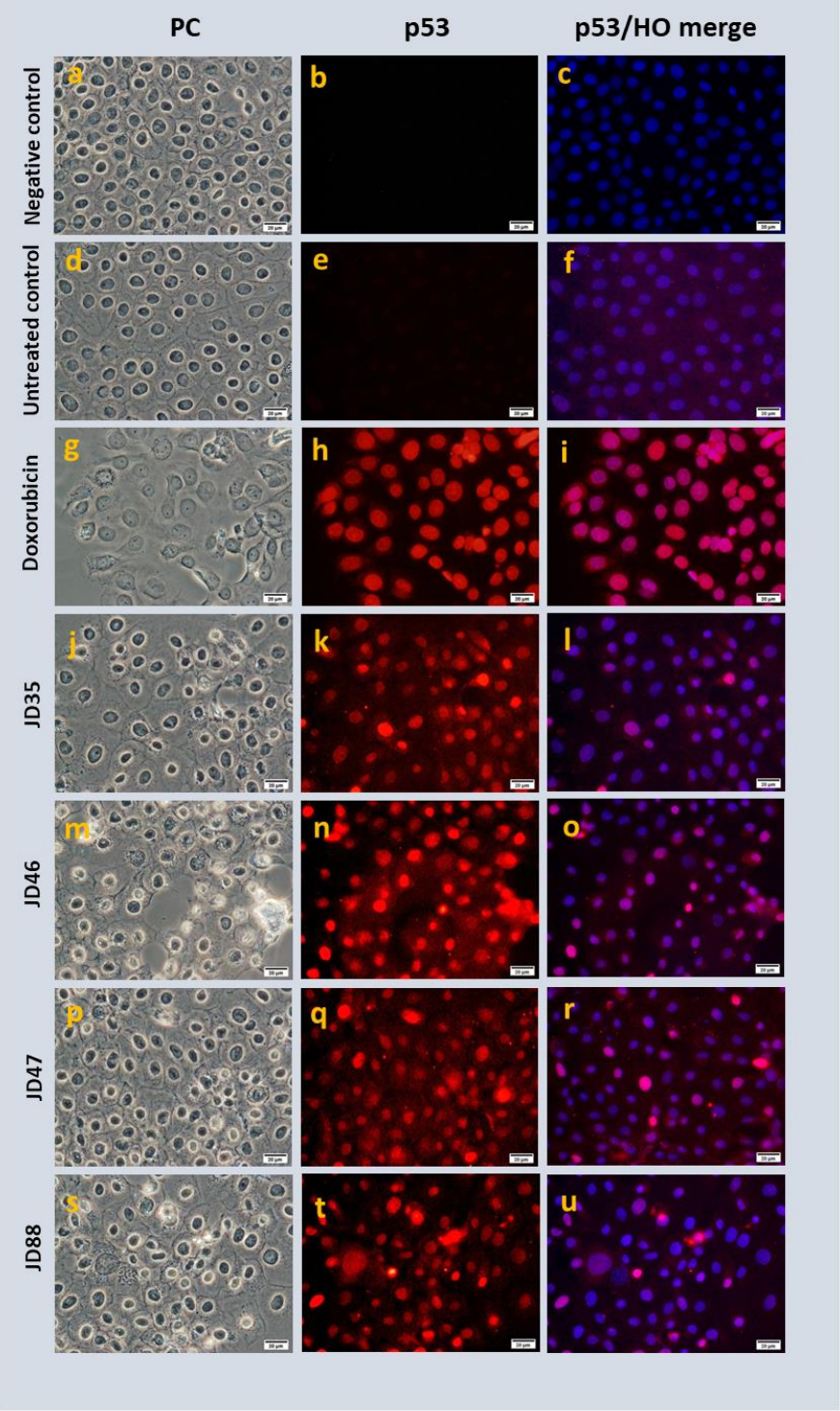

Figure 3.15 Photomicrographs showing p53 expression in A549 lung cancer cells post-treatment with copper-imidazo[1,2-*a*]pyridines and doxorubicin. A549 cells were treated with 10 µM of JD35, 7 µM of JD46, 4 µM of JD47, 4 µM of JD88, and 10 µM of doxorubicin for 20 hours. The detection of p53 expression was performed employing immunofluorescence. The cellular nuclei were counterstained using HO. Observation of cells was conducted with an Olympus BX41 epifluorescence microscope at 400× magnification, deploying U-MWG2 and U-MNIB3 filter cubes. Images were captured with an Olympus Dp72 camera. Further processing was achieved using the Olympus CellSens software package. Scale bar: 20 µm.

Table 3.3 Quantitative representation of the percentage of A549 cells demonstrating p53 expression after a 20-hour treatment with copper-imidazo[1,2-*a*]pyridines and doxorubicin. The table categorises cells based on the observed intensity of the p53 signal. Experiments were conducted in duplicate to ensure the reliability and reproducibility of the findings.

Complexes	% p53 signal	% high intensity p53 signal	% low intensity p53 signal
Untreated control	5%	0%	5%
Doxorubicin	100%	100%	0%
JD35	79%	23%	56%
JD46	87%	44%	43%
JD47	64%	20%	44%
JD88	87%	29%	58%

Figure 3.15, panels b, e, h, k, n, q, and t demonstrate p53 expression, while panels c, f, i, l, o, r, and u show merged images of p53 expression with HO stain. In these panels it can be observed that the bright blue stain of the nucleus from the HO stain and the red p53 fluorescence of the treated cells overlap accurately to produce a bright purple colour in lower intensity signals and a violet colour in higher intensity signals. This suggests the nuclear localization of p53. The antibody-negative control (panels a-c) confirmed the specificity of the p53 signal observed, while the antibody-positive untreated control (panels d-f) suggested low cytoplasmic p53 levels and potential nuclear presence. Doxorubicin treatment (panels g-i) resulted in a vivid nuclear p53 signal in all cells, although the drug's contribution to this fluorescence should be considered given its innate red fluorescence.

Treatment with JD35 (panels j-l) led to nuclear p53 signals in 79% of cells, with 23% showing high-intensity signals. JD46 treatment (panels m-o) resulted in nuclear p53 expression in 87% of cells, with an almost equal distribution between high- and low-intensity signals. For JD47 (panels p-r), 64% of cells displayed nuclear p53 expression, with a predominance of low-intensity signals. Finally, JD88 treatment (panels s-u) caused nuclear p53 signals in 87% of cells, with most exhibiting low-intensity signals. The phase contrast micrographs in panels j, m, p, and s suggest that cells with significant cellular damage tend to display brighter fluorescence signals.

All the copper-imidazo[1,2-*a*]pyridines influenced the expression of p53 in A549 cells, this p53 signal aligned with the HO stain of the nucleus, suggesting nuclear localisation of

p53.Specifically, the antibody used in this study was sensitive to p53 phosphorylated at S15. JD46 and JD88 treatments resulted in pronounced p53 signals. However, the distinction in p53 expression across different treatments was subtle, suggesting that all copper complexes had some level of influence on p53 expression.

3.9 The effect of JD88 and doxorubicin on the apoptotic proteome profile of A549 cells

Apoptosis is a regulated cellular mechanism that governs cell death, involving an intricate interplay of proteins and enzymes central to its initiation, regulation, and execution. Analysing the expression of these proteins in cells subjected to cytotoxic agents gives insight into the changes in the apoptotic protein levels leading up to cell death.

This study evaluated the modification in the apoptotic proteome profile of A549 lung cancer cells after exposure to the highly active copper complex, JD88, and the standard chemotherapy drug, doxorubicin. The Proteome Profiler Human Apoptosis Array Kit (R&D Systems) was used to detect these modifications, as delineated in Section 2.12. The resulting data are illustrated in Figures 3.16 through 3.26. Table 3.4 delineates the coordinates coupled with protein identities. Meanwhile, Table 3.5 offers a grading metric for categorising the baseline protein expression levels, derived from pixel density values. Furthermore, Table 3.6 illustrates the percentage deviation in protein expression compared to the untreated control for JD88 and doxorubicin.

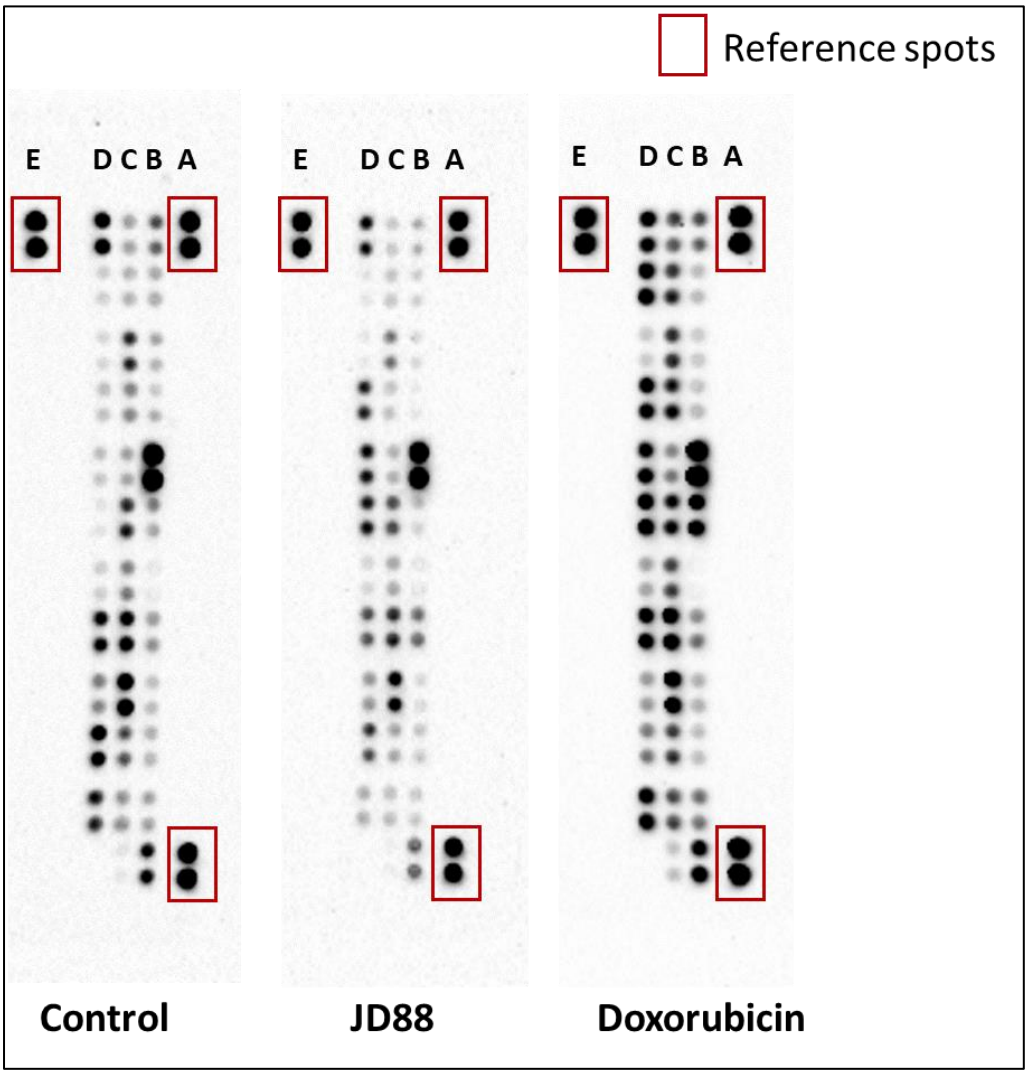

Figure 3.16 Chemiluminescent signals on nitrocellulose membrane arrays indicating the expression levels of apoptosis-related proteins in A549 cells. Cells were subjected to an 18-hour treatment with 4 µM of JD88 and 4 µM of doxorubicin. The membrane was incubated with a cell lysate containing 400 µg of protein. The resulting chemiluminescent images were documented using the BIO-RAD ChemiDoc™ MP Imager. Proteins are represented in duplicate across lanes A to E, with reference spots highlighted in red. (Specific protein coordinates are reported in Table 3.4.)

Table 3.4 Coordinates for Human Apoptosis Array. This table lists the coordinates corresponding to various apoptotic regulatory proteins within the human apoptosis array used in this study.

Coordinate	Target/Control	Coodinate	Target/Control
A1, A2	Reference Spots	C13, C14	HO-2/HMOX2
A23, A24	Reference Spots	C15, C16	HSP27
B1, B2	Bad	C17, C18	HSP60
B3, B4	Bax	C19, C20	HSP70
B5, B6	Bcl-2	C21, C22	HTRA2/Omi
B7, B8	Bcl-x	C23, C24	Livin
B9, B10	Pro-Caspase-3	D1, D2	PON2
B11, B12	Cleaved Caspase-3	D3, D4	p21/CIP1/CDKN1A
B13, B14	Catalase	D5, D6	p27/Kip1
B15, B16	cIAP-1	D7, D8	Phospho-p53 (S15)
B17, B18	cIAP-2	D9, D10	Phospho-p53 (S46)
B19, B20	Claspin	D11, D12	Phospho-p53 (S392)
B21, B22	Clusterin	D13, D14	Phospho-Rad17 (S635)
B23, B24	Cytochrome c	D15, D16	SMAC/Diablo
C1, C2	TRAIL R1/DR4	D17, D18	Survivin
C3, C4	TRAIL R2/DR5	D19, D20	TNF RI/TNFRSF1A
C5, C6	FADD	D21, D22	XIAP
C7, C8	Fas/TNFRSF6/CD95	D23, D24	PBS (Negative Control)
C9, C10	HIF-1α	E1, E2	Reference Spots
C11, C12	HO-1/HMOX1/HSP32		

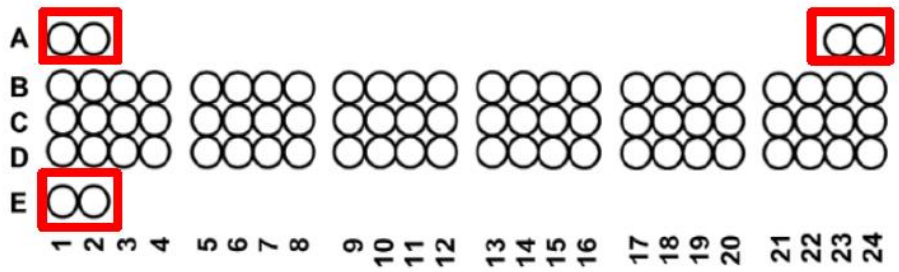

Figure 3.17 Depiction of the coordinates for proteins in the human apoptosis array. Each protein related to apoptosis is represented by two identical spots. Reference spots are highlighted in red

Table 3.5 The grading system based on pixel density that is used to classify different levels of protein expression.

Pixel density	Protein expression level
0 - 50 000	Very low
50 000 - 200 000	Low
200 000 - 400 000	Moderate
400 000 - 600 000	Moderately high
600 000 - 900 000	High
900 000 >	Very high

Table 3.6 Baseline expression levels of apoptotic regulatory proteins in A549 cells, accompanied by the relative percentage variation post-treatment. The table also delineates the statistical significance of these differences when compared with untreated A549 control cells.

Protein	Baseline expression level	JD88		Doxorubicin	
		% Change	Significance	% Change	Significance
Bad	moderate	-60	***	+33	**
Bax	low	-45	***	+20	***
Bcl-2	low	-43	***	+19	*
Bcl-x	low	-60	**	+61	**
Pro-Caspase-3	very high	+21	***	-7	**
Cleaved Caspase-3	moderate	-30	*	+449	***
Catalase	very low	+42	***	+13	*
cIAP-1	moderate	+49	**	+68	**
cIAP-2	low	-21	**	+67	***
Claspin	low	-29	***	+11	*
Clusterin	low	-32	***	+150	***
Cytochrome c	moderately high	-30	*	+101	***
TRAIL R1/DR4	low	-44	*	+170	***
TRAIL R2/DR5	low	-21	ns	+331	***
FADD	moderate	-35	***	+47	***
Fas/TNFRSF6/CD95	moderate	-45	*	+206	***
HIF-1α	moderate	-6	ns	+115	***
HO-1/HMOX1/HSP32	moderately high	-8	ns	+85	***
HO-2/HMOX2	moderate	-20	*	+113	***
HSP27	High	-20	*	+81	***
HSP60	very high	-35	***	+5	ns
HSP70	moderate	-35	**	+83	***
HTRA2/Omi	moderate	-34	*	+122	***
Livin	Very low	+21	**	+150	***
PON2	High	-41	***	+8	*
p21/CIP1/CDKN1A	low	-41	***	+888	***
p27/Kip1	low	-20	**	+80	***
Phospho-p53 (S15)	low	+225	***	+587	***
Phospho-p53 (S46)	low	+258	***	+563	***
Phospho-p53 (S392)	low	+415	***	+970	***
Phospho-Rad17 (S635)	low	-5	ns	+135	***
SMAC/Diablo	moderately high	-32	***	+88	***
Survivin	moderate	-26	***	-4	ns
TNF RI/TNFRSF1A	High	-55	***	-53	***
XIAP	moderately high	-62	***	91	***

The positive (+) sign shows increased protein expression, while the negative (-) sign indicates decreased protein expression. One-way ANOVA followed by the Dunnet's post-hoc comparisons test was performed, and analysis shows that ns is non-significant; *$p<0.05$ is poorly significant; **$p<0.01$ is moderately significant; and *** $p<0.001$ is highly significant.

3.9.1 Effect of JD88 and doxorubicin on the expression of phosphorylated p53 in A549 cells

The tumour suppressor protein, p53, orchestrates the regulation of numerous genes that stimulate apoptotic cell death. The phosphorylation of p53 at serine residues, specifically at positions 15, 46, and 392, is crucial for maintaining its stability (Siliciano *et al*., 1997).

Figure 3.18 and Table 3.6 depict the expression patterns of p53 in A549 lung cancer cells, where wild-type p53 is predominant. Phospho-p53 (S15) was poorly expressed in untreated control A549 cells. However, treatment with JD88 and doxorubicin significantly increased its expression by 225% and 587%, respectively. Baseline expression of Phospho-p53 (S46) was low, JD88 and doxorubicin caused a highly significant increase of 258% and 563%, respectively. Phospho-p53 (S392) was expressed at a low level in A549 control cells. JD88 caused a highly significant increase of 415%, and doxorubicin caused a highly significant increase of 970% of the protein in the treated cells relative to the control cells.

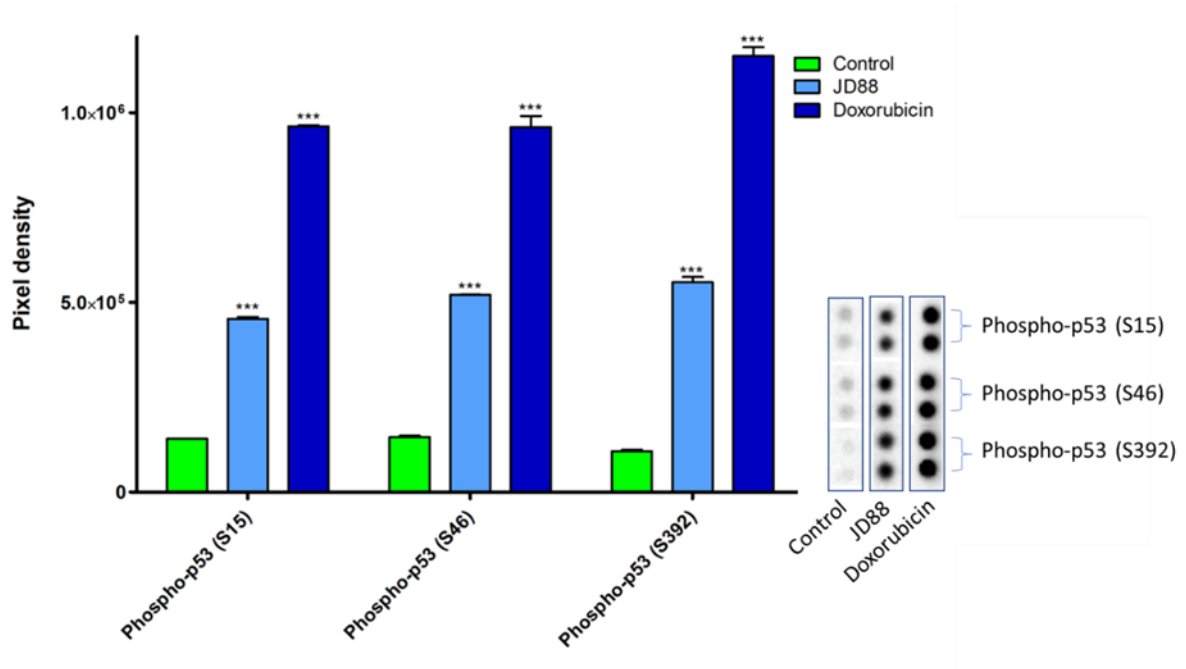

Figure 3.18 Effect of JD8 and doxorubicin on the expression of phosphorylated p53. A549 cells were treated with 4 µM of JD88 and 4 µM, of doxorubicin for 18 hours. Arrays were incubated with 400 µg of each cell lysate. Array data was analysed by one-way ANOVA ($p < 0.05$) followed by Dunnett's post-hoc comparison test. (NS; non-significant; *$p < 0.1$; is non-significant; **$p < 0.05$ = significant; ***$p < 0.01$ = highly significant).

3.9.2 Effect of JD88 and doxorubicin on the expression of p21 and p27

The expression profiles of p21 (Cip1) and p27 (Kip1), two cell cycle regulatory proteins, are demonstrated in Figure 3.19 following the treatment of A549 cells with JD88 and doxorubicin.

p21, with a low baseline expression in A549 control cells, decreased by 41% with high significance following JD88 treatment and increased 888% with high significance after treatment with doxorubicin. p27, with poor baseline expression in A549 control cells, had a significant decrease of 20% after JD88 treatment and a highly significant increase of 80% post-doxorubicin treatment.

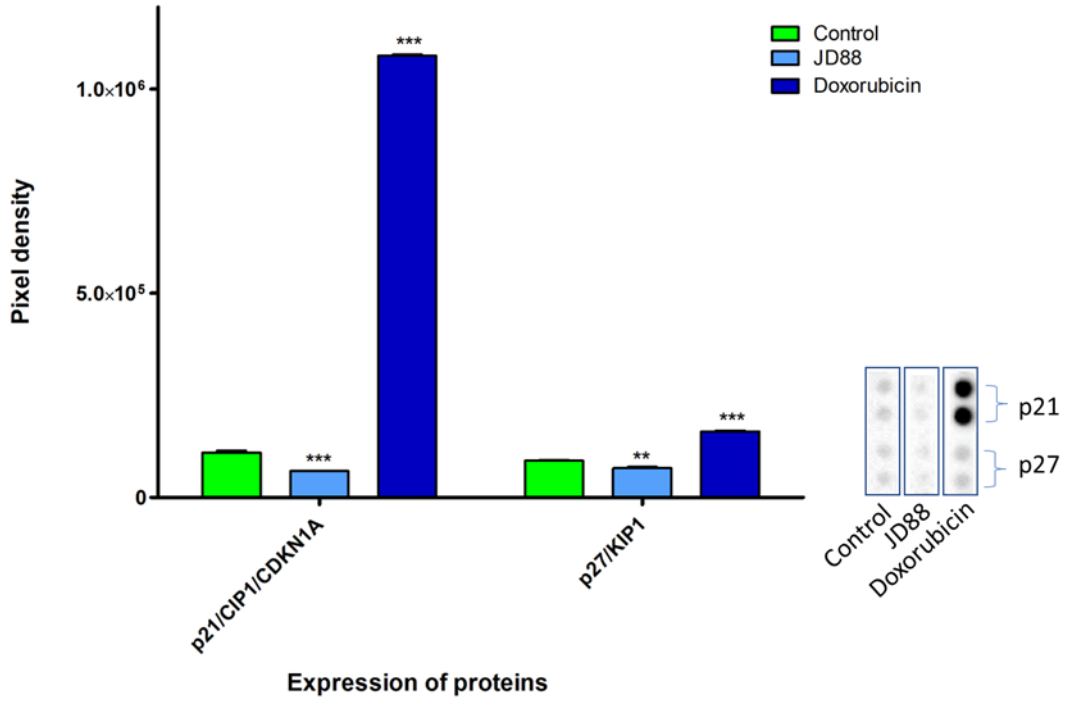

Figure 3.19 Effect of JD88 and doxorubicin on p21 and p27. A549 cells were treated with 4 µM of JD88 and 4 µM, of doxorubicin for 18 hours. Arrays were incubated with 400 µg of each cell lysate. Array data was analysed by one-way ANOVA ($p < 0.05$), followed by Dunnett's post-hoc comparison test. (NS; non-significant; *$p < 0.1$; is non-significant; **$p < 0.05$ = significant; ***$p < 0.01$ = highly significant.

3.9.3 Effect of JD88 and doxorubicin on BCL-2 family protein levels

The B-cell Lymphoma-2 (BCL-2) family proteins play pivotal roles in the regulation of programmed cell death, with members either promoting (Bad and Bax) or inhibiting apoptosis (Bcl-2 and Bcl-x). Figure 3.20 displays the influence of JD88 and doxorubicin on BCL-2 family protein expression in A549 cells.

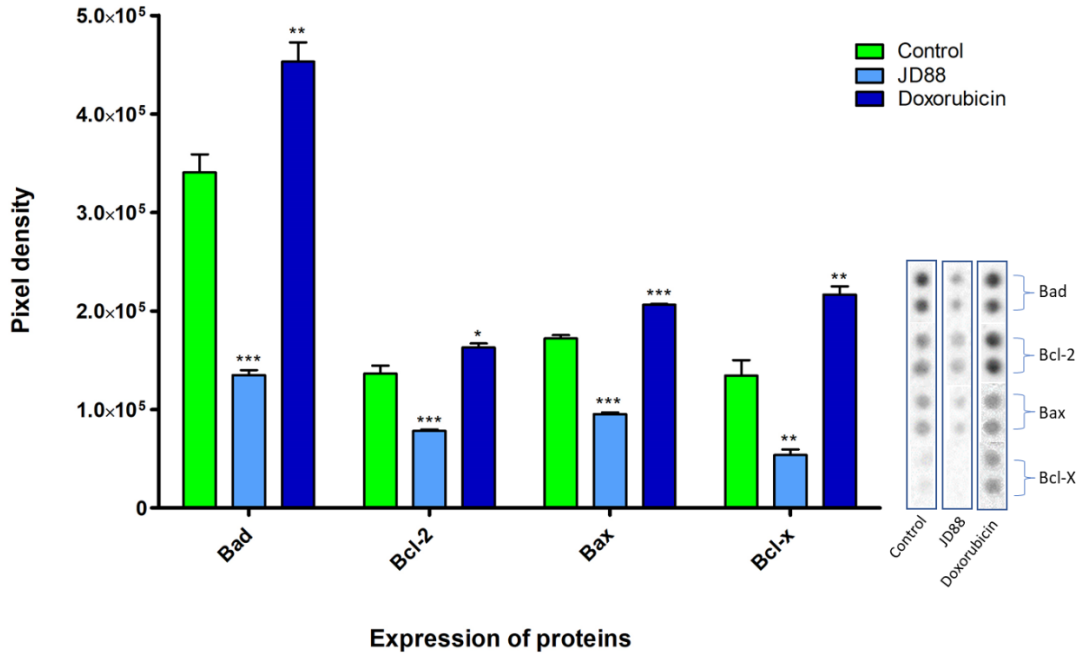

Figure 3.20 Effect of JD88 and doxorubicin on the expression of BCL-2 family proteins Bad, Bcl-2, Bax and Bcl-x. A549 cells were treated with 4 µM of JD88 and 4 µM, of doxoxorubicin for 18 h. Arrays were incubated with 400 µg of each cell lysate. Array data was analysed by one-way ANOVA ($p < 0.05$) followed by Dunnett's *post-hoc* comparison test. (NS; non-significant; *$p < 0.1$; is non-significant; **$p < 0.05$ = significant; ***$p < 0.01$ = highly significant).

The baseline expression for Bad protein was moderate in A549 control cells. Treatment with JD88 led to a significant decrease of 60%, while doxorubicin significantly increased its expression by 33% relative to control cells (Table 3.6; Figure 3.20).

The Bcl-2 protein, known to inhibit apoptosis by preserving mitochondrial membrane integrity, exhibited a low-level baseline expression in A549 control cells. Post-treatment with JD88, showed significant reduction in its levels by 43% and treatment with doxorubicin caused a poorly significant increase of 19%, as detailed in Table 3.6 and Figure 3.20

Bax, another member of this family with a role in the mitochondrial apoptotic process, presented with a low expression in control cells. Upon treatment, JD88 significantly decreased Bax levels by 45%, whereas doxorubicin significantly increased it by 20%, all represented in Table 3.6 and Figure 3.20.

Lastly, the Bcl-x protein, an inhibitor of apoptosis, initially displayed a low expression in A549 control cells. However, following treatment, JD88 led to a significant decrease of 60%, whereas

doxorubicin significantly increased the levels by 61%, as evidenced in Table 3.6 and Figure 3.20.

3.9.4 Effect of JD88 and doxorubicin on the expression of inhibitor of apoptosis proteins cIAP-1, cIAP-2, livin, survivin and XIAP

Members of the inhibitor of apoptosis (IAP) protein family are often overexpressed in cancer, affecting tumour cell survival, chemo-resistance, and disease progression (Silke and Meier, 2013). The impact of JD88 and doxorubicin on the expression of these proteins in A549 cells is shown in Table 3.6 and Figure 3.21.

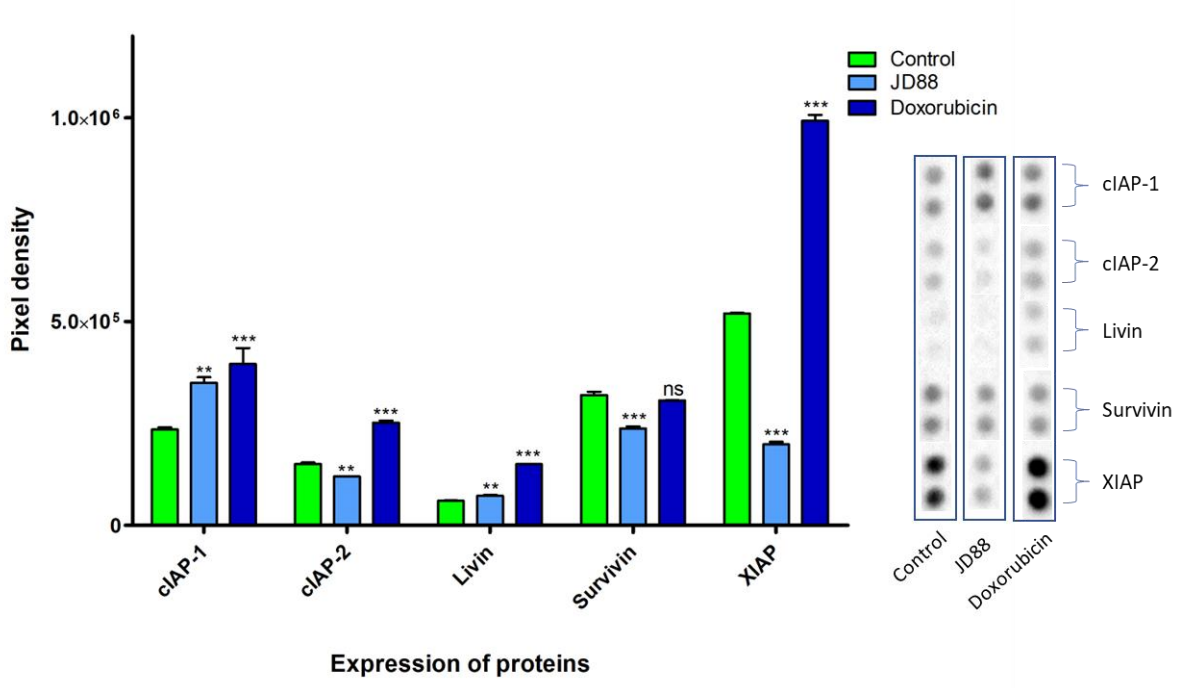

Figure 3.21 Effect of JD88 and doxorubicin on the expression of inhibitor of apoptosis proteins cIAP-1, cIAP-2, livin, survivin, and XIAP. A549 cells were treated with 4 µM of JD88 and 4 µM of doxorubicin for 18 hours. Arrays were incubated with 400 µg of each cell lysate. Array data was analysed by one-way ANOVA ($p < 0.05$) followed by Dunnett's post-hoc comparison test. (NS; non-significant; *$p < 0.1$= poorly significant; **$p < 0.05$ = significant; ***$p < 0.01$ = highly significant).

cIAP-1 had a moderate baseline expression in A549 control cells. After treatment with JD88, there was a significant increase of 49% in the protein level, while there was a significant increase of 68% in the protein level following treatment with doxorubicin. Similarly, cIAP-2 showed low expression in the A549 control cells. JD88 led to a 21% significant decrease in the protein level, while doxorubicin resulted in a 67% highly significant increase. Results are shown in Table 3.6 and Figure 3.21.

Survivin, moderately expressed in the A549 control cells, displayed a highly significant decrease of 26% with JD88 and a non-significant decrease of 4% with doxorubicin. These results are depicted in Table 3.6 and Figure 3.21.

For livin, which was present at low levels in the A549 control cells, JD88 and doxorubicin treatments resulted in a significant 21% and a highly significant 150% increases, respectively, as shown in Table 3.6 and Figure 3.21.

XIAP exhibited a moderately high baseline expression in control cells. Upon treatment, JD88 led to a significant 62% decrease, while doxorubicin resulted in a high 91% increase, as shown in Table 3.6 and Figure 3.21.

3.9.5 Effect of JD88 and doxorubicin on the expression of SMAC/Diablo and HTRA2/Omi

SMAC/Diablo and HTRA2/Omi are pro-apoptotic proteins. SMAC/Diablo showed a moderately high baseline expression in untreated A549 control cells. Upon treatment with JD88 and doxorubicin, the protein levels changed by a highly significant decrease of 32% and a highly significant increase of 88%, respectively. HTRA2/Omi, which had a moderate expression in control cells, had a 34% poorly significant decrease and a 122% highly significant increase post-treatment with JD88 and doxorubicin, respectively. These results are presented in Table 3.6 and Figure 3.22.

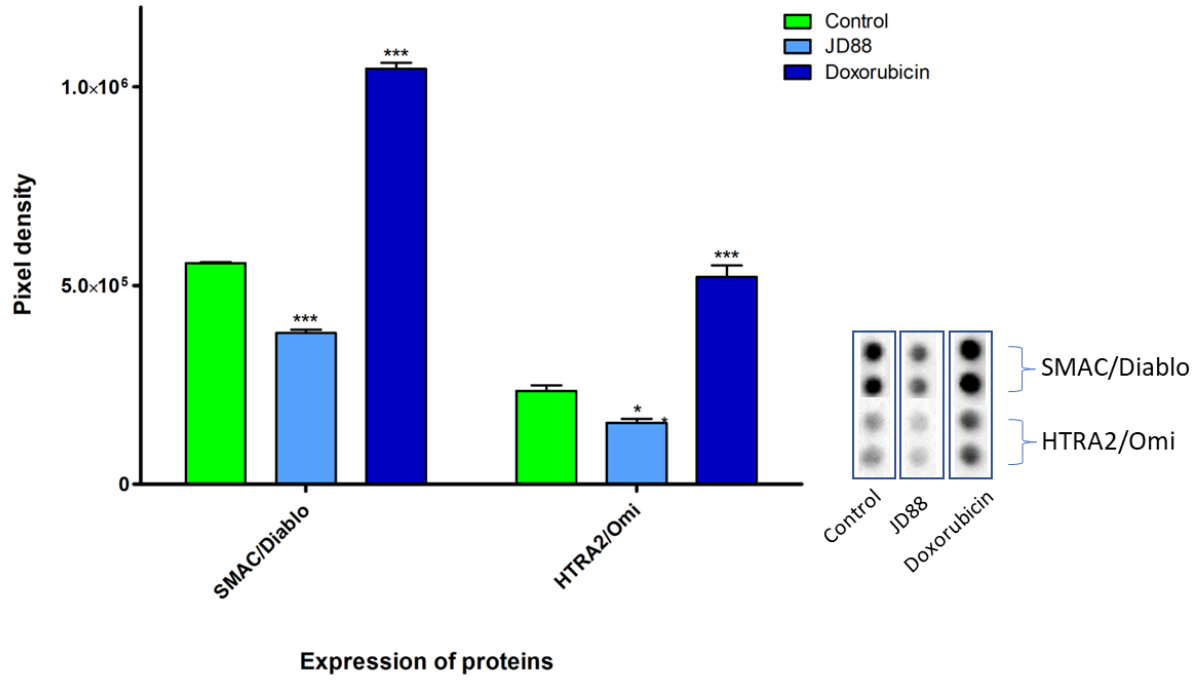

Figure 3.22 Effect of JD88 and doxorubicin on SMAC/Diablo and HTRA2/Omi. A549 cells were treated with 4 µM of JD88 and 4 µM of doxorubicin for 18 hours. Arrays were incubated with 400 µg of each cell lysate. Array data was analysed by one-way ANOVA ($p < 0.05$) followed by Dunnett's post-hoc comparison test. (NS; non-significant; *$p < 0.1$= poorly significant; **$p < 0.05$ = significant; ***$p < 0.01$ = highly significant).

3.9.6 Effect of JD88 and doxorubicin on procaspase-3 and cleaved caspase-3

Procaspase-3, the inactive homodimer form of caspase-3, was expressed at a notably high level in untreated A549 control cells. Treatment with JD88 and doxorubicin resulted in a significant increase of 21% and an insignificant decrease of 7%, respectively. While cleaved caspase-3, the active form, had a moderate baseline expression in A549 cells and underwent a significant decrease of 30% with JD88 and a highly significant decrease of 449% with doxorubicin. The results are shown in Table 3.6 and Figure 3.23.

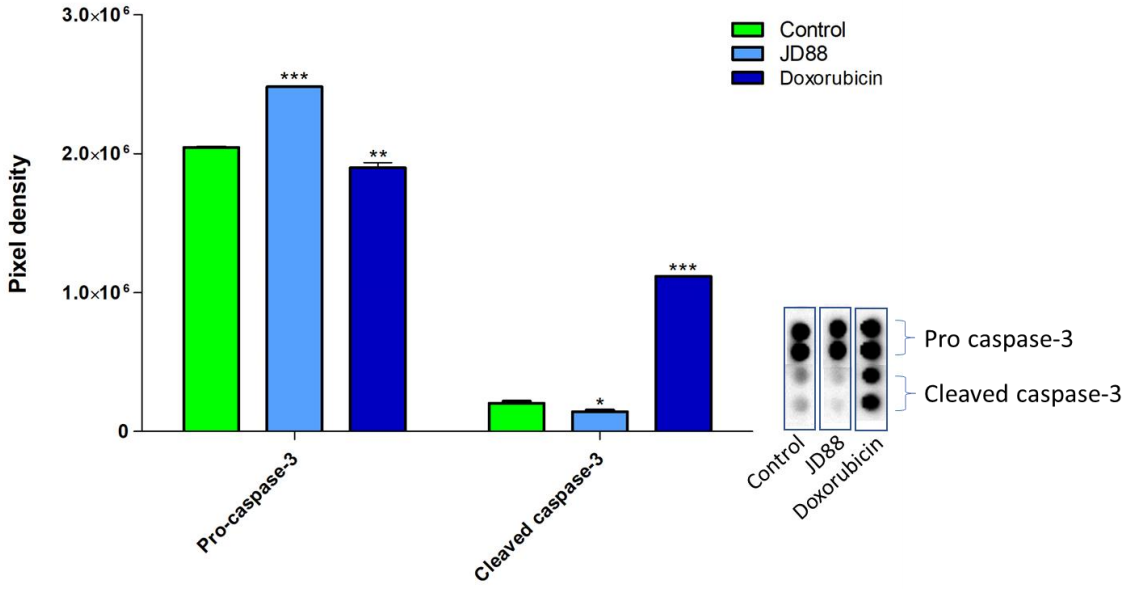

Figure 3.23 Effect of JD88 and doxorubicin on caspase 3. A549 cells were treated with 4 µM of JD88 and 4 µM of doxorubicin for 18 hours. Arrays were incubated with 400 µg of each cell lysate. Array data was analysed by one-way ANOVA ($p < 0.05$) followed by Dunnett's post-hoc comparison test. (NS; non-significant; *$p < 0.1$; is non-significant; **$p < 0.05$ = significant; ***$p < 0.01$ = highly significant).

3.9.7 Effect of JD88 and doxorubicin on the expression of HIF-1α, PON2, HMOX1, and HMOX2 during apoptosis

HIF-1α in untreated A549 control cells exhibited moderate baseline expression. Following treatment, JD88 led to a non-significant decrease of 6%, while doxorubicin resulted in a highly significant increase of 115%. Results are displayed in Table 3.6 and Figure 3.24.

PON2, with high expression in control cells, had a 41% highly significant decrease and an 8% poorly significant increase post-JD88 and doxorubicin treatment, respectively (Table 3.6 and Figure 3.24).

For HMOX1 in untreated A549 control cells, there was a moderately high baseline expression. JD88 treatment led to a non-significant decrease of 8%, whereas doxorubicin prompted a significant increase of 85%. Conversely, HMOX2, with its moderate baseline expression in A549 cells, showed a poorly significant decrease of 20% with JD88 and a highly significant increase of 113% with doxorubicin. These results are detailed in Table 3.6 and Figure 3.24.

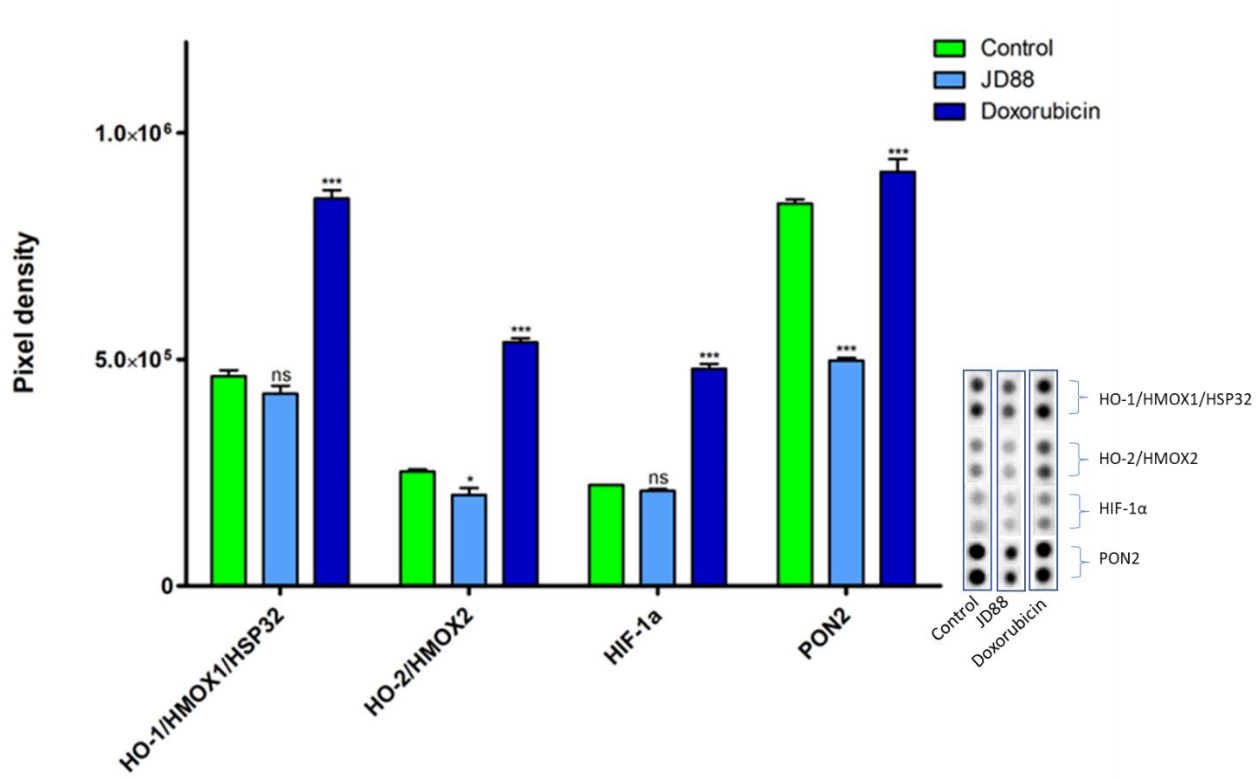

Figure 3.24 Effect of JD88 and doxorubicin on HMOX1, HMOX2, HIF 1α, and PON2. A549 cells were treated with 4 µM of JD88 and 4 µM of doxorubicin for 18 hours. Arrays were incubated with 400 µg of each cell lysate. Array data was analysed by one-way ANOVA ($p < 0.05$) followed by Dunnett's post-hoc comparison test. (NS; non-significant; *$p < 0.1$; is non-significant; **$p < 0.05$ = significant; ***$p < 0.01$ = highly significant).

3.9.8 Effect of JD88 and doxorubicin on the expression of heat shock proteins

Heat shock proteins (HSPs) are highly regulated proteins expressed by cells in response to numerous stresses. Figure 3.25 shows the expression profile of HSP in A549 cells treated with JD88 and doxorubicin.

HSP27, initially showing high expression in untreated A549 control cells, experienced a 20% poorly significant decrease following JD88 treatment, while doxorubicin led to an 81% highly significant increase. HSP60, with very high baseline expression in the A549 control cells, showed a significant 35% decrease post-JD88 treatment and a non-significant 5% increase post-doxorubicin treatment. In contrast, HSP70, with moderate baseline expression in A549 control cells, underwent a 35% significant decrease and an 83% highly significant increase after JD88 and doxorubicin treatment, respectively.

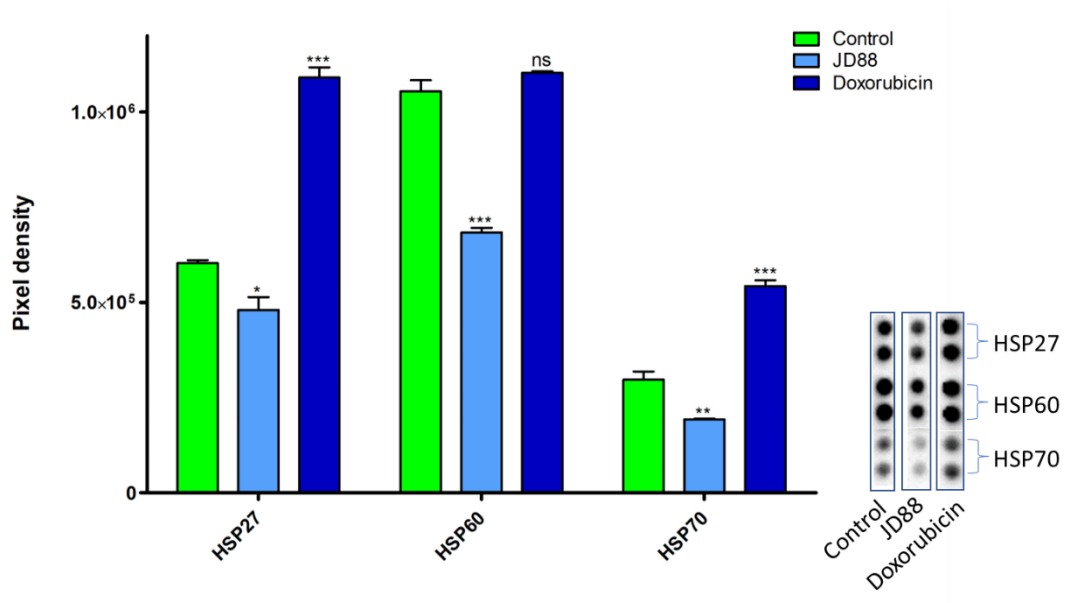

Figure 3.25 Effect of JD88 and doxorubicin on heat shock proteins. A549 cells were treated with 4 µM of JD88 and 4 µM, of doxorubicin for 18 hours. Arrays were incubated with 400 µg of each cell lysate. Array data was analysed by one-way ANOVA ($p < 0.05$) followed by Dunnett's post-hoc comparison test. (NS; non-significant; *$p < 0.1$; is non-significant; **$p < 0.05$ = significant; ***$p < 0.01$ = highly significant).

3.9.9 Effect of JD88 on the expression of death receptor proteins

The death receptor protein, TRAIL R1/DR4, expressed at low levels in A549 control cells, showed a significant decrease of 44% with JD88 treatment, and a significant increase of 170% with doxorubicin treatment. Similarly, TRAIL R2/DR5, with poor baseline expression in A549 control cells, had a non-significant 21% decrease and a significant 331% increase with JD88 and doxorubicin treatments, respectively (Table 3.6, Figure 3.26). FADD, another death receptor protein, starting with moderate expression in A549 control cells, showed a 35% significant decrease and a 47% significant increase after JD88 and doxorubicin treatment, respectively. Fas, another key death receptor protein, showed a moderate expression in A549 control cells. Post treatment, JD88 significantly decreased its expression by 45% while doxorubicin significantly increased it by 206%, respectively. Lastly, TNF R1, with high baseline expression in A549 control cells, showed significant 55% and 53% decreases under JD88 and doxorubicin treatment, respectively.

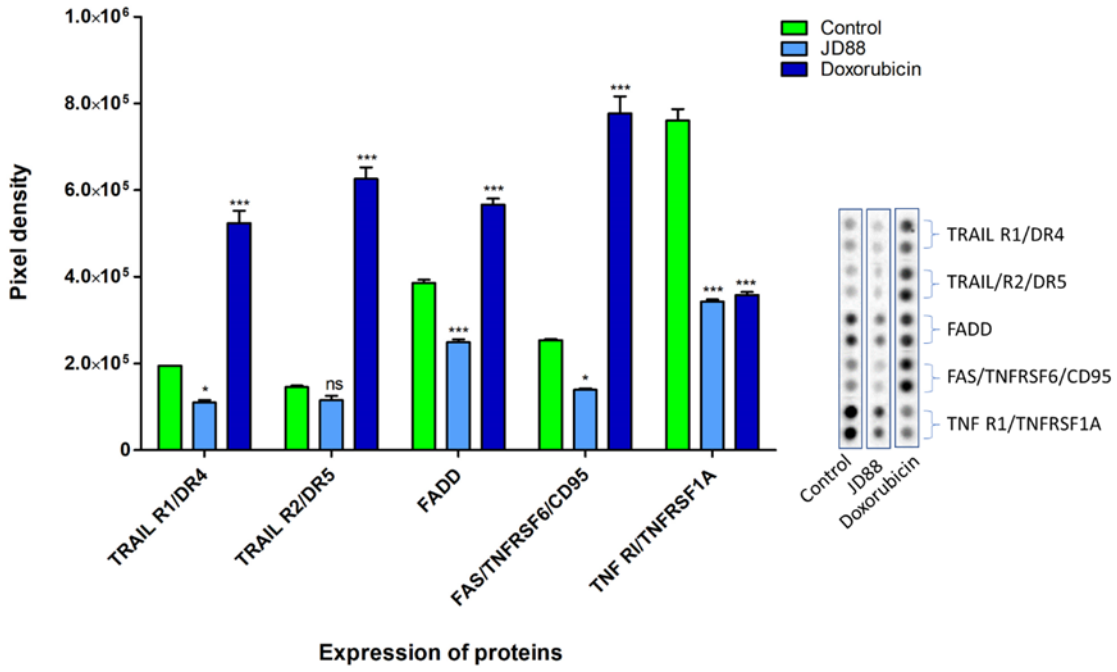

Figure 3.26 Effect of JD88 and doxorubicin on death receptor proteins TRAIL R1, TRAIL R2, FADD, FAS, and TNF R1. A549 cells were treated with 4 µM of JD88 and 4 µM, of doxorubicin for 18 h. Arrays were incubated with 400 µg of each cell lysate. Array data was analyzed by one-way ANOVA ($p < 0.05$) followed by Dunnett's post-hoc comparison test. (NS; non-significant; *$p < 0.1$; is non-significant; **$p < 0.05$ = significant; ***$p < 0.01$ = highly significant).

Chapter IV: Discussion

4. Overview

Lung cancer represents a substantial global health concern, accounting for 11.4% of cancer diagnoses and 18% of related deaths in 2020 (Ferlay *et al*., 2021). Therapies targeting EGFR, ALK, and KRAS pathways, like crizotinib, exhibit response rates of 60-80%, surpassing traditional chemotherapy (Guo *et al*., 2015). However, resistance due to mutations in these kinase inhibitors necessitates diverse therapeutic approaches (Giunta *et al*., 2022). Despite progress in targeted therapies affecting lung cancer treatment outcomes, the significant cost remains a notable barrier. Consequently, platinum-based chemotherapy, particularly cisplatin-based doublets, persists as the standard care in advanced NSCLC (Rossi and Di Maio, 2016). However, its clinical utility is limited by chemoresistance and severe adverse reactions (Tchounwou *et al*., 2021). Hence, extensive research into alternative metals and their complexes has been explored. Copper has emerged as one such metal warranting investigation.

Copper's essential role in various metalloenzymes offers a unique perspective in cancer therapy. Numerous copper complexes have shown promise in preclinical studies, hindering tumour progression and metastasis (McGivern *et al*., 2018; Santini *et al*., 2014). Organic ligand complexes based on copper have been thoroughly investigated as anticancer agents, demonstrating significant activity across multiple cancer cell lines, including breast, colorectal, leukaemic and cervical (Bhat *et al*., 2011; Palanimuthu *et al*., 2013; Qiu *et al*., 2015; Jany *et al*., 2015; Dam *et al*., 2017).

This study's objective was to elucidate the cytotoxicity of copper complexes in A549 lung cancer cells, determining their mode of cell death and analysing their impact on apoptotic regulatory proteins and associated genes. The aim was to identify potential anticancer agents targeting A549 lung cancer cells from a diverse compound library, encompassing copper-imidazo[1,2-*a*]pyridine complexes (JDs), copper-theophylline conjugates (ADs), copper-complexed OM compounds, and novel epidermal growth factor receptor kinase inhibitors (EKIs). This chapter will discuss the obtained results.

4.1 The cytotoxicity of copper-imidazo[1,2-*a*]pyridine complexes in A549 lung cancer cells

The cytotoxicity of the EKIs, ADs, OM compounds and copper-imidazo[1,2-*a*]pyridine complexes, was assessed through MTT assays at 48 hours post-exposure, and the IC_{50} values of the most potent agents were subsequently determined.

Copper-imidazo[1,2-*a*]pyridines exhibited the highest cytotoxicity, followed by AD3 and OM compounds. The EKIs demonstrated minimal efficacy, particularly at concentrations of 5 μM and 50 μM, resulting in their exclusion from further investigations. A549 cells are known to have a wild-type EGFR gene and the lack of effectiveness of EKIs—designed to primarily target mutated EGFR—indicates that EGFR may not be the principal factor driving cancer cell proliferation in this specific cell line (Giard *et al*., 1972; Korrodi-Gregorio *et al*., 2016).

The IC_{50} results showed that copper-imidazo[1,2-*a*]pyridine complexes, namely JD35, JD46, JD47, and JD88, displayed potent cytotoxicity, with IC_{50} values below 5 μM. These findings are consistent with prior research, indicating the significant anticancer effects of copper-imidazo[1,2-*a*]pyridine complexes against various types of cancer cells, including breast, colorectal, and leukaemia cells, with similar IC_{50} values (Dam *et al*., 2017; Harmse *et al*., 2019; Ismail *et al*., 2022). In contrast, AD3 and OM compounds demonstrated higher IC_{50} values, underscoring the superior effectiveness of the copper-imidazo[1,2-*a*]pyridine complexes.

Traditional chemotherapeutic agents such as 5-fluorouracil, doxorubicin, and cisplatin were evaluated for comparison. Doxorubicin had the lowest IC_{50} value of 6.25 ± 0.28 μM among the other agents and was therefore selected as a control for this study. Furthermore, statistical analysis showed that the copper-imidazo[1,2-*a*]pyridine complexes were significantly more potent than doxorubicin ($p < 0.05$).

The IC_{50} values for copper-imidazo[1,2-*a*]pyridine complexes in this study align closely with those reported for other copper coordination complexes. For instance, Gul *et al*., (2020) reported IC_{50} values of 3.05 ± 0.3 μM and 6.04 ± 0.5 μM in A549 cells after a 48-hour exposure to isoquinoline-based copper(II) complexes. Jadeja *et al*., (2017) also reported IC_{50} values ranging from 3.2 to 6.8 μM 24 hours post-treatment with copper(II) mixed ligand complexes. Similarly, Naso *et al*., (2020) reported an IC_{50} value of 3.6 μM for a ternary copper(II) complex of 5-hydroxytryptophan and 1,10-phenanthroline on A549 cells based on a 24-hour MTT assay.

A comparative analysis of the copper-imidazo[1,2-*a*]pyridine complexes, JD35, JD46, JD47, and JD88 reveals that specific structural components significantly dictate their anticancer activities. JD35, identified as an amine nitrate, demonstrated lower potency (IC_{50}: 3.37±0.34 μM) than its amine diacetate counterparts JD46, JD47, and JD88. JD46, lacking halogen substitution, displayed reduced potency (IC_{50}: 2.40±0.15 μM) compared to JD47 and JD88, both featuring bromine substitutions at the 5th and 6th positions of the imidazopyridine ring. The presence of bromine at the 6th position in JD88 corresponded with notably increased

efficacy. This corroborates Ismail *et al*.'s (2022) findings, highlighting the heightened cytotoxicity of JD88 in K562 and HL-60 leukaemia cell lines (IC_{50}: 1.7±0.3 μM and 2.2±0.5 μM, respectively). Conversely, Dam *et al*. (2017) observed superior potency for JD46 in HT-29 colorectal cancer cells (IC_{50}: 0.8±0.2 μM), underscoring its specificity across different cancer types.

In A549 cells, JD88 emerged as the most effective complex, closely followed by JD47, JD46, and JD35. Consequently, these complexes were selected for further investigation.

4.2. The effect of copper-imidazo[1,2-*a*]pyridines on A549 lung cancer cell morphology

The impact of the four most active copper-imidazo[1,2-*a*]pyridine complexes, JD35, JD46, JD47, and JD88, on A549 lung cancer cell morphology was evaluated following the assessment of low IC_{50} values. At 18 hours post-treatment, distinct morphological changes were observed, consistent with indicators of apoptotic cell death. Phase-contrast images showed cytoplasmic vacuolisation, a characteristic often associated with cellular distress preceding cell death (Shubin *et al*., 2016). Notably, this observation was absent in doxorubicin-treated cells.

The absence of propidium iodide (PI) staining in the nuclei across all treatments suggested the lack of necrosis, indicating a more controlled form of cell death. This regulated cell death is pivotal in minimising inflammation and tissue damage typically linked with uncontrolled necrosis in cancer treatment (Khalid and Azimpouran, 2023). These findings are consistent with previous studies that have assessed the copper-imidazo[1,2-*a*]pyridine complexes and found no evidence of necrosis (Harmse *et al*., 2019, Ismail *et al*., 2022). This reinforces the concept that necrosis is not a common mechanism of cell death triggered by the copper-imidazo[1,2-*a*]pyridines.

Furthermore, observations of chromatin condensation and nuclear fragmentation across all treatments suggested early stages of apoptosis, possibly excluding autophagic cell death where nuclear fragmentation is typically not observed (Galluzzi *et al*., 2018). These observations align with similar morphological changes reported by Harmse *et al*. (2019) and Ismail *et al*. (2022) in colorectal and leukaemia cell lines, respectively.

Distinctive red fluorescing lysosomes were notably observed in acridine orange-stained cells treated with copper complexes, except for JD46. Acridine orange accumulation in lysosomes is well-established (Vermes and Haanen, 1994). Lysosomes play a role in initiating apoptosis

through protease release (Vermes and Haanen, 1994; Zhang *et al*., 2021), suggesting heightened lysosomal activity and supporting the likelihood of apoptotic cell death.

Collectively, these morphological changes, absence of necrotic cell death, nuclear fragmentation, and increased lysosomal activity suggest the potential induction of apoptosis by copper-imidazo[1,2-*a*]pyridine complexes in A549 lung cancer cells. However, these observations based on morphological changes necessitate further validation through additional assays.

4.3 The effect of copper-imidazo[1,2-*a*]pyridine complexes on Annexin-v binding in A549 cells

Following treatment with copper complexes and doxorubicin, the mechanism of cell death in A549 cells was investigated, focusing on apoptosis. Apoptosis involves the loss of plasma membrane phospholipid asymmetry, resulting in phosphatidylserine (PS) externalization, which can be detected by Annexin V binding (Op Den Kamp, 1979; Vermes *et al*., 1995; Lee *et al*., 2013). The presence of propidium iodide (PI) in cells undergoing apoptosis indicates late apoptosis or a possible transition to secondary necrosis (Crowley *et al*., 2016a; Wlodkowic *et al*., 2011).

In this study, Annexin V binding was examined at 6 and 18 hours post-treatment with copper-imidazo[1,2-*a*]pyridines and doxorubicin in A549 cells. The results showed a time-dependent increase in apoptosis induced by these complexes. At 6 hours post-treatment, cells in all treatments exhibited Annexin-V binding alone, with JD88 displaying the highest percentage. By 18 hours, all treated cells showed both Annexin-V and PI staining, indicating late-stage apoptosis or secondary necrosis. Compared to doxorubicin, the copper complexes displayed higher Annexin V binding, implying their prompt initiation of apoptosis.

Secondary necrosis, distinct from primary necrosis, involves cellular disintegration and content release in *in vitro* cultures and is typically characterized by lysosomal leakage and cell swelling (Silva, 2010; Rogers *et al*., 2017. These features were not observed in prior morphological studies of A549 cells treated with these copper complexes. Hence, the transition to dual Annexin V and PI staining at 18 hours likely signifies late-stage apoptosis rather than secondary necrosis in this cell line.

These findings reinforce a time-dependent shift from early to late apoptosis following the administration of copper complexes. This is in line with previous research that observed a similar induction of Annexin-V binding to PS by a copper complex, $Cu(SBCM)_2$ showing the

transition from early to late apoptosis (Foo *et al*., 2019). Furthermore, other studies examining copper-imidazo[1,2-*a*]pyridine complexes found that HL-60 and K562 leukaemia cells treated with these complexes also showed early and late stage apoptosis with Annexin V binding at 14 hours and dual Annexin V binding and PI staining at 18 hours (Ismail *et al.,* 2022). This aligns with the observations made in this study and supports the induction of apoptosis by these copper complexes.

4.4 The effect of copper-imidazo[1,2-*a*]pyridine complexes on caspase-3/7 activity in A549 cells

Apoptosis is orchestrated by a cascade of caspases, including initiator and effector caspases like caspases-3 and -7, which cause the degradation of cellular components, including DNA fragmentation (Taylor *et al*., 2008; Martin *et al*., 2012). These caspases specifically cleave the DEVD amino acid sequence on the C-terminal side of the aspartic acid residues. This cleavage is a critical step in the initiation of apoptosis, leading to the activation of downstream effector molecules that cause apoptosis (Peterson *et al*., 2010).

This study evaluated the capacity of copper complexes to activate caspase-3/7, in comparison to the positive control, doxorubicin. Treatments were administered at their respective IC_{80} concentrations, and caspase-3/7 activity was measured at 24 and 48 hours after treatment.

JD46 notably triggered caspase-3/7 activity in 80% of cells after 24 hours, followed by JD47 and doxorubicin. JD35 and JD88 exhibited the least caspase-3/7 activity at this treatment period. By 48 hours, all complexes and doxorubicin had over 80% cell activity for caspase 3/7. This is expected since caspase 3/7 activation is considered a late event. The copper complexes induced higher caspase 3/7 activity than doxorubicin at both time points, affirming their apoptosis-inducing ability in A549 cells.

Observations from other studies align with the findings of this research, where copper-imidazo[1,2-*a*]pyridines induced peak caspase-3/7 activation in HL60 and K562 leukaemia cells at 14 and 24 hours post-treatment, respectively (Ismail *et al*., 2022). A similar trend was observed in HT-29 colorectal cells, where a threefold increase in caspase-3/7 activity was noted 20 hours post-treatment with copper-imidazo[1,2-*a*]pyridines, JD46 and JD88 (Harmse *et al*., 2019). These findings confirm the consistent activation of caspase-3/7 by copper-imidazo[1,2-*a*]pyridines across different cell lines. The variation in peak caspase-3/7 activity levels could be attributed to the differential cellular responses to the treatment, which may be influenced by factors such as cell type, treatment duration, and the specific copper complex used.

In addition, an increase in caspase-3/7 activity was noted in A549 cells treated with Cu(II) flavonoid complexes at both 24 and 48 hours post treatment, aligning with this study (Done *et al*., 2022). Caspase-3/7 activation was also identified as a primary indicator of apoptosis in A549 cells treated with specific [CuL5 (H_2O)] copper complexes (Ribeiro *et al*., 2021).

These findings collectively validate the pro-apoptotic potential of copper complexes, particularly the copper-imidazo[1,2-*a*]pyridines. Their ability to activate caspase-3/7 in A549 cells, supported by data from other cell lines such as HL-60, K562, and HT-29, suggests a consistent apoptotic mechanism of cell death.

4.5 The effect of copper-imidazo[1,2-*a*]pyridines on caspase-8 activity in A549 cells

Caspases, particularly initiator caspases, play a critical role in orchestrating apoptosis. Their activation distinguishes intrinsic and extrinsic apoptotic pathways, mediated by caspase-8 and caspase-9, respectively. Procaspase-8 dimerizes within a death-inducing signalling complex (DISC) during the extrinsic apoptosis pathway, which forms around a specific death receptor. This complex activates caspase-8 to ultimately trigger caspase-3/7 (Tummers and Green, 2017).

Treatment of A549 cells with copper-imidazo[1,2-*a*]pyridines and doxorubicin significantly raised caspase-8 activity at concentrations corresponding to their IC_{80} values at both 24 and 48 hours post-treatment. At 24 hours, JD35, JD46, and JD47 treatments demonstrated the highest caspase-8 activity, while at 48 hours, overall increased caspase-8 activity was observed across all treatments, with JD46 displaying the highest elevation followed by JD47, and JD88 showing the most notable increase in caspase-8 activity. Notably, A549 cells with heightened caspase-8 activity showed significant cellular damage, while cells maintaining structural integrity exhibited muted caspase-8 signals. Conversely, doxorubicin-treated cells showed extensive red fluorescence beyond the nucleus, aligning with increased caspase-8 activity, consistent with previous findings on doxorubicin-treated A549 cells (Poornima *et al*., 2014; Lee *et al*., 2011).

The observed increase of caspase-8 activity in A549 cells post-treatment is an unusually late event as it should occur earlier and it differs from results observed in other cell lines. A modest 20% increase in the activation of caspase-8 in HL-60 cells was reported, while in K562 cells, no significant caspase-8 induction was observed post treatment with copper-imidazo[1,2-*a*]pyridines (Ismail *et al*., 2022). Similarly, in HT29 colorectal cancer cells, specific copper-imidazo[1,2-*a*]pyridines did not activate caspase-8 within a 24-hour period (Harmse *et al*.,

2019). This suggests that copper-imidazo[1,2-*a*]pyridines may not uniformly stimulate caspase-8 activity or activate an extrinsic apoptotic pathway across all cell types.

In contrast, the copper complex [Cu(L)(2imi)] activated both intrinsic and extrinsic apoptotic pathways in the HepG2 liver cell line, showing significant caspase-8 activity (Rezaei *et al*., 2019). Another copper complex, (II)-N-(2-hydroxy-3-methoxy-benzaldehyde)-alaninate, was identified to induce apoptosis *via* both pathways (Banerjee *et al*., 2016). These varied observations emphasize the diverse apoptotic potential of copper complexes across different cell lines and the pivotal role of the ligand attached to copper complex.

These diverse responses in caspase-8 induction by copper-imidazo[1,2-*a*]pyridine complexes, notably their significant effect on the A549 cell line, suggest its heightened sensitivity to caspase-8 induction compared to other cell lines and may suggest the activation of the extrinsic apoptosis. However, the simultaneous activation of caspase-3/7 alongside caspase-8 which should be an earlier event to caspase-3/7 prompts further inquiry into the specific apoptotic pathways involved.

4.6 The effect of copper-imidazo[1,2-*a*]pyridines on reactive oxygen species in A549 cells

Reactive oxygen species (ROS), such as hydroxyl radicals (HO), superoxide radicals (O_2), and hydrogen peroxide (H_2O_2), serve as secondary messengers in various cellular signalling pathways, notably in ROS-mediated cell death (Redza-Dutordoir and Averill-Bates, 2016). Physiologically, moderate ROS levels have essential functions, while excessive amounts can result in detrimental effects by damaging cellular components like proteins, nucleic acids, and lipids, often activating apoptotic pathways (Redza-Dutordoir and Averill-Bates, 2016). Copper-containing metal complexes have been associated with increased ROS, leading to potential toxicity and mitochondrial dysfunction, triggering apoptosis (Kowol *et al*., 2012).

This study evaluated the ROS-inducing capabilities of copper-imidazo[1,2-*a*]pyridine complexes and doxorubicin at their IC_{80} concentrations. JD35 and JD88 treatments demonstrated a notable increase in ROS at 6 hours, with JD35 maintaining high levels at 18 hours while JD88 decreased to 30% at 18 hours. In contrast, JD46 and JD47 initially induced ROS at 6 hours, which drastically decreased to less than 2% by 18 hours. Doxorubicin, a recognised ROS inducer (Weis, 1992), showed 90% and 70% ROS-positive cells at 6 hours and 18 hours, respectively.

This observed ROS pattern suggests a transient, notable surge in ROS mainly at 6 hours post-treatment. Correspondingly, Harmse *et al*., (2019) documented ROS production in HT29 cells after treatment with copper-imidazo[1,2-*a*]pyridine complexes, observing peak levels at 6 hours, consistent with this study's findings. The pronounced increase in ROS at 6 hours, declining by 18 hours, highlights the transient nature of ROS generation by these complexes.

Done *et al*., (2022) observed a dose- and time-dependent increase in ROS with a Cu(II) flavonoid complex. Similarly, Naso *et al*., (2020) reported a 240% surge in ROS levels in A549 cells after a 4-hour treatment with a ternary copper(II) complex, Cu5HTPphen. Jadeja *et al*., (2017), using mixed ligand Cu(II) complexes derived from 4-acyl pyrazolones, noted heightened ROS levels in A549 cells, indicating potential downstream mitochondrial damage due to ROS production. These results reinforce the theory of ROS-mediated apoptosis triggered by copper complexes, aligning with this study's findings that copper-imidazo[1,2-*a*]pyridine complexes effectively induce ROS formation in A549 cells, potentially inducing intrinsic apoptosis *via* mitochondrial membrane damage.

4.7 The effect of copper-imidazo[1,2-*a*]pyridines on mitochondrial membrane potential in A549 cells

ROS have been associated with influencing MMP, leading to mitochondrial dysfunction (Done *et al*., 2022; Jadeja *et al*., 2017; Periasamy *et al*., 2020). MMP, an early indicator of apoptosis, is disrupted by damages to the mitochondrial membrane, causing the release of pro-apoptotic factors like cytochrome c, apoptosis-inducing factor, and SMAC/Diablo into the cytosol, ultimately activating caspase-9 and caspase-3/7, initiating the intrinsic apoptotic pathway (Wong, 2011).

The alterations in MMP were evaluated in A549 cells treated with copper-imidazo[1,2-*a*]pyridine complexes and doxorubicin at their IC_{80} concentrations and measured at 12 and 18 hours post-treatment using the JC-1 assay. Typically, intact MMP exhibits red fluorescence with JC-1 forming red aggregates in mitochondria, while decreased MMP results in green fluorescence, indicating MMP loss (Tait and Green, 2010; De Biasi *et al*., 2015).

Untreated A549 cells showed red JC-1 fluorescence, indicating intact mitochondrial function. Doxorubicin-treated cells showed a 40% and 50% reduction in MMP at 12 and 18 hours, respectively. In contrast, JD35, JD46, JD47, and JD88 compounds displayed approximately a 60% MMP reduction at 12 hours, escalating to nearly 90% by 18 hours, suggesting a higher potential for inducing mitochondrial dysfunction compared to doxorubicin.

These findings align with similar studies where a substantial MMP loss was observed in HT-29 cells treated with copper-imidazo[1,2-*a*]pyridine complexes (Harmse *et al*., 2019). Similarly, MMP disruption by copper-imidazo[1,2-*a*]pyridine complexes was also evident in HL-60 and K562 cells following treatment with JD88 and JD47 at their IC_{75} concentrations for 14 and 24 hours, respectively (Ismail *et al*., 2022). Other copper complexes such as those investigated by Naso *et al*., (2020) showed a dose-dependent reduction in MMP in A549 cells treated with Cu5HTPphen, while, Periasamy *et al*., (2020) highlighted the alteration of ROS levels by the copper complex [Cu(tdp)(phen)]+, indicating the interplay between ROS and the observed MMP changes. These results suggest that copper-imidazo[1,2-*a*]pyridines lead to MMP loss, potentially mediated by ROS generation.

4.8 Immunohistochemical analysis of copper-imidazo[1,2-*a*]pyridines on p21 and p53 Expression"

Following the assessment of apoptotic markers, this study further explored the impact of copper-imidazo[1,2-*a*]pyridines on the expression of the cell cycle regulatory proteins p21 and p53 through immunohistochemistry techniques. These proteins are integral to cell cycle regulation and the DNA damage response, and ascertain their role in potentially mediating DNA damage.

4.8.1 The effect of copper-imidazo[1,2-*a*]pyridines on nuclear p21 in A549 Lung Cancer Cells

P21, a key regulator of cell division, ensures the accurate replication of parental DNA and functions as part of the DNA damage response (Kreis *et al*., 2019; Waga *et al*., 1994). Nuclear p21 inhibits damaged cells from progressing through mitosis and is a significant marker for DNA damage, restraining DNA polymerase and impeding the replication fork (Waga *et al*., 1994; Cazzalini *et al*., 2010). Elevated nuclear p21 expression indicates a DNA damage response and potentially triggers apoptosis (Fujiwara *et al*., 2008; Abbas and Dutta, 2009). Activation of the Akt/PKB signalling pathway results in the cytoplasmic relocation of p21, diminishing its cell cycle inhibitory capacity (Mauro *et al*., 2012).

Immunohistochemistry techniques were employed to assess changes in p21 expression in A549 lung cancer cells after exposure to the copper-imidazo[1,2-*a*]pyridines and doxorubicin. Treatment with the copper-imidazo[1,2-*a*]pyridines increased nuclear p21 expression especially in JD35, indicating a DNA damage response. Cells displaying intensified p21 expression showed morphological changes suggestive of cell damage. Doxorubicin-treated cells exhibited the most intense nuclear p21 fluorescence, a compound known to induce DNA

damage (He *et al*., 2020). Notably, limited information exists concerning the impact of other copper complexes on nuclear p21 expression in A549 cells.

These results suggest that copper-imidazo[1,2-*a*]pyridines, especially JD35, may enhance nuclear p21 expression and related pathways, implicating a potential preference for apoptosis by these complexes.

4.8.2 The effect of copper-imidazo[1,2-*a*]pyridines on nuclear phospho-p53(S15) expression in A549 cells

The p53 protein, a pivotal tumour suppressor, regulates DNA repair, cell cycle arrest, and apoptosis (Redza-Dutordoir and Averill-Bates, 2016). It triggers the transcription of proteins such as Bax, Bid, and Apaf-1 that set off the intrinsic pathway, as well as Fas and Fas-L, which trigger the extrinsic pathway of apoptosis. Furthermore, p53 can translocate from the cytoplasm to the mitochondria, enhancing MOMP and releasing pro-apoptotic proteins, thereby facilitating apoptosis (Redza-Dutordoir and Averill-Bates, 2016). The altered function and localization of p53 play intricate roles in various cancers, including lung cancer (Abuetabh *et al*., 2022).

Immunohistochemistry techniques were used to evaluate changes in p53 expression in A549 lung cancer cells after exposure to copper-imidazo[1,2-*a*]pyridines (JD35, JD46, JD47, and JD88) and doxorubicin. Post-treatment, a significant increase in nuclear phospho-p53(S15) signal was observed, particularly after JD46 and JD88 treatments. This increase corresponded with observable cellular damage, indicating potential DNA damage resulting from the treatments.

The heightened phospho-p53(S15) suggests inhibition of degradation by mouse double minute 2 homolog (MDM2), which is responsible for the nuclear export of p53 to the cytoplasm where it is degraded (Abraha and Ketema, 2016). This increased nuclear phospho-p53 suggests enhanced p53 stabilization and nuclear accumulation, which aids in its apoptotic function (Inoue *et al*., 2005). The intensified phospho-p53 correlates with earlier observations of increased ROS formation, often linked to p53 activation in response to DNA damage induced by ROS (Shi *et al*., 2021). Copper complexes have been known to stimulate ROS production, subsequently upregulating p53 expression (Shao *et al*., 2019).

In response to DNA damage, p53 must be protected from MDM2 ubiquitination and degradation. The phosphorylation of p53 on amino acid residues by kinases such as Checkpoint kinase (Chk) 1 and 2 and ATM modifies the domain recognized by MDM2, thereby preventing

the p53-MDM2 interaction. As a result, MDM2 is unable to initiate the ubiquitinylation of p53, allowing p53 to avoid degradation and increase cellular concentrations (Weinburg, 2014).

The immunohistochemistry assessment revealed significant changes in nuclear phospho-p53(S15) expression following exposure to copper-imidazo[1,2-*a*]pyridines and doxorubicin, indicating potential mechanisms of DNA damage in A549 cells induced by these treatments. These findings implicate ROS-mediated p53 activation and provide a compelling argument for further investigation into the anticancer potential of copper-imidazo[1,2-*a*]pyridine complexes.

4.9 The effect of JD88 on apoptosis-associated proteins in A549 Cells

To evaluate the effects of the highly active copper complex JD88 and the positive control, doxorubicin, on apoptosis-associated regulatory proteins in A549 cells, proteome array data was analysed. The proteome array evaluated the effect of JD88 on apoptosis-related proteins post-confirmation of cell death through apoptosis.

4.9.1 The effect of JD88 on phospho-p53(S15) expression in A549 Cells

In A549 lung cancer cells, where wild-type p53 predominates (Guntur *et al.*, 2010.), baseline expression levels of three phosphorylated species of p53 were notably low. However, upon treatment with JD88 and doxorubicin, there was a substantial and statistically significant increase in the expression levels of these three phosphorylated forms of p53. Specifically, phospho-p53 (S15) expression was increased by 225% with JD88 and 587% with doxorubicin. Similarly, phospho-p53 (S46) levels increased by 258% and 563%, respectively. The most notable change was observed in phospho-p53 (S392), showing an increase of 415% and 970% with JD88 and doxorubicin, respectively. This substantial increase coincides with the immunohistochemistry results showing elevated phospho-p53(S15) expression 20 hours post-treatment with JD88. These findings are consistent with p53's role as a tumour suppressor protein, triggering growth arrest and apoptosis upon sensing cellular stress (Levine and Oren, 2009).

It is well-documented in existing literature that the phosphorylation of specific serine residues—S15, S46, and S392—plays a pivotal role in determining p53's stability and transcriptional activation capacity (Lui *et al*., 2019). Post-translational modifications, such as phosphorylation, acetylation, and ubiquitination, significantly modulate p53's stability and function (Siliciano *et al*., 1997). For instance, phosphorylation of serine 15 by ataxia telangiectasia mutated kinases (ATM) stabilizes mutant p53. Conversely, serine 46 phosphorylation, mediated by kinases homeodomain-interacting protein kinase 2 (HIK2) and

dual-specificity tyrosine phosphorylation-regulated kinase 2 (DYRK2), has been associated with p53's pro-apoptotic functions. Moreover, serine 392 phosphorylation, facilitated by cyclin-dependent kinase 9(CDK9), regulates p53's transcriptional activity (Hientz *et al*., 2017).

In assessing other studies on the influence of copper complexes on the p53 pathway, Harmse *et al*., (2019) reported that copper-imidazo[1,2-*a*]pyridines JD47 and JD88 downregulated the expression of mutated p53 in HT-29 colorectal cancer cells, leading to apoptosis. This effect was attributed to the presence of a gain-of-function mutation, R273H, in HT-29 cells, causing mutated p53 accumulation (Yue *et al*., 2017). This explains the elevated expression of phosphorylated p53 forms in untreated HT-29 cells compared to A549 cells where wild-type p53 levels were low. Conversely, Ismail *et al*., (2022) discovered that in HL-60 and K562 cells, p53 is not essential for initiating apoptotic cell death, indicating that these cell lines can undergo apoptosis without accumulating wild-type p53. These findings highlight the cell line-dependent effects of copper-imidazo[1,2-*a*]pyridines on p53 and underscore the complexity and variability of the p53 pathway's involvement across different cancer types. Particularly in A549 cell lines, the significant increase in p53 is an important event for apoptosis as it will overcome the anti-apoptotic events that may have been activated in the pathway upon treatment with copper-imidazo[1,2-*a*]pyridines such as JD88, as it is a powerful inducer of apoptosis through various mechanisms.

4.9.2 The effect of JD88 on p21 and p27 expression in A549 Cells

Imbalances in cell growth and death, largely regulated by proteins governing the cell cycle, often underlie the development of human cancers. Central to these regulations are cyclins, cyclin-dependent kinases (CDKs), and CDK inhibitors. Reduced expression or functionality of the G1-checkpoint CDK inhibitors, p21 (Cip1) and p27 (Kip1), is linked to cancer. Additionally, their loss may lead to drug resistance, although conflicting studies suggest their potential in tumour development (Abukhdeir and Park, 2008).

In this study, the changes in the expression of p21 and p27 were evaluated in A549 lung cancer cells after treatment with JD88 and doxorubicin as part of the proteome array analysis.

p21, known for inducing cell cycle arrest post-DNA damage under the governance of the tumour suppressor p53 (He *et al*., 2020), displayed low baseline expression in A549 cancer cells. JD88 treatment significantly reduced p21 levels, whereas doxorubicin significantly increased its expression. Interestingly, these findings contrast with the observed increase in nuclear p21 expression during immunohistochemistry experiments. Nuclear p21 typically

signifies cell cycle arrest, while its cytoplasmic presence is associated with aggressive tumours and poorer prognosis (Abbas and Dutta, 2009). It is important to note that cell lysates used in this study included both nuclear and cytoplasmic proteins, necessitating further investigations to elucidate this contrast.

p27, another vital regulator inhibiting CDKs and modulating the cell cycle (James *et al*., 2008), displayed low baseline expression in A549 cells. While JD88 treatment decreased p27 levels insignificantly, doxorubicin significantly increased p27 expression. Notably, p27's growth-inhibitory function is associated with nuclear localization, while cytoplasmic localization is linked to increased metastasis and poor survival (Razavipour *et al*., 2020). However, the localization of p27 was not determined in this study and merits further investigation.

4.9.3 The effect of JD88 on anti-apoptotic and pro-apoptotic bcl-2 family proteins in A549 cells

The BCL-2 protein family, pivotal in regulating apoptosis, comprises anti-apoptotic proteins like Bcl-2 and Bcl-xL, along with pro-apoptotic proteins including Bax and Bad (Hardwick and Soane, 2013). Imbalances within these proteins, marked by increased expression of anti-apoptotic or decreased expression of pro-apoptotic proteins, contribute to cancer cell survival and treatment resistance (Czabotar *et al*., 2014).

The precise mechanism underlying the regulation of apoptosis by BCL-2 family proteins is their control over MOMP. Anti-apoptotic proteins such as Bcl-2 and Bcl-xL prevent MOMP, impeding cytochrome c release and preventing cell death. Conversely, pro-apoptotic proteins such as Bax and Bad promote MOMP, facilitating cytochrome c release, apoptosome formation, and initiating apoptosis (Shamas-Din *et al*., 2013).

Initially, baseline expression of Bad and Bcl-xL was moderate, while Bcl-2 and Bax were low in A549 cells. Exposure to JD88 significantly decreased the expression of both pro-apoptotic proteins (Bad and Bax) and anti-apoptotic proteins (Bcl-2 and Bcl-xL). Conversely, doxorubicin treatment significantly increased Bad, Bcl-2, and Bcl-xL expression and significantly decreased Bax expression. However, considering the low baseline expression of Bax, this might have a minimal effect on the cells. Diverse effects on these proteins have been observed in other studies with copper complexes, suggesting varied responses to JD88 (Ismail *et al*., 2022; Harmse *et al*., 2019).

The observed reduction in the expression of pro-apoptotic proteins Bad and Bax following JD88 treatment in A549 cells may initially appear paradoxical, however, the fate of a cell often

depends on the equilibrium between pro- and anti-apoptotic proteins, rather than individual protein levels (Zhang *et al*., 2000). Normally, this balance prevents unnecessary cell death, however, in cancer cells, there is a shift toward anti-apoptotic proteins, promoting cancer cell survival (Hata *et al*., 2015). The decrease in anti-apoptotic Bcl-2 and Bcl-xL by JD88 might shift this balance, promoting apoptosis, despite the lower levels of Bad and Bax. Furthermore, the highly significant increase in the phosphorylated forms of p53 by JD88 which supports these pro-apoptotic proteins may counteract this inhibitory effect by JD88.

Considering the central role of the Bcl-2 family in apoptosis regulation, the diminished Bcl-2 and Bcl-xL expression in A549 cells treated with JD88, along with reduced pro-apoptotic proteins Bad and Bax, suggests that JD88 may stimulate apoptosis by inhibiting anti-apoptotic mechanisms and shifting the protein balance to favour apoptosis.

4.9.4 The effect of JD88 on inhibitors of apoptosis proteins in A549 cells

The inhibitor of the apoptosis (IAP) protein family plays a critical role in cell survival by preventing apoptosis, making them attractive targets in cancer therapy (Silke and Meier, 2013).

XIAP, characterized by a low baseline level in untreated A549 cells, inhibits caspases involved in apoptosis such as caspase-9, caspase-3, and caspase-7 (Obexer and Ausserlechner, 2014). Post JD88 exposure, XIAP expression significantly decreased by 62%, suggesting a potential reduction in its anti-apoptotic effects, thus favouring apoptosis. Conversely, doxorubicin treatment significantly increased XIAP levels by 91%, hinting at a resistance mechanism. In a study with HT-29 cells, the highly expressed XIAP protein was also significantly suppressed by similar copper-imidazo[1,2-*a*]pyridines in line with this study's observations(Harmse *et al*., 2019). Contrarily, in HL-60 leukaemia cells, the copper-imidazo[1,2-*a*]pyridines significantly increased XIAP expression (Ismail *et al*., 2022). These observed variations in XIAP expression in different studies highlight diverse cellular responses to the copper-imidazo[1,2-*a*]pyridines among different cell lines.

cIAP-1 and cIAP-2 showed distinct responses upon JD88 and doxorubicin treatment. In A549 control cells, cIAP-1 had moderate baseline expression levels. Post-treatment, JD88 and doxorubicin caused a significant increase of 49% and 68% in cIAP-1 levels, respectively. Conversely, cIAP-2 demonstrated low baseline levels in A549 cells. JD88 treatment led to a significant 21% decrease, while doxorubicin induced a significant 67% increase in cIAP-2 expression. These alterations in cIAP-1 and cIAP-2 expressions potentially affect the NF-κB pathway, a crucial contributor to cancer cell survival and chemoresistance (Xia *et al*., 2014).

The NF-κB pathway regulates the transcription of various survival proteins, where cIAPs modulate both canonical and non-canonical NF-κB pathways (Hoesel and Schmid, 2013; Liu *et al*., 2017). Despite the significant increase in cIAP-1 following JD88 treatment, the concurrent reduction in cIAP-2 levels post-JD88 exposure may hint at a possible inhibition of the NF-κB pathway. This inference is further supported by the simultaneous decrease in XIAP levels post-JD88 treatment. Consequently, JD88's varying effects on cIAP-1 and cIAP-2 suggest its potential to disrupt the NF-κB-mediated transcriptional loop, which could favour apoptosis.

Survivin, moderately expressed in the A549 control cells, displayed a significant decrease of 26% with JD88 and a non-significant decrease with doxorubicin. Survivin is linked with aggressive tumour behaviour and drug resistance (Mobahat *et al*., 2014; Garg *et al*., 2016). The simultaneous reduction of survivin and XIAP by JD88 suggests a wider impact on cellular defences against apoptosis. Survivin's role in stabilizing XIAP and inhibiting its function, along with SMAC/Diablo, indicates JD88's potential to target multiple anti-apoptotic proteins, rendering cells more vulnerable to apoptosis.

Livin, present at low levels in A549 cells, notably increased by 21% and 150% post-JD88 and doxorubicin treatments respectively. The rise in livin levels after JD88 might indicate a compensatory mechanism, influencing the balance between XIAP and SMAC/Diablo, potentially sensitizing A549 cells to apoptosis (Yan, 2011; Fulda, 2014). However, this increase could also suggest a resistance mechanism triggered by treatment.

These findings highlight the impact of copper-imidazo[1,2-*a*]pyridine complexes such as JD88 on IAP protein expression in A549 lung cancer cells, resulting in reduced levels of XIAP, cIAP-2, and survivin which are some pivotal proteins in cancer. These alterations suggest JD88's potential to inhibit anti-apoptotic mechanisms and NF-κB signalling, thereby heightening cancer cell susceptibility to apoptosis. However, the observed increase in livin expression following JD88 treatment implies a possible compensatory or resistance mechanism.

4.9.5 The effect of JD88 on SMAC/Diablo and HTRA2/Omi expression in A549 cells

SMAC/Diablo and HTRA2/Omi are known to inhibit anti-apoptotic proteins, such as XIAP and survivin, thereby promoting caspase activation and apoptosis (Fulda, 2014).

Baseline expressions of SMAC/Diablo were moderate, and JD88 treatment resulted in a decrease, while doxorubicin caused a nearly 90% increase. Similarly, HTRA2/Omi showed a 34% decrease post-JD88 treatment and a 122% increase after doxorubicin treatment.

The decrease in SMAC/Diablo post-JD88 treatment, given its crucial role as an XIAP antagonist, could be of concern (Fulda, 2014). However, JD88 effectively reduced XIAP expression in A549 cells, indicating that JD88 initiates apoptosis through pathways not solely reliant on SMAC/Diablo regulation. Moreover, the high baseline levels of SMAC/Diablo in untreated A549 cells may also suggest its availability for possible involvement in promoting apoptosis.

Similarly, the decline in HTRA2/Omi expression post-JD88 treatment suggests an alternative mechanism for inducing apoptosis. While HTRA2/Omi typically opposes XIAP, its reduced expression post-JD88 treatment did not inhibit apoptosis. This aligns with Gmeiner *et al*., (2015), where HTRA2/Omi inhibition instigated apoptosis in prostate cancer cells, highlighting the complex roles of apoptotic proteins in cell death mediation. A decrease in SMAC/Diablo expression in HT-29 colorectal cancer cells post-JD88 treatment, consistent with this study was observed and similarly, apoptosis occurred despite this decrease (Harmse *et al.*, 2919). Conversely, an increase in SMAC/Diablo levels was observed in HL-60 and K562 leukaemia cells post-JD88 treatment (Ismail *et al*., 2022). These variations highlight the unique effects of JD88 on different proteins, dependent on the specific cell line context.

The experimental data suggest that despite SMAC/Diablo and HTRA2/Omi downregulation by JD88, IAPs, such as XIAP, which are controlled by these proteins, were still suppressed by the complex. This highlights the concept that JD88 may induce apoptosis by offsetting the balance between anti- and pro-apoptotic proteins through reducing those proteins that inhibit apoptosis so that a lower threshold for apoptosis induction may be reached.

4.9.6 The effect of JD88 on HIF-1α, PON2, HMOX1, and HMOX2 expression in A549 cells

The effects of stress-related proteins post JD88 and Doxorubicin were assessed in the protein array. Both compounds differentially altered the expression of HIF-1α, PON2, HMOX1, and HMOX2, proteins which are crucial in cellular stress responses.

HMOX1 (HO-1/HSP32) and HMOX2 (HO-2), are recognised as stress-induced survival factors (Jozkowicz *et al*., 2007). These proteins are vital for cellular defence against oxidative stress, guarding against free radical damage (Chiang *et al*., 2018). In untreated A549 cells,

HMOX1 showed moderately high expression. Post-JD88 treatment, its expression declined insignificantly, while doxorubicin led to a significant 85% increase. Conversely, HMOX2 exhibited moderate baseline expression, insignificantly decreasing after JD88 treatment, and significantly increasing by 113% with doxorubicin. These findings align with doxorubicin's known role as a free radical producer, increasing oxidative stress-inducing proteins *via* the Nrf2/ARE pathway (Pronk *et al*., 2014). While JD88 treatment did not significantly impact HMOX1 and HMOX2 in A549 cells, other studies involving similar compounds noted moderate expressions of HMOX1 and HMOX2 in untreated HT-29 colorectal cancer cells. These showed a significant upregulation in HMOX1 while minimally affecting HMOX2 post-JD88 treatment (Harmse *et al*., 2019). Additionally, minimal HMOX1 expression was observed in untreated HL-60 and K562 leukaemia cells, with a marked increase noted in HL-60 cells post-treatment with active copper-imidazo[1,2-*a*]pyridines (Ismail *et al*., 2022). This highlights the variation in the responses of various cell types to these compounds.

HIF-1α, a key regulator of HMOX1 gene transcription linked to hypoxia-induced apoptosis (Greijer and Van der Wall, 2004), showed moderate expression in A549 control cells. Its expression decreased non-significantly after JD88 treatment but significantly increased by 115% after doxorubicin treatment. In contrast, a similar study on HT-29 cells reported a significant increase in HIF-1α expression post-treatment with copper-imidazo[1,2-*a*]pyridines, suggesting a cell-type-specific response (Harmse *et al*., 2019).

PON2, a protein with antioxidative functions, shields cells from oxidative stress and counters ER stress-induced apoptosis (Witte *et al*., 2011). Baseline expression of PON2's was high and decreased significantly by 41% with JD88 treatment but was not affected after treatment with doxorubicin. Reduced PON2 expression can intensify ROS production, inducing apoptosis (Parween and Gupta, 2022). Given the increase in ROS production following JD88 treatment the decrease of PON2 may have compromised the cells' antioxidative defence, increasing ROS levels and promoting apoptosis.

4.9.7 The effect of JD88 on heat shock proteins in A549 cells

Proteomic analysis showed changes in the expression of heat shock proteins (HSPs) in A549 lung cancer cells post-treatment with JD88 and doxorubicin.

HSP27 baseline expression was high in untreated A549 cells. This was modified and insignificantly suppressed by JD88 post-treatment, whereas doxorubicin significantly increased HSP27 expression by 81%. Given the prevalent upregulation of HSP27 in various

cancers and its association with an unfavourable prognosis (Ciocca and Calderwood, 2005), the significant increase post-doxorubicin treatment might contribute to chemotherapy resistance. Supporting this, Lampros *et al*., (2022) found that HSP27 often enhances the Akt/mTOR signalling cascade and inhibits p53, obstructing chemotherapy-induced apoptosis. Given that p53 was highly upregulated in both JD88 and doxorubicin-treated cells, the effects of HSP27 may be overcome, therefore enabling apoptosis to proceed after these treatments.

The baseline expression of HSP60 was high in A549 cells. Post-treatment, JD88 led to a significant 35% decrease, whereas doxorubicin caused a non-significant increase in the expression of the protein. Considering HSP60's role as a crucial chaperonin in proper protein folding and its anti-apoptotic activity (Gupta and Knowlton, 2002), the reduction following JD88 treatment suggests potential pro-apoptotic activity.

HSP70, moderately expressed at baseline in A549 cells, had a significant 35% reduction post-JD88 exposure and an 83% significant increase post-doxorubicin treatment. Known for its anti-apoptotic and cytoprotective characteristics (Beere and Green, 2001), the decreased expression post-JD88 suggests a potential shift towards a pro-apoptotic environment, possibly challenging its protective role in chemotherapy.

Numerous studies have demonstrated the impact of reduced HSP levels on tumour progression. For instance, reduced HSP70 expression has been associated with impeded cancer cell growth, migration, and invasion across various cancer types (Cyran and Zhitkovich, 2022). While this data supports the hypothesis that diminished HSP levels could enhance cancer cell susceptibility to apoptosis, further research is necessary to delineate the direct impact of JD88 on apoptotic pathways.

4.9.8 The effect of JD88 on procaspase-3 and cleaved caspase-3 in A549 cells

Caspase-3 is a crucial player in the execution phase of cell apoptosis. It exists in cells as an inactive precursor, procaspase-3, which is activated through cleavage to form active caspase-3 (McIlwain *et al*., 2013). The high level of procaspase-3 expression in control A549 cells suggests a potential for these cells to undergo apoptosis when appropriately stimulated.

Treatment with JD88 resulted in a significant increase in procaspase-3 levels, suggesting that JD88 may be inducing apoptosis in these cells. However, the decrease in cleaved caspase-3 levels indicates that the conversion of procaspase-3 to its active form may be inhibited. This could potentially be due to the presence of inhibitors of apoptosis proteins (IAPs) that can block

caspase activation (Fulda and Vucic, 2012.). Conversely, treatment with doxorubicin resulted in a decrease in procaspase-3 levels, which could be due to the conversion of procaspase-3 to its active form. However, the highly significant decrease in cleaved caspase-3 levels suggests that doxorubicin treatment may be leading to the degradation of active caspase-3.

The activation of caspase 3/7 in apoptotic marker assays for both JD88 and doxorubicin, despite the decrease in cleaved caspase-3 levels, suggests that other caspases or pathways may be involved in the induction of apoptosis. Caspase-7, like caspase-3, is also an executioner caspase and can carry out a similar role in the apoptosis process (McIlwain *et al*., 2013). Therefore, it is possible that caspase-7 could be compensating for the decrease in cleaved caspase-3 levels.

These results highlight the complex nature of the apoptotic response and suggest that both JD88 and doxorubicin may be influencing apoptosis in A549 cells through different mechanisms. Further studies are needed to fully understand these mechanisms and their implications for the anticancer potential of JD88.

4.9.9 The effect of JD88 on death receptor proteins in A549 cells

Death receptors, such as TRAIL R1/DR4, TRAIL R2/DR5, Fas/TNFRSF6, and TNF RI, play crucial roles in the extrinsic apoptosis pathway. The binding of death ligands to these receptors initiates the pathway, leading to the formation of the death-inducing signalling complex (DISC) and subsequent caspase-8 activation, triggering apoptosis (Oh and Sun, 2021; Sayers, 2011).

In the A549 control cells, baseline expression of both TRAIL R1/DR4 and TRAIL R2/DR5 was low. Following treatment TRAIL R1/DR4's expression significantly decreased by 44% with JD88 and increased by 170% with doxorubicin. In a similar manner, TRAIL R2/DR5 demonstrated a non-significant decrease of 21% with JD88 and a significant increase of 331% with doxorubicin. The increase in these receptors with doxorubicin suggests its potential to promote apoptosis in A549 cells, consistent with its recognized role in inducing death receptor expressions across varied cell types (Zhao and Zhang, 2017). However, JD88's effects on apoptosis signalling pathways appear to operate differently, not relying on cell death signalling. This is in contrast to a similar study where treatment of HT-29 colorectal cancer cells with JD88 induced a significant increase in TRAIL R2/DR5 expression where it was initially low at baseline (Harmse *et al*., 2019).

Fas expression was moderate at baseline in A549 cells, decreasing significantly by 45% and 206% with JD88 and doxorubicin treatment respectively. FADD, also moderately expressed at

baseline in A549 cells, showed a significant 35% reduction post-JD88 treatment and a 47% increase with doxorubicin treatment.

TNF RI, with high baseline expression in A549 cells, was significantly reduced by 55% and 53% with JD88 and doxorubicin treatment, respectively. The decreased expression of TNF-R1 following JD88 treatment is notable as TNF-R1 is essential for NF-κB signalling and its reduced expression could restrict NF-κB transcriptional activity. Given the diverse roles of NF-κB in cell survival, inflammation, immunity, apoptosis, and cancer progression (Brenner *et al*., 2015), this potential restriction might be linked to JD88's pro-apoptotic effects in A549 cells.

The downregulation of death receptors by JD88 treatment suggests its potential to induce apoptosis through alternative mechanisms. This aligns with the observed increased activation of caspase-8 at 24 and 48 hours after treatment with JD88 in the apoptotic marker assays. This caspase-8 activity, possibly arising from other upstream signals likely converges on caspase-8 activation. In a similar context, caspase-8 activation can also be triggered by ER stress responses, independent of death receptor involvement (Szegezdi *et al*., 2006).

V. Conclusion

The purpose of this study was to identify new compounds that may be beneficial in the treatment of lung cancer and to study their mechanisms of inducing cell death. Four different classes of compounds, the epidermal growth factor receptor kinase inhibitors (EKIs), copper-imidazo[*1,2-a*]pyridine complexes (JDs), copper-theophylline conjugates (AD compounds), as well as copper-complexed OM compounds were evaluated. The copper-imidazo[1,2-*a*]pyridines were the most active in inhibiting cell growth in A549 lung cancer cells, with IC_{50} values in the low micromolar range. Therefore, the copper-imidazo[1,2-*a*]pyridines were further investigated to determine their mode of cell death and were found to induce apoptotic cell death. Immunohistochemistry assays showed that changes in p21 and p53 expression and distribution were important contributors to copper complex-induced apoptosis. Furthermore, apoptotic proteomics analysis on the most potent copper-imidazo[1,2-a]pyridine, JD88, showed that the copper complex changed the profile of the apoptotic proteome.

5.1 Copper-imidazo[1,2-*a*]pyridines are cytotoxic on the A549 cell line

In this study the cytotoxic activity of 20 compounds belonging to four classes of agents against A549 lung cancer cells was evaluated. The copper-imidazo[1,2-*a*]pyridine complexes were found to be the most cytotoxic, with JD35, JD46, JD47 and JD88 identified as the most potent having all having IC_{50} values less than 4 µM. Further investigation into the structure-activity function of the complexes also showed that halogen substitutions at the 5^{th} or 6^{th} positions of the copper-imidazo[1,2-*a*]pyridine complexes, as seen with JD47 and JD88, increased their cytotoxicity.

5.2 Copper-imidazo[1,2-*a*]pyridines induce apoptosis in A549 lung cancer cells

The morphological evaluation of A549 cells treated with the most active copper-imidazo[1,2-*a*]pyridine complexes, particularly JD35, JD46, JD47, and JD88, showed the absence of necrotic cell death and indicated that apoptosis was the most likely form of cell death. This was supported by changes in the morphology of the cells such as vacuolisation, fragmented nuclei, chromatin condensation, lysosomal aggregation, and nuclear fragmentation, which are all features of apoptosis. No signs of necrosis were observed, which is important since, unlike necrosis, apoptosis does not contribute to inflammation, which is associated with tumour lysis syndrome and patient morbidity.

Apoptosis as a cell death mechanism of the copper-imidazo[1,2-*a*]pyridines (JD35, JD46, JD47 and JD88) was further supported by the increased presence of phosphatidyl-serine on the outer

leaflet of the plasma membranes of treated A549 cells as indicated by Annexin-V binding. After 18 hours post-treatment with these complexes, there was an increase in dual Annexin-V/PI staining, indicating mid to late apoptosis. These findings suggest that apoptotic changes are already evident after 6 hours of exposure to the compounds since Annexin-V binding is an early indicator of apoptosis.

All copper-imidazo[1,2-*a*]pyridines caused an increase in caspase-3/7 activity after 24 and 48 hours post treatment, with JD46 showing the highest increase in caspase 3/7 activity at both treatment periods. Taken together, the translocation of PS and the increase in caspase-3/7 activity provides further evidence for apoptotic cell death.

5.3 Copper-imidazo[1,2-*a*]pyridines induce reactive oxygen species in A549 lung cancer cells

Copper-imidazo[1,2-*a*]pyridine complexes induce the production of ROS in A549 lung cancer cells. The intensity of ROS production was found to be time-dependent, with highest ROS observed at 6 hours after treatment. The complexes JD35 and JD88 were found to be the most potent inducers of ROS at both 6 and 18 hours, while JD46 and JD47 were less active.

The production of ROS is known to induce oxidative stress, which can lead to DNA damage, trigger apoptosis, and cause cell death. Therefore, the ability of copper-imidazo[1,2-*a*]pyridine complexes to induce ROS production in lung cancer cells further suggests that they are cytotoxic and may mediate apoptotic cell death by oxidative stress. Since cancer cells have a high metabolic rate and innate oxidative stress, the additional oxidative stress caused by the copper complexes would be sufficient to activate apoptotic pathways.

Moreover, the heightened ROS levels in A549 cells post treatment with the complexes suggest potential downstream mitochondrial damage due to ROS production, potentially inducing intrinsic apoptosis *via* mitochondrial membrane damage.

5.4 Copper-imidazo[1,2-*a*]pyridines induce intrinsic and extrinsic apoptosis in A549 lung cancer cells

The loss of MMP in A549 lung cancer cells after treatment with the copper-imidazo[1,2-*a*]pyridines, lead to mitochondrial dysfunction and apoptosis. The active complexes JD35, JD46, JD47, and JD88 displayed granular green fluorescence and the absence of red fluorescence at 12 hours post treatment, indicating a loss in MMP. By 18 hours, all cells treated with the copper complexes showed predominantly smooth green fluorescence, indicative of low membrane potential and mitochondrial disruption. These findings suggest that a loss of

MMP is the key mechanism by which these complexes induce apoptosis in lung cancer cells and suggest activation of the intrinsic apoptotic pathway, potentially mediated by ROS generation.

Treatment of A549 cells with copper-imidazo[1,2-*a*]pyridines significantly increased caspase-8 activity after 24 and 48 hours, with JD46 demonstrating the highest elevation in caspase-8 activity during both treatment periods. Interestingly, heightened caspase-8 activity corresponded to significant cellular damage, while cells maintaining structural integrity displayed subdued caspase-8 signals. This unexpected finding indicates a delayed caspase-8 activation, contrary to its typical early occurrence. Notably, such delayed activation is associated with the inhibition of the NFKB pathway. This suggests a complex interplay between caspase-8 and the NFKB pathway, where caspase-8 activation may act as a late event contributing to cellular damage rather than an early trigger of apoptosis. This unexpected role of caspase-8 in the inhibition of the NFKB pathway highlights the intricate regulatory mechanisms underlying the cytotoxic effects of copper-imidazo[1,2-*a*]pyridines in A549 cells.

5.5 Immunohistochemical analysis of copper-imidazo[1,2-a]pyridines shows nuclear p21 and nuclear phospho-p53(S15) expression in A549 cells

The immunohistochemical analysis of the impact of copper-imidazo[1,2-*a*]pyridines on p21 and p53 expression in A549 lung cancer cells provided significant insights into the potential anticancer mechanisms of these complexes.

An increase in nuclear p21 expression was observed in all cells treated with copper-imidazo[1,2-*a*]pyridines, especially following JD35 treatment. This increase suggests a DNA damage response, implying that copper-imidazo[1,2-*a*]pyridines could potentially enhance the expression of nuclear p21 and associated pathways, thereby favouring apoptosis.

In addition, post-treatment, there was a substantial increase in nuclear phospho-p53(S15) signal in all treatments, especially after JD46 and JD88 treatments. This increase, which was concurrent with visible cellular damage, suggests potential DNA damage induced by these complexes. This implies that copper-imidazo[1,2-*a*]pyridines induce DNA damage, leading to the activation of p53. This observation is consistent with previous findings of increased ROS formation, often associated with p53 activation in response to DNA damage. The ROS stimulation by the copper-imidazo[1,2-*a*]pyridines can potentially upregulate p53 expression and trigger apoptosis, which may be a significant contributor to the cytotoxic activity and

apoptosis induction in these complexes. Furthermore, the elevated phospho-p53(S15) signal indicates the inhibition of degradation by MDM2, resulting in enhanced p53 stabilization and nuclear accumulation, which facilitates its apoptotic function.

Collectively, these findings suggest that copper-imidazo[1,2-*a*]pyridines may induce DNA damage, leading to the activation of p21 and p53, key regulators of cell cycle and apoptosis. However, further investigations are necessary to fully comprehend the complex roles of p21 and p53 in mediating the observed effects and to explore the potential of copper-imidazo[1,2-*a*]pyridines as anticancer agents.

5.6 The most active copper-imidazo[1,2-a]pyridine-JD88 modulates the apoptotic proteome expression in A549 lung cancer cells

The findings of the proteomics analysis suggest that JD88, the most potent copper-imidazo[1,2-a]pyridine, induces apoptosis in A549 lung cancer cells by affecting several key proteins and pathways.

5.6.1 JD88 increases the expression of phosphorylated p53 in A549 cells

JD88 significantly upregulated three phosphorylated forms of p53: phospho-p53 (S15), phospho-p53 (S46), and phospho-p53 (S392). These phosphorylation events are recognized for their role in enhancing p53's stability and transcriptional activation, critical for its function as a tumour suppressor protein that triggers growth arrest and apoptosis in response to cellular stress. This pronounced elevation of multiple p53 species, particularly in A549 cells where wild-type p53 typically exists at low levels, holds immense significance. It has the potential to counteract anti-apoptotic pathways that may arise following treatment with copper-imidazo[1,2-*a*]pyridines such as JD88, especially since p53 activates pro-apoptotic proteins. Furthermore, this significant increase in p53 species may have the main influence on JD88's cytotoxicity and function.

5.6.2 JD88 decreased expression of pro-apoptotic Bax and Bad and anti-apoptotic Bcl-2 and Bcl-xL proteins

JD88 treatment in A549 cells demonstrated a reduction in both pro-apoptotic Bad and Bax proteins, alongside the anti-apoptotic Bcl-2 and Bcl-xL proteins. This alteration in the pro- and anti-apoptotic protein balance, particularly the decrease in anti-apoptotic Bcl-2 and Bcl-xL by JD88, potentially encourages apoptosis despite lower levels of Bad and Bax. The substantial increase in p53 following JD88 treatment might counteract this downregulation of pro-apoptotic proteins, as it is known to enhance their expression. This suggests that by decreasing

anti-apoptotic proteins and activating proteins such as p53 that support apoptosis, JD88 can shift the pro- and anti-apoptotic protein balance and push cells towards a pro-apoptotic state *via* the intrinsic mitochondrial pathway, which is supported by findings indicating disruption of MMP in A549 cells from the apoptotic marker assays.

5.6.3 JD88 suppressed IAP expression and, SMAC/Diablo and HTRA2/Omi expression, in A549 cells

JD88 significantly suppressed IAPs, notably XIAP, cIAP-2, and survivin, in A549 cells. It also reduced pro-apoptotic HTRA2/Omi and SMAC/Diablo. Despite these reductions, JD88 consistently inhibited IAPs, promoting apoptosis. Its ability to decrease XIAP levels, a potent inhibitor of caspase enzymes, indicates JD88's capacity to counteract the anti-apoptotic effects of IAPs. This is reinforced by the observed increase in caspase 3/7 activity in apoptotic marker assays. Notably, JD88 altered cIAP-1 and cIAP-2 levels, increasing cIAP-1 while suppressing cIAP-2. These changes may suppress the NF-κB pathway, crucial for cancer cell survival and chemoresistance. The concurrent decrease in IAP levels supports this, given that NF-κB regulates IAP transcription, thereby impacting their expression.

5.6.4 JD88 decreased expression of death receptor proteins in A549 cells

JD88 treatment led to a notable decrease in death receptors, specifically TRAIL R1/DR4, TRAIL R2/DR5, Fas/TNFRSF6, and TNF RI, indicating its potential to induce apoptosis through alternate mechanisms. This aligns with the observed increased caspase-8 activation at 24 and 48 hours post JD88 treatment in apoptotic marker assays, suggesting a pathway beyond death receptor activation.

Furthermore, TNF-R1 expression was reduced in JD88-treated A549 cells. This reduction in TNF-R1 expression is significant as TNF-R1 plays a pivotal role in NF-κB signaling. Its decreased expression suggests a potential limitation in NF-κB transcriptional activity. Considering NF-κB's various cell functions, including survival, inflammation, immunity, and cancer progression, this inhibition might contribute to JD88's pro-apoptotic effects in A549 cells.

5.6.5 JD88 decreased the expression of HSPs, HMOX-2 and PON2

JD88 treatment resulted in decreased expression of heat shock proteins 27, 60, and 70, known for their inhibitory role on p53, cytoprotective functions, and anti-apoptotic effects, contributing to tumour progression. This decrease in HSP levels supports the hypothesis that lowering HSP levels may render cancer cells more susceptible to apoptosis.

Additionally, JD88 induced oxidative stress and apoptotic cell death by hindering the protective actions of HMOX-2 and reducing PON2 expression. Decreased PON2 expression can amplify ROS generation, leading to apoptosis. Considering the elevated ROS production following JD88 treatment, the reduced PON2 expression might have compromised the cells' antioxidant defence, elevating ROS levels, and promoting apoptosis

5.7 Summary of investigation

The results of this study demonstrate that copper-imidazo[1,2-*a*]pyridine complexes possess potent cytotoxic activity against A549 lung cancer cells. The four most potent complexes, JD35, JD46, JD47, and JD88 had IC_{50} values less than 4 μM, and induced apoptosis in A549 cells by modifying cell morphology, inducing ROS production, increasing Annexin-V binding, activating caspase-3/7 and caspase-8, and causing a loss of mitochondrial membrane potential. These findings highlight the potential of copper-imidazo[1,2-*a*]pyridine complexes as effective anticancer agents that induce apoptosis in cancer cells.

Furthermore, this study provides insight into the mechanism of cell death induced by these complexes. The study shows that the mechanism of cell death involves the activation of cellular proteins such as p21 and p53. These proteins were previously implicated in the apoptosis pathway, providing further support for the involvement of apoptosis in the cell death induced by these complexes.

In the context of the proteomics analysis, JD88, the most potent copper-imidazo[1,2-a]pyridine, demonstrate diverse effects on apoptosis-related proteins in A549 lung cancer cells. It notably increases the expression of multiple phosphorylated p53 species (S15, S46 and S392), essential for stabilizing and activating p53, known to induce cell cycle arrest and apoptosis under stress conditions. Simultaneously, JD88 causes a shift in the expression balance of pro- and anti-apoptotic proteins, reducing Bax, Bad, Bcl-2, and Bcl-xL. These alterations potentially push cells towards apoptosis *via* the intrinsic mitochondrial pathway. Furthermore, JD88 suppresses inhibitors of apoptosis (IAPs) like XIAP, cIAP-2 and survivin, while concurrently affecting HTRA2/Omi and SMAC/Diablo, reinforcing apoptotic signalling pathways. In addition to these effects, JD88 also downregulated death receptors and TNF-R1, possibly initiating apoptosis through alternate routes and limiting NF-κB signalling. Finally, JD88's action on HSPs, HMOX-2, and PON2 highlight its potential to sensitize cancer cells to apoptosis by decreasing their protective and anti-apoptotic functions and increasing oxidative stress-mediated apoptosis.

These comprehensive findings emphasize that the overall balance between pro- and anti-apoptotic proteins, rather than any specific protein target, determine whether cells survive or undergo apoptosis upon treatment with copper-imidazo[1,2-*a*]pyridine complexes.

5.8 Limitations

This study provides valuable insights into the potential of copper-imidazo[1,2-a]pyridine complexes in treating lung cancer cells. However, it is essential to acknowledge some limitations. Primarily, the research focused on one lung cancer cell line, necessitating the investigation of multiple cell lines to confirm the broad efficacy of these complexes.

One significant limitation of this study was the lack of investigation into the effects of the test compounds, JD35, JD46, JD47, and JD88, on non-tumour human cell lines, such as BEAS-2Bs, especially during the screening phases of the study. This would have yielded much-needed scientific knowledge on the possible toxic effects of these compounds on normal epithelial cells in the lungs. Many chemotherapeutic agents, especially platinum-based drugs, although effective against cancerous cells, are known to be harmful to normal human cells. Therefore, assessing the viability or cytotoxic effects of these compounds on non-tumour human cell lines would have provided crucial information about their selectivity and safety.

Expanding into *in vivo* animal studies would provide further insight into their effectiveness and any potential adverse reactions, thereby providing stronger evidence for future clinical trials. Despite these limitations, the study has laid a solid foundation for further research into the therapeutic potential of copper-imidazo[1,2-a]pyridine complexes in the treatment of lung cancer. Future studies should aim to address these limitations to provide a more comprehensive understanding of these complexes' therapeutic potential.

5.9 Future directions

Future research should prioritize expanding into animal studies and toxicity evaluations alongside pharmacokinetic investigations to determine the availability and potential toxicity of the copper-imidazo[1,2-*a*]pyridine complexes. Additional studies encompassing other lung cancer cell lines and *in vivo* validation are necessary to confirm their effectiveness. Evaluating these compounds' harm in normal cells and their effectiveness against drug resistance is crucial. Furthermore, exploring 3D cell culture models preceding animal studies may provide deeper insights into these complexes' mechanisms of action. Structural modifications in these complexes should also be considered to improve their cytotoxic activity and specificity towards cancer cells.

In conclusion**,** this study offers promising evidence regarding the potential of copper-imidazo[1,2-*a*]pyridine complexes against A549 lung cancer cells. These findings warrant further investigation to determine the potential clinical application of these complexes as future anti-cancer agents.

References

Abbas, T. and Dutta, A., 2009. p21 in cancer: intricate networks and multiple activities. *Nature Reviews Cancer*,*9*(6), pp.400-414.

Abraha, A.M. and Ketema, E.B., 2016. Apoptotic pathways as a therapeutic target for colorectal cancer treatment. *World journal of gastrointestinal oncology*,*8*(8), p.583.

Abuetabh, Y., Wu, H.H., Chai, C., Al Yousef, H., Persad, S., Sergi, C.M. and Leng, R., 2022. DNA damage response revisited: the p53 family and its regulators provide endless cancer therapy opportunities. *Experimental & Molecular Medicine*, *54*(10), pp.1658-1669.

Abukhdeir, A.M. and Park, B.H., 2008. P21 and p27: roles in carcinogenesis and drug resistance. *Expert reviews in molecular medicine*, *10*, p.e19.

Akhtar, N. and Bansal, J.G., 2017. Risk factors of Lung Cancer in nonsmokers. *Current problems in cancer*, *41*(5), pp.328-339.

Alberts, B., Johnson, A., Lewis, J., Raff, M., Roberts, K. and Walter, P., 2015. Cancer as a microevolutionary process. In *Molecular Biology of the Cell. 4th edition*. Garland Science.

Al-Shahrabani, F., Vallböhmer, D., Angenendt, S. and Knoefel, W.T., 2014. Surgical strategies in the therapy of non-small cell lung cancer. *World Journal of Clinical Oncology*, *5*(4), p.595.

Amos, C.I., Wu, X., Broderick, P., Gorlov, I.P., Gu, J., Eisen, T., Dong, Q., Zhang, Q., Gu, X., Vijayakrishnan, J. and Sullivan, K., 2008. Genome-wide association scan of tag SNPs identifies a susceptibility locus for lung cancer at 15q25. 1. *Nature genetics*, *40*(5), pp.616-622.

Azzoli, C.G., Baker Jr, S., Temin, S., Pao, W., Aliff, T., Brahmer, J., Johnson, D.H., Laskin, J.L., Masters, G., Milton, D. and Nordquist, L., 2009. American Society of Clinical Oncology clinical practice guideline update on chemotherapy for stage IV non–small-cell lung cancer. *Journal of clinical oncology*,*27(36*), p.6251-6266

Baig, S., Seevasant, I., Mohamad, J., Mukheem, A., Huri, H.Z. and Kamarul, T., 2016. Potential of apoptotic pathway-targeted cancer therapeutic research: Where do we stand?. *Cell death & disease*, *7*(1), pp.e2058-e2058.

Banerjee, K., Basu, S., Das, S., Sinha, A., Biswas, M.K. and Choudhuri, S.K., 2016. Induction of intrinsic and extrinsic apoptosis through oxidative stress in drug-resistant cancer by a newly synthesised Schiff base copper chelate. *Free radical research*, *50*(4), pp.426-446.

Beere, H.M. and Green, D.R., 2001. Stress management–heat shock protein-70 and the regulation of apoptosis. *Trends in cell biology*, *11*(1), pp.6-10.

Berrouet, C., Dorilas, N., Rejniak, K.A. and Tuncer, N., 2020. Comparison of drug inhibitory effects (IC 50) in monolayer and spheroid cultures. *Bulletin of Mathematical Biology*, *82*(6), p.68.

Bhat, S.S., Kumbhar, A.A., Heptullah, H., Khan, A.A., Gobre, V.V., Gejji, S.P. and Puranik, V.G., 2011. Synthesis, electronic structure, DNA and protein binding, DNA cleavage, and anticancer activity of fluorophore-labeled copper (II) complexes. *Inorganic chemistry*, *50*(2), pp.545-558.

Bialik, S., Dasari, S.K. and Kimchi, A., 2018. Autophagy-dependent cell death–where, how and why a cell eats itself to death. *Journal of cell science*, *131*(18), p.jcs215152.

Borghaei, H., Paz-Ares, L., Horn, L., Spigel, D.R., Steins, M., Ready, N.E., Chow, L.Q., Vokes, E.E., Felip, E., Holgado, E. and Barlesi, F., 2015. Nivolumab versus docetaxel in advanced nonsquamous non–small-cell lung cancer. *New England Journal of Medicine*, *373*(17), pp.1627-1639.

Bradford MM (1976). A rapid and sensitive method for quantitating microgram quantities of protein utilising the principle of protein-dye binding. *Anal Biochem* **72:** 248-254.

Brenner, D., Blaser, H. and Mak, T.W., 2015. Regulation of tumour necrosis factor signalling: live or let die. *Nature Reviews Immunology*, *15*(6), pp.362-374.

Burnet, M., 1957. Cancer—a biological approach: I. The processes of control. II. The significance of somatic mutation. *British medical journal*, *1*(5022), p.779.

Cai, Y.Y., Li, L., Zhu, X.M., Lu, J.P., Liu, X.H. and Lin, F.C., 2022. The crucial role of the regulatory mechanism of the Atg1/ULK1 complex in fungi. *Frontiers in Microbiology*, *13*, p.1019543.

Cai, Z., Jitkaew, S., Zhao, J., Chiang, H.C., Choksi, S., Liu, J., Ward, Y., Wu, L.G. and Liu, Z.G., 2014. Erratum: Plasma membrane translocation of trimerised MLKL protein is required for TNF-induced necroptosis. *Nature Cell Biology*, *16*(2), pp.200-200.

Cazzalini, O., Scovassi, A.I., Savio, M., Stivala, L.A. and Prosperi, E., 2010. Multiple roles of the cell cycle inhibitor p21CDKN1A in the DNA damage response. *Mutation Research/Reviews in Mutation Research*, *704*(1-3), pp.12-20.

Chan, F.K.M., Luz, N.F. and Moriwaki, K., 2015. Programmed necrosis in the cross talk of cell death and inflammation. *Annual review of immunology*, *33*, pp.79-106.

Ciocca, D.R. and Calderwood, S.K., 2005. Heat shock proteins in cancer: diagnostic, prognostic, predictive, and treatment implications. *Cell stress & chaperones*, *10*(2), pp.86-103.

Cooper, W.A., Lam, D.C., O'Toole, S.A. and Minna, J.D., 2013. Molecular biology of lung cancer. *Journal of thoracic disease*, *5*(Suppl 5), p.S479.

Crowley, L.C., Chojnowski, G. and Waterhouse, N.J., 2016a. Measuring the DNA content of cells in apoptosis and at different cell-cycle stages by propidium iodide staining and flow cytometry. *Cold Spring Harbor Protocols*, *2016*(10), pp.pdb-prot087247.

Crowley, L.C., Marfell, B.J., Scott, A.P., Boughaba, J.A., Chojnowski, G., Christensen, M.E. and Waterhouse, N.J., 2016b. Dead cert: measuring cell death. *Cold Spring Harb. Protoc*, *2016*(12), pp.1064-1072.

Cruz, C.S.D., Tanoue, L.T. and Matthay, R.A., 2011. Lung cancer: epidemiology, etiology, and prevention. *Clinics in chest medicine*, *32*(4), pp.605-644.

Cyran, A.M. and Zhitkovich, A., 2022. Heat shock proteins and HSF1 in cancer. *Frontiers in Oncology*, *12*.

Czabotar, P.E., Lessene, G., Strasser, A. and Adams, J.M., 2014. Control of apoptosis by the BCL-2 protein family: implications for physiology and therapy. *Nature reviews Molecular cell biology*, *15*(1), pp.49-63.

Dam, J., Ismail, Z., Kurebwa, T., Gangat, N., Harmse, L., Marques, H.M., Lemmerer, A., Bode, M.L. and de Koning, C.B., 2017. Synthesis of copper and zinc 2-(pyridin-2-yl) imidazo [1, 2-*a*] pyridine complexes and their potential anticancer activity. *European journal of medicinal chemistry*, *126*, pp.353-368

Dam, J., Ismail, Z., Kurebwa, T., Gangat, N., Harmse, L., Marques, H.M., Lemmerer, A., Bode, M.L. and de Koning, C.B., 2017. Synthesis of copper and zinc 2-(pyridin-2-yl) imidazo [1, 2-a] pyridine complexes and their potential anticancer activity.*European journal of medicinal chemistry*, *126*, pp.353-368

De Biasi, S., Gibellini, L. and Cossarizza, A., 2015. Uncompensated polychromatic analysis of mitochondrial membrane potential using JC-1 and multilaser excitation. *Current protocols in cytometry*, *72*(1), pp.7-32.

de Groot, P. and Munden, R.F., 2012. Lung cancer epidemiology, risk factors, and prevention. *Radiologic Clinics*, *50*(5), pp.863-876.

Dhup, S., Kumar Dadhich, R., Ettore Porporato, P. and Sonveaux, P., 2012. Multiple biological activities of lactic acid in cancer: influences on tumor growth, angiogenesis and metastasis. *Current pharmaceutical design*, *18*(10), pp.1319-1330.

Done, G., Ari, F., Akgun, O., Akgun, H., Cevatemre, B. and Gençkal, H.M., 2022. The Mechanism for Anticancer and Apoptosis-Inducing Properties of Cu (II) Complex with Quercetin and 1, 10-Phenanthroline. *ChemistrySelect*, *7*(38), p.e202203242.

Estaquier, J., Vallette, F., Vayssiere, J.L. and Mignotte, B., 2012. The mitochondrial pathways of apoptosis. *Advances in mitochondrial medicine*, pp.157-183.

Evans, M., 2013. Lung cancer: needs assessment, treatment and therapies. *British Journal of Nursing*, *22*(Sup17), pp.S15-S22.

Ferlay, J., Colombet, M., Soerjomataram, I., Parkin, D.M., Piñeros, M., Znaor, A. and Bray, F., 2021. Cancer statistics for the year 2020: An overview. *International Journal of Cancer*, *149*(4), pp.778-789.Fiala, C. and Diamandis, E.P., 2020. Mutations in normal tissues—some diagnostic and clinical implications. *BMC Medicine*, *18*(1), pp.1-9.

Foo, J.B., Ng, L.S., Lim, J.H., Tan, P.X., Lor, Y.Z., Loo, J.S.E., Low, M.L., Chan, L.C., Beh, C.Y., Leong, S.W. and Yazan, L.S., 2019. Induction of cell cycle arrest and apoptosis by copper complex Cu (SBCM) 2 towards oestrogen-receptor positive MCF-7 breast cancer cells. *RSC advances*, *9*(32), pp.18359-18370

Freshney, R.I., 2015. *Culture of animal cells: a manual of basic technique and specialised applications*. John Wiley & Sons.

Fujiwara, K., Daido, S., Yamamoto, A., Kobayashi, R., Yokoyama, T., Aoki, H., Iwado, E., Shinojima, N., Kondo, Y. and Kondo, S., 2008. Pivotal role of the cyclin-dependent kinase inhibitor p21WAF1/CIP1 in apoptosis and autophagy. *Journal of Biological Chemistry*, *283*(1), pp.388-397.

Fulda, S. and Vucic, D., 2012. Targeting IAP proteins for therapeutic intervention in cancer. *Nature Reviews Drug discovery*, *11*(2), pp.109-124.

Fulda, S., 2014. Molecular Pathways: Targeting Inhibitor of Apoptosis Proteins in Cancer—From Molecular Mechanism to Therapeutic ApplicationTargeting IAP Proteins in Cancer. *Clinical Cancer Research*, *20*(2), pp.289-295.

Gadgeel, S.M., Ramalingam, S.S. and Kalemkerian, G.P., 2012. Treatment of lung cancer. *Radiologic Clinics, 50(5)*, pp.961-974.

Galluzzi, L., Vitale, I., Aaronson, S.A., Abrams, J.M., Adam, D., Agostinis, P., Alnemri, E.S., Altucci, L., Amelio, I., Andrews, D.W. and Annicchiarico-Petruzzelli, M., 2018. Molecular mechanisms of cell death: recommendations of the Nomenclature Committee on Cell Death 2018. *Cell Death & Differentiation*, *25*(3), pp.486-541.

Gao, Y.-L., Zhai, J.-H., and Chai, Y.-F. (2018). Recent Advances in the Molecular Mechanisms Underlying Pyroptosis in Sepsis. *Mediators Inflamm.* 2018, 1–7.

Garg, H., Suri, P., Gupta, J.C., Talwar, G.P. and Dubey, S., 2016. Survivin: a unique target for tumor therapy. *Cancer cell international*, *16*(1), pp.1-14.

Garraway, L.A. and Lander, E.S., 2013. Lessons from the cancer genome. *Cell*, *153*(1), pp.17-37.

Gazdar, A.F., Girard, L., Lockwood, W.W., Lam, W.L. and Minna, J.D., 2010. Lung cancer cell lines as tools for biomedical discovery and research. *Journal of the National Cancer Institute*, *102*(17), pp.1310-1321.

Giard, D.J., Aaronson, S.A., Todaro, G.J., Arnstein, P., Kersey, J.H., Dosik, H. and Parks, W.P., 1973. *In vitro* cultivation of human tumors: establishment of cell lines derived from a series of solid tumors. *Journal of the National Cancer Institute*, *51*(5), pp.1417-1423.

Giunta, E.F., Signori, A., West, H.J., Metro, G., Friedlaender, A., Parikh, K., Banna, G.L. and Addeo, A., 2022. Beyond crizotinib: a systematic review and meta-analysis of the next-generation ALK inhibitors as first-line treatment for ALK-translocated lung cancer. *Frontiers in Oncology*, *12*, p.921854.

Globocan, 2020. Global Cancer Observatory. International Agency for Research on Cancer, World Health Organization, Lyon, France. Available at: https://gco.iarc.fr/.

Gmeiner, W.H., Boyacioglu, O., Stuart, C.H., Jennings-Gee, J. and Balaji, K.C., 2015. The cytotoxic and pro-apoptotic activities of the novel fluoropyrimidine F10 towards prostate

cancer cells are enhanced by Zn2+-chelation and inhibiting the serine protease Omi/HtrA2. *The Prostate*, *75*(4), pp.360-369.

Greijer, A.E. and Van der Wall, E., 2004. The role of hypoxia-inducible factor 1 (HIF-1) in hypoxia-induced apoptosis. *Journal of clinical pathology*, *57*(10), pp.1009-1014.

Groves-Kirkby, C.J., Timson, K., Shield, G., Denman, A.R., Rogers, S. and Phillips, P.S., 2011. Lung-cancer reduction from smoking cessation and radon remediation: a preliminary cost-analysis in Northamptonshire, UK. *Environment International*, *37*(2), pp.375-382.

Gul, N.S., Khan, T.M., Chen, M., Huang, K.B., Hou, C., Choudhary, M.I., Liang, H. and Chen, Z.F., 2020. New copper complexes inducing bimodal death through apoptosis and autophagy in A549 cancer cells. *Journal of Inorganic Biochemistry*, *213*, p.111260.

Guntur, V.P., Waldrep, J.C., Guo, J.J., Selting, K. and Dhand, R., 2010. Increasing p53 protein sensitizes non-small cell lung cancer to paclitaxel and cisplatin *in vitro*. *Anticancer research*, *30*(9), pp.3557-3564.

Guo, L., Zhang, H., Shao, W. and Chen, B., 2015. Crizotinib as a personalised alternative for targeted anaplastic lymphoma kinase rearrangement in previously treated patients with non-small-cell lung cancer. *Drug design, development and therapy*, pp.5491-5497.

Hanahan, D. and Weinberg, R.A., 2011. Hallmarks of cancer: the next generation. *Cell*, *144*(5), pp.646-674.

Hardwick, J.M. and Soane, L., 2013. Multiple functions of BCL-2 family proteins. *Cold Spring Harbor perspectives in biology*, *5*(2), p.a008722.

Harmse, L., Gangat, N., Martins-Furness, C., Dam, J. and de Koning, C.B., 2019. Copper-imidazo [1, 2-a] pyridines induce intrinsic apoptosis and modulate the expression of mutated p53, haem-oxygenase-1 and apoptotic inhibitory proteins in HT-29 colorectal cancer cells. *Apoptosis*, *24*(7), pp.623-643.

Hassan, M., Watari, H., AbuAlmaaty, A., Ohba, Y. and Sakuragi, N., 2014. Apoptosis and molecular targeting therapy in cancer. *BioMed research international*, *2014*.

Hata, A.N., Engelman, J.A. and Faber, A.C., 2015. The BCL2 family: key mediators of the apoptotic response to targeted anticancer therapeutics. *Cancer Discovery*, *5*(5), pp.475-487.

He, Y., Wang, Z., Hu, Y., Yi, X., Wu, L., Cao, Z. and Wang, J., 2020. Sensitive and selective monitoring of the DNA damage-induced intracellular p21 protein and unraveling the role of the p21 protein in DNA repair and cell apoptosis by surface plasmon resonance. *Analyst*, *145*(10), pp.3697-3704.

Helgason, G.V., Holyoake, T.L. and Ryan, K.M., 2013. Role of autophagy in cancer prevention, development and therapy. *Essays in biochemistry*, *55*, pp.133-151.

Herbst, R.S., Baas, P., Kim, D.W., Felip, E., Pérez-Gracia, J.L., Han, J.Y., Molina, J., Kim, J.H., Arvis, C.D., Ahn, M.J. and Majem, M., 2016. Pembrolizumab versus docetaxel for previously treated, PD-L1-positive, advanced non-small-cell lung cancer (KEYNOTE-010): a randomised controlled trial. *The Lancet*, *387*(10027), pp.1540-1550.

Herbst, R.S., Heymach, J.V. and Lippman, S.M., 2008. Lung Cancer. *New England Journal of Medicine*, 359(13), pp.1367–1380.

Hientz, K., Mohr, A., Bhakta-Guha, D. and Efferth, T., 2017. The role of p53 in cancer drug resistance and targeted chemotherapy. *Oncotarget*, *8*(5), p.8921.

Hirsch, F.R., Scagliotti, G.V., Mulshine, J.L., Kwon, R., Curran Jr, W.J., Wu, Y.L. and Paz-Ares, L., 2017. Lung cancer: current therapies and new targeted treatments. *The Lancet*, *389(10066)*, pp.299-311.

Hoesel, B. and Schmid, J.A., 2013. The complexity of NF-κB signaling in inflammation and cancer. *Molecular cancer*, *12*(1), pp.1-15.

Howlader, N.N.A.K.M., Noone, A.M., Krapcho, M., Garshell, J., Neyman, N., Altekruse, S.F., Kosary, C.L., Yu, M., Ruhl, J., Tatalovich, Z. and Cho, H., 2013. SEER cancer statistics review, 1975–2010. *Bethesda, MD: National Cancer Institute*, *21*, p.12.

Huang, K., Zhang, J., O'Neill, K.L., Gurumurthy, C.B., Quadros, R.M., Tu, Y. and Luo, X., 2016. Cleavage by caspase 8 and mitochondrial membrane association activate the BH3-only protein Bid during TRAIL-induced apoptosis. *Journal of Biological Chemistry*, *291*(22), pp.11843-11851.

Inoue, T., Wu, L., Stuart, J. and Maki, C.G., 2005. Control of p53 nuclear accumulation in stressed cells. *FEBS letters*, *579*(22), pp.4978-4984.

International Agency for Research on Cancer, 2020. South Africa. [online] Available at: https://gco.iarc.fr/today/data/factsheets/populations/710-south-africa-fact-sheets.pdf [Accessed (5 May 2022)]

Ismail, Z., Dam, J., Penny, C., de Koning, C.B. and Harmse, L., 2022. Copper-imidazo [1, 2-a] pyridines differentially modulate pro-and anti-apoptotic protein and gene expression in HL-60 and K562 leukaemic cells to cause apoptotic cell death. *Biochimica et Biophysica Acta (BBA)-Molecular Cell Research*, *1869*(1), p.119160.

Jadeja, R.N., Vyas, K.M., Upadhyay, K.K. and Devkar, R.V., 2017. *In vitro* apoptosis-inducing effect and gene expression profiles of mixed ligand Cu (II) complexes derived from 4-acyl pyrazolones on human lung cancer cells. *RSC advances*, *7*(28), pp.17107-17116.

Jany, T., Moreth, A., Gruschka, C., Sischka, A., Spiering, A., Dieding, M., Wang, Y., Samo, S.H., Stammler, A., Bögge, H. and Fischer von Mollard, G., 2015. Rational design of a cytotoxic dinuclear Cu2 complex that binds by molecular recognition at two neighbouring phosphates of the DNA backbone. *Inorganic chemistry*, *54*(6), pp.2679-2690.

Jones, G.S. and Baldwin, D.R., 2018. Recent advances in the management of lung cancer. *Clinical Medicine*, *18*(Suppl 2), p.s41-s46.

Jozkowicz, A., Was, H. and Dulak, J., 2007. Heme oxygenase-1 in tumors: is it a false friend?. *Antioxidants & redox signaling*, *9*(12), pp.2099-2118.

Jung, C.H., Jun, C.B., Ro, S.H., Kim, Y.M., Otto, N.M., Cao, J., Kundu, M. and Kim, D.H., 2009. ULK-Atg13-FIP200 complexes mediate mTOR signalling to the autophagy machinery. *Molecular biology of the cell*, *20*(7), pp.1992-2003.

Karimian, A., Ahmadi, Y. and Yousefi, B., 2016. Multiple functions of p21 in cell cycle, apoptosis and transcriptional regulation after DNA damage. *DNA repair*, *42*, pp.63-71.

Kerr, J. F., A. H. Wyllie, and Currie A. R**.,** 1972. Apoptosis: a basic biological phenomenon with wide-ranging implications in tissue kinetics. *Br. J. Cancer*. 26**:**239-257.

Khalid, N. and Azimpouran, M., 2023. Necrosis. In: StatPearls [Internet]. Treasure Island (FL): StatPearls Publishing; 2023 Jan-. [cited 2023 Mar 6]. Available from: https://www.ncbi.nlm.nih.gov/books/NBK557627/

Knudson Jr, A.G., 1971. Mutation and cancer: statistical study of retinoblastoma. *Proceedings of the National Academy of Sciences*, *68*(4), pp.820-823.

Korrodi-Gregorio, L., Soto-Cerrato, V., Vitorino, R., Fardilha, M. and Perez-Tomas, R., 2016. From proteomic analysis to potential therapeutic targets: Functional profile of two lung cancer cell lines, A549 and SW900, widely studied in pre-clinical research. *PLoS One*, *11*(11), p.e0165973.

Kowol, C.R., Heffeter, P., Miklos, W., Gille, L., Trondl, R., Cappellacci, L., Berger, W. and Keppler, B.K., 2012. Mechanisms underlying reductant-induced reactive oxygen species formation by anticancer copper (II) compounds. *JBIC Journal of Biological Inorganic Chemistry*, *17*(3), pp.409-423.

Kristeleit, H., Enting, D. and Lal, R., 2011. Basic science of lung cancer. *European Journal of Cancer*, *47*(Supplement 3), pp.s319-s321.

Landi, M.T., Chatterjee, N., Yu, K., Goldin, L.R., Goldstein, A.M., Rotunno, M., Mirabello, L., Jacobs, K., Wheeler, W., Yeager, M. and Bergen, A.W., 2009. A genome-wide association study of lung cancer identifies a region of chromosome 5p15 associated with risk for adenocarcinoma. *The American Journal of Human Genetics*, *85*(5), pp.679-691.

Langthaler, S., Rienmüller, T., Scheruebel, S., Pelzmann, B., Shrestha, N., Zorn-Pauly, K., Schreibmayer, W., Koff, A. and Baumgartner, C., 2021. A549 in-silico 1.0: A first computational model to simulate cell cycle-dependent ion current modulation in the human lung adenocarcinoma. *PLoS Computational Biology*, *17*(6), p.e1009091.

Lee, H., Kim, S., Choi, B.H., Park, M.T., Lee, J., Jeong, S.Y., Choi, E.K., Lim, B.U., Kim, C. and Park, H.J., 2011. Hyperthermia improves therapeutic efficacy of doxorubicin carried by mesoporous silica nanocontainers in human lung cancer cells. *International Journal of Hyperthermia*, *27*(7), pp.698-707.

Lee, S.H., Meng, X.W., Flatten, K.S., Loegering, D.A. and Kaufmann, S.H., 2013. Phosphatidylserine exposure during apoptosis reflects bidirectional trafficking between plasma membrane and cytoplasm. *Cell Death & Differentiation*, *20*(1), pp.64-76.

Levine, A. J., & Oren, M. (2009). The first 30 years of p53: growing ever more complex. Nat Rev Cancer, 9(10), 749-758.

Li, H., Fang, H., Chang, L., Qiu, S., Ren, X., Cao, L., Bian, J., Wang, Z., Guo, Y., Lv, J. and Sun, Z., 2021. TC2N: a novel vital oncogene or tumor suppressor gene in cancers. *Frontiers in Immunology*, *12*, p.764749.

Lieber, M., Todaro, G., Smith, B., Szakal, A. and Nelson-Rees, W., 1976. A continuous tumour-cell line from a human lung carcinoma with properties of type II alveolar epithelial cells. *International Journal of Cancer*, *17*(1), pp.62-70.

Liu, Y., Tavana, O. and Gu, W., 2019. p53 modifications: exquisite decorations of the powerful guardian. *Journal of molecular cell biology*, *11*(7), pp.564-577.

Lopez, J. and Tait, S.W.G., 2015. Mitochondrial apoptosis: killing cancer using the enemy within. *British Journal of Cancer*, *112*(6), pp.957-962.

Martens, S. and Fracchiolla, D., 2020. Activation and targeting of ATG8 protein lipidation. *Cell discovery*, *6*(1), p.23.

Martin, S.J., Henry, C.M. and Cullen, S.P., 2012. A perspective on mammalian caspases as positive and negative regulators of inflammation. *Molecular cell*, *46*(4), pp.387-397.

Mauro, M., Rego, M.A., Boisvert, R.A., Esashi, F., Cavallo, F., Jasin, M. and Howlett, N.G., 2012. p21 promotes error-free replication-coupled DNA double-strand break repair. *Nucleic acids research*, *40*(17), pp.8348-8360.

McGivern, T.J.P., Afsharpour, S. and Marmion, C.J., 2018. Copper complexes as artificial DNA metallonucleases: from Sigman's reagent to next generation anti-cancer agent?. *Inorganica Chimica Acta*, *472*, pp.12-39.

McGivern, T.J.P., Afsharpour, S. and Marmion, C.J., 2018. Copper complexes as artificial DNA metallonucleases: from Sigman’s reagent to next generation anti-cancer agent?. *Inorganica Chimica Acta*, *472*, pp.12-39.

McIlwain, D.R., Berger, T. and Mak, T.W., 2013. Caspase functions in cell death and disease. *Cold Spring Harbor perspectives in biology*, *5*(4), p.a008656.

Mendo, A.S., Figueiredo, S., Roma-Rodrigues, C., Videira, P.A., Ma, Z., Diniz, M., Larguinho, M., Costa, P.M., Lima, J.C., Pombeiro, A.J. and Baptista, P.V., 2015. Characterisation of antiproliferative potential and biological targets of a copper compound containing 4′-phenyl terpyridine. *JBIC Journal of Biological Inorganic Chemistry*, *20*(6), pp.935-948.

Micheau, O., 2018. Regulation of TNF-related apoptosis-inducing ligand signaling by glycosylation. *International journal of molecular sciences*, *19*(3), p.715.

Mokhtari, R.B., Homayouni, T.S., Baluch, N., Morgatskaya, E., Kumar, S., Das, B. and Yeger, H., 2017. Combination therapy in combating cancer. *Oncotarget*, *8*(23), p.38022.

Morris, D.H., Yip, C.K., Shi, Y., Chait, B.T. and Wang, Q.J., 2015. Beclin 1-Vps34 complex architecture: Understanding the nuts and bolts of therapeutic targets. *Frontiers in biology*, *10*, pp.398-426.

Mosmann, T., 1983. Rapid colorimetric assay for cellular growth and survival: application to proliferation and cytotoxicity assays. *Journal of immunological methods*, *65*(1-2), pp.55-63.

Naimi, A., Movassaghpour, A.A., Hagh, M.F., Talebi, M., Entezari, A., Jadidi-Niaragh, F. and Solali, S., 2018. TNF-related apoptosis-inducing ligand (TRAIL) as the potential therapeutic target in hematological malignancies. *Biomedicine & Pharmacotherapy*, *98*, pp.566-576.

Naso, L.G., Medina, J.J.M., D'Alessandro, F., Rey, M., Rizzi, A., Piro, O.E., Echeverría, G.A., Ferrer, E.G. and Williams, P.A., 2020. Ternary copper (II) complex of 5-hydroxytryptophan and 1, 10-phenanthroline with several pharmacological properties and an adequate safety profile. *Journal of Inorganic Biochemistry*, *204*, p.110933.

NCCN, 2022. Non–Small Cell Lung Cancer, Version 3.2022, NCCN Clinical Practice Guidelines in Oncology. *Journal of the National Comprehensive Cancer Network*, 20(5). Available at: https://doi.org/10.6004/jnccn.2022.0025

Negrini, S., Gorgoulis, V.G. and Halazonetis, T.D., 2010. Genomic instability—an evolving hallmark of cancer. *Nature Reviews Molecular cell biology*, *11*(3), pp.220-228.

Nencioni, A., Cea, M., Montecucco, F., Longo, V.D., Patrone, F., Carella, A.M., Holyoake, T.L. and Helgason, G.V., 2013. Autophagy in blood cancers: biological role and therapeutic implications. *haematologica*, *98*(9), p.1335.

Obexer, P. and Ausserlechner, M.J., 2014. X-linked inhibitor of apoptosis protein–a critical death resistance regulator and therapeutic target for personalised cancer therapy. *Frontiers in oncology*, *4*, p.197.

Obexer, P. and Ausserlechner, M.J., 2014. X-linked inhibitor of apoptosis protein–a critical death resistance regulator and therapeutic target for personalised cancer therapy. *Frontiers in oncology*, *4*, p.197.

Oh, Y.T. and Sun, S.Y., 2021. Regulation of cancer metastasis by trail/death receptor signaling. *Biomolecules*, *11*(4), p.499.

O'Neill, K.L., Huang, K., Zhang, J., Chen, Y. and Luo, X., 2016. The inactivation of prosurvival Bcl-2 proteins activates Bax/Bak through the outer mitochondrial membrane. *Genes & development*, *30*(8), pp.973-988.

Op Den Kamp, J.A.K., 1979. Lipid asymmetry in membranes.

Oun, R., Moussa, Y.E. and Wheate, N.J., 2018. The side effects of platinum-based chemotherapy drugs: a review for chemists. *Dalton transactions*, *47*(19), pp.6645-6653.

Ozaki, T. and Nakagawara, A., 2011. Role of p53 in cell death and human cancers. *Cancers*, *3*(1), pp.994-1013.

Palanimuthu, D., Shinde, S.V., Somasundaram, K. and Samuelson, A.G., 2013. *In vitro* and *in vivo* anticancer activity of copper bis (thiosemicarbazone) complexes. *Journal of medicinal chemistry*, *56*(3), pp.722-734.

Park, Y.H., Jeong, M.S. and Jang, S.B., 2016. Structural insights of homotypic interaction domains in the ligand-receptor signal transduction of tumor necrosis factor (TNF). *BMB reports*, *49*(3), p.159-166.

Parkin, D.M., Bray, F., Ferlay, J. and Jemal, A., 2014. Cancer in Africa 2012. *Cancer Epidemiology and Prevention Biomarkers*, *23*(6), pp.953-966. (Parkin *et al*.2012)

Parween, F. and Gupta, R.D., 2022. Insights into the role of paraoxonase 2 in human pathophysiology. *Journal of Biosciences*, *47*(1), p.4.

Pecorino, L., 2016. *Molecular biology of cancer: mechanisms, targets, and therapeutics*. Oxford University Press, USA

Periasamy, V.S., Riyasdeen, A., Rajendiran, V., Palaniandavar, M., Krishnamurthy, H., Alshatwi, A.A. and Akbarsha, M.A., 2020. Induction of redox-mediated cell death in ER-positive and ER-negative breast cancer cells by a copper (II)-phenolate complex: an *in vitro* and in silico study. *Molecules*, *25*(19), p.4504.found that:

Peterson, Q.P., Goode, D.R., West, D.C., Botham, R.C. and Hergenrother, P.J., 2010. Preparation of the caspase-3/7 substrate Ac-DEVD-pNA by solution-phase peptide synthesis. *nature protocols*, *5*(2), pp.294-302.

Pierzynska-Mach A, Janowski PA, Dobrucki JW (2014). Evaluation of acridine orange, LysoTracker Red, and quinacrine as fluorescent probes for long-term tracking of acidic vesicles. *Cytometry A.* **85**(8)**:** 729-737. doi: 710.1002/cyto.a.22495

Pirker, R. and Filipits, M., 2016. Personalised treatment of advanced non-small-cell lung cancer in routine clinical practice. *Cancer and Metastasis Reviews*, *35*, pp.141-150.

Pistritto, G., Trisciuoglio, D., Ceci, C., Garufi, A. and D'Orazi, G., 2016. Apoptosis as anticancer mechanism: function and dysfunction of its modulators and targeted therapeutic strategies. *Aging (Albany NY)*, *8*(4), p.603-619.

Poornima, P., Kumar, V.B., Weng, C.F. and Padma, V.V., 2014. Doxorubicin-induced apoptosis was potentiated by reference in human lung adenocarcinoma, A549 cells. *Food and chemical toxicology*, *68*, pp.87-98.

Pronk, T.E., van der Veen, J.W., Vandebriel, R.J., van Loveren, H., de Vink, E.P. and Pennings, J.L., 2014. Comparison of the molecular topologies of stress-activated transcription factors HSF1, AP-1, NRF2, and NF-κB in their induction kinetics of HMOX1. *Biosystems*, *124*, pp.75-85.

Qiu, L., Lv, G., Guo, L., Chen, L., Luo, S., Zou, M. and Lin, J., 2015. Synthesis, crystal structure and antitumor effect of a novel copper (II) complex bearing zoledronic acid derivative. *European Journal of Medicinal Chemistry*, *89*, pp.42-50.

Razavipour, S.F., Harikumar, K.B. and Slingerland, J.M., 2020. p27 as a transcriptional regulator: new roles in development and cancer. *Cancer research*, *80*(17), pp.3451-3458.

Reddy, P., Zuma, K., Shisana, O., Jonas, K. and Sewpaul, R., 2015. Prevalence of tobacco use among adults in South Africa: results from the first South African National Health and Nutrition Examination Survey. *South African Medical Journal*, *105*(8), pp.648-655.

Redza-Dutordoir, M. and Averill-Bates, D.A., 2016. Activation of apoptosis signalling pathways by reactive oxygen species. *Biochimica et Biophysica Acta (BBA)-Molecular Cell Research*, *1863*(12),pp.2977-2992.

Rezaei, A., Mahmoodi, M., Mohammadizadeh, F., Mohamadi, M., Hajizadeh, M.R., Mirzaei, M.R. and Khanamani Falahati-pour, S., 2019. A novel copper (II) complex activated both extrinsic and intrinsic apoptotic pathways in liver cancerous cells. *Journal of Cellular Biochemistry*, *120*(8), pp.12280-12289.

Ribatti, D., Nico, B. and Crivellato, E., 2015. The development of the vascular system: a historical overview. *Vascular Morphogenesis*, pp.1-14.

Ribeiro, N., Bulut, I., Cevatemre, B., Teixeira, C., Yildizhan, Y., André, V., Adão, P., Pessoa, J.C., Acilan, C. and Correia, I., 2021. Cu (II) and V (IV) O complexes with tri-or tetradentate ligands based on (2-hydroxybenzyl)-L-alanines reveal promising anticancer therapeutic potential. *Dalton Transactions*, *50*(1), pp.157-169

Rogers, C., Fernandes-Alnemri, T., Mayes, L., Alnemri, D., Cingolani, G. and Alnemri, E.S., 2017. Cleavage of DFNA5 by caspase-3 during apoptosis mediates progression to secondary necrotic/pyroptotic cell death. *Nature communications*, *8*(1), p.14128.

Rossi, A. and Di Maio, M., 2016. Platinum-based chemotherapy in advanced non-small-cell lung cancer: optimal number of treatment cycles. *Expert review of anticancer therapy*, *16*(6), pp.653-660.

Ruiz-Azuara, L. and E Bravo-Gomez, M., 2010. Copper compounds in cancer chemotherapy. *Current medicinal chemistry*, *17*(31), pp.3606-3615

Sakamuru, S., Attene-Ramos, M.S. and Xia, M., 2016. Mitochondrial membrane potential assay. *High-throughput screening assays in toxicology*, pp.17-22.

Salimi, M., Abdi, K., Kandelous, H.M., Hadadzadeh, H., Azadmanesh, K., Amanzadeh, A. and Sanati, H., 2015. Antiproliferative effects of copper (II)–polypyridyl complexes in breast cancer cells through inducing apoptosis. *BioMetals*, *28*(2), pp.267-278

Sandström, N., Johansson, M., Jekunen, A. and Andersén, H., 2023. Socioeconomic status and lifestyle patterns in the most common cancer types-community-based research. *BMC Public Health*, *23*(1), p.1722.

Santini, C., Pellei, M., Gandin, V., Porchia, M., Tisato, F. and Marzano, C., 2013. Advances in copper complexes as anticancer agents. *Chemical Reviews, 114(1)*, pp.815-862.

Santini, C., Pellei, M., Gandin, V., Porchia, M., Tisato, F. and Marzano, C., 2014. Advances in copper complexes as anticancer agents. *Chemical reviews*, *114*(1), pp.815-862.

Schabath, M.B. and Cote, M.L., 2019. Cancer progress and priorities: lung cancer. *Cancer Epidemiology and Prevention Biomarkers*, 28(10), pp.1563-1579.

Schreiber, R., 2016. *Tumor immunology*. Academic Press.

Schroder, K., Muruve, D.A. and Tschopp, J., 2009. Innate immunity: cytoplasmic DNA sensing by the AIM2 inflammasome. *Current biology*, *19*(6), pp.R262-R265.

Shalini, S., Dorstyn, L., Dawar, S. and Kumar, S., 2015. Old, new and emerging functions of caspases. *Cell Death & Differentiation*, *22*(4), pp.526-539.

Shamas-Din, A., Kale, J., Leber, B. and Andrews, D.W., 2013. Mechanisms of action of Bcl-2 family proteins. *Cold Spring Harbor perspectives in biology*, *5*(4), p.a008714.

Shao, J., Li, M., Guo, Z., Jin, C., Zhang, F., Ou, C., Xie, Y., Tan, S., Wang, Z., Zheng, S. and Wang, X., 2019. TPP-related mitochondrial targeting copper (II) complex induces p53-dependent apoptosis in hepatoma cells through ROS-mediated activation of Drp1. *Cell Communication and Signaling*, *17*(1), pp.1-18.

Shay, J.W., 2016. Role of telomeres and telomerase in aging and cancer. *Cancer discovery*, *6*(6), pp.584-593.

Shi, T., van Soest, D.M., Polderman, P.E., Burgering, B.M. and Dansen, T.B., 2021. DNA damage and oxidant stress activate p53 through differential upstream signaling pathways. *Free Radical Biology and Medicine*, *172*, pp.298-311.

Shubin, A.V., Demidyuk, I.V., Komissarov, A.A., Rafieva, L.M. and Kostrov, S.V., 2016. Cytoplasmic vacuolisation in cell death and survival. *Oncotarget*, *7*(34), p.55863.

Sigman, D.S., Landgraf, R., Perrin, D.M. and Pearson, L., 1996. Nucleic acid chemistry of the cuprous complexes of 1, 10-phenanthroline and derivatives. *Metal ions in biological systems*, *33*, pp.485-514.

Siliciano, J.D., Canman, C.E., Taya, Y., Sakaguchi, K., Appella, E. and Kastan, M.B., 1997. DNA damage induces phosphorylation of the amino terminus of p53. *Genes & development*, *11*(24), pp.3471-3481.

Siliciano, J.D., Canman, C.E., Taya, Y., Sakaguchi, K., Appella, E. and Kastan, M.B., 1997. DNA damage induces phosphorylation of the amino terminus of p53. *Genes & development*, *11*(24), pp.3471-3481.

Silke, J. and Meier, P., 2013. Inhibitor of apoptosis (IAP) proteins–modulators of cell death and inflammation. *Cold Spring Harbor perspectives in biology*, *5*(2), p.a008730.

Silke, J. and Meier, P., 2013. Inhibitor of apoptosis (IAP) proteins–modulators of cell death and inflammation. *Cold Spring Harbor perspectives in biology*, *5*(2), p.a008730.

Smiley, S.T., Reers, M., Mottola-Hartshorn, C., Lin, M., Chen, A., Smith, T.W., Steele Jr, G.D. and Chen, L.B., 1991. Intracellular heterogeneity in mitochondrial membrane potentials revealed by a J-aggregate-forming lipophilic cation JC-1. *Proceedings of the National Academy of Sciences*, *88*(9), pp.3671-3675.

Steven, A., Fisher, S.A. and Robinson, B.W., 2016. Immunotherapy for lung cancer. *Respirology*, *21*(5), pp.821-833.

Sung, H., Ferlay, J., Siegel, R.L., Laversanne, M., Soerjomataram, I., Jemal, A. and Bray, F., 2021. Global cancer statistics 2020: GLOBOCAN estimates of incidence and mortality worldwide for 36 cancers in 185 countries. *CA: a cancer journal for clinicians*, *71*(3), pp.209-249.

Szegezdi, E., Logue, S. E., Gorman, A. M., & Samali, A. (2006). Mediators of endoplasmic reticulum stress-induced apoptosis. EMBO Reports, 7(9), 880-885.

Tait, S.W. and Green, D.R., 2010. Mitochondria and cell death: outer membrane permeabilization and beyond. *Nature reviews Molecular cell biology*, *11*(9), pp.621-632.

Tamayo, L.V., Da Silva, J.G., Quintão, M.C., Duarte, H.A., Louro, S.R. and Beraldo, H., 2017. Investigation of the physicochemical properties of trans-4-stilbenecarboxaldehyde-derived hydrazones and their copper (II) complexes. *Polyhedron*, *134*, pp.199-206.

Tan, Y., Chen, Q., Li, X., Zeng, Z., Xiong, W., Li, G., Li, X., Yang, J., Xiang, B. and Yi, M., 2021. Pyroptosis: a new paradigm of cell death for fighting against cancer. *Journal of Experimental & Clinical Cancer Research*, *40*(1), pp.1-15.

Tchounwou, P.B., Dasari, S., Noubissi, F.K., Ray, P. and Kumar, S., 2021. Advances in our understanding of the molecular mechanisms of action of cisplatin in cancer therapy. *Journal of experimental pharmacology*, pp.303-328.

Timmerman, R., Paulus, R., Galvin, J., Michalski, J., Straube, W., Bradley, J., Fakiris, A., Bezjak, A., Videtic, G., Johnstone, D. and Fowler, J., 2010. Stereotactic body radiation therapy for inoperable early-stage lung cancer. *Jama*, *303(11)*, pp.1070-1076

Travis, W.D., Brambilla, E., Nicholson, A.G., Yatabe, Y., Austin, J.H., Beasley, M.B., Chirieac, L.R., Dacic, S., Duhig, E., Flieder, D.B. and Geisinger, K., 2015. The 2015 World

Health Organization classification of lung tumors: impact of genetic, clinical and radiologic advances since the 2004 classification. *Journal of thoracic oncology*, *10*(9), pp.1243-1260.

Travis, W.D., Brambilla, E., Noguchi, M., Nicholson, A.G., Geisinger, K., Yatabe, Y., Ishikawa, Y., Wistuba, I., Flieder, D.B., Franklin, W. and Gazdar, A., 2013. Diagnosis of lung adenocarcinoma in resected specimens: implications of the 2011 International Association for the Study of Lung Cancer/American Thoracic Society/European Respiratory Society classification. *Archives of Pathology and Laboratory Medicine*, *137*(5), pp.685-705.

Truong, T., Hung, R.J., Amos, C.I., Wu, X., Bickeböller, H., Rosenberger, A., Sauter, W., Illig, T., Wichmann, H.E., Risch, A. and Dienemann, H., 2010. Replication of lung cancer susceptibility loci at chromosomes 15q25, 5p15, and 6p21: a pooled analysis from the International Lung Cancer Consortium. *Journal of the National Cancer Institute*, *102*(13), pp.959-971.

Tummers, B. and Green, D.R., 2017. Caspase-8: regulating life and death. *Immunological reviews*, *277*(1), pp.76-89.

Tutton, S. and Lieberman, P.M., 2017. A role for p53 in telomere protection. *Molecular & cellular oncology*, *4*(6), p.e1143078.

Usman, M., Zaki, M., Khan, R.A., Alsalme, A., Ahmad, M. and Tabassum, S., 2017. Coumarin centered copper (II) complex with appended-imidazole as cancer chemotherapeutic agents against lung cancer: molecular insight *via* DFT-based vibrational analysis. *RSC advances*, *7*(57), pp.36056-36071.

Van Eeden, Ronwyn, Mariza Tunmer, Agneta Geldenhuys, Simon Nayler, and Bernardo Leon Rapoport. "Lung Cancer in South Africa." *Journal of Thoracic Oncology* 15, no. 1 (2020): 22-28.

Vande Walle, L. and Lamkanfi, M.P., 2016. Pyroptosis. *Current Biology* 26(13)**:** R568-R572.

Vandenabeele, P., Vanden Berghe, T. and Festjens, N., 2006. Caspase inhibitors promote alternative cell death pathways. *Science's STKE*, *2006*(358), pp.pe44-pe44.

Vermes, I. and Haanen, C., 1994. Apoptosis and programmed cell death in health and disease. *Advances in clinical chemistry*, *31*, pp.177-246.

Waga, S., Hannon, G.J., Beach, D. and Stillman, B., 1994. The p21 inhibitor of cyclin-dependent kinases controls DNA replication by interaction with PCNA. *Nature*, *369*(6481), pp.574-578.

Wang, S., Liu, Y., Zhang, L. and Sun, Z., 2022. Methods for monitoring cancer cell pyroptosis. *Cancer Biology & Medicine*, *19*(4), p.398.

Warburg, O., Wind, F. and Negelein, E., 1927. The metabolism of tumours in the body. *The Journal of General Physiology*, *8*(6), p.519.

Weinberg, R.A., 2013. The Nature of Cancer. The Biology of Cancer, New York: Garland Science.

Weiss, R.B., 1992, December. The anthracyclines: will we ever find a better doxorubicin?. In *Seminars in oncology* (Vol. 19, No. 6, pp. 670-686).

West, L., Vidwans, S.J., Campbell, N.P., Shrager, J., Simon, G.R., Bueno, R., Dennis, P.A., Otterson, G.A. and Salgia, R., 2012. A novel classification of lung cancer into molecular subtypes. *PloS one*, *7*(2), p.e31906.

Witte, I., Altenhöfer, S., Wilgenbus, P., Amort, J., Clement, A.M., Pautz, A., Li, H., Förstermann, U. and Horke, S., 2011. Beyond reduction of atherosclerosis: PON2 provides apoptosis resistance and stabilises tumor cells. *Cell death & disease*, *2*(1), pp.e112-e112.

Wood, D.E., Kazerooni, E., Baum, S.L., Dransfield, M.T., Eapen, G.A., Ettinger, D.S., Hou, L., Jackman, D.M., Klippenstein, D., Kumar, R. and Lackner, R.P., 2015. Lung cancer screening, version 1.2015. *Journal of the National Comprehensive Cancer Network*, *13*(1), pp.23-34.

Woodard, G.A., Jones, K.D. and Jablons, D.M., 2016. Lung cancer staging and prognosis. *Lung cancer*, pp.47-75.

World Health Organization. *Noncommunicable Diseases (NCD)*, 2022. Available online at: https://www.who.int/gho/ncd/mortality_morbidity/en/ (accessed May 14, 2022).

Xia, Y., Shen, S. and Verma, I.M., 2014. NF-κB is an active player in human cancers. *Cancer immunology research*, *2*(9), pp.823-830.

Xie, T., Peng, W., Yan, C., Wu, J., Gong, X. and Shi, Y., 2013. Structural insights into RIP3-mediated necroptotic signaling. *Cell reports*, *5*(1), pp.70-78.

Xiong, Z., Wu, J., Sun, Y., Bai, M., Niu, F. and Jin, T., 2020. Variants in multiple genes are associated with oesophagal cancer risk in a Chinese Han population: A case–control study. *The Journal of Gene Medicine*, *22*(12), p.e3266.

Yang, Y., Sun, M., Wang, L. and Jiao, B., 2013. HIFs, angiogenesis, and cancer. *Journal of cellular biochemistry*, *114*(5), pp.967-974.

Yuan, M., Huang, L.L., Chen, J.H., Wu, J. and Xu, Q., 2019. The emerging treatment landscape of targeted therapy in non-small-cell lung cancer. *Signal transduction and targeted therapy*, *4*(1), pp.1-14.

Zehra, S., Tabassum, S. and Arjmand, F., 2021. Biochemical pathways of copper complexes: progress over the past 5 years. *Drug Discovery Today*, *26*(4), pp.1086-1096.

Zhang, L., Yu, J., Park, B.H., Kinzler, K.W. and Vogelstein, B., 2000. Role of BAX in the apoptotic response to anticancer agents. *Science*, *290*(5493), pp.989-992.

Zhao, L. and Zhang, B., 2017. Doxorubicin induces cardiotoxicity through upregulation of death receptors mediated apoptosis in cardiomyocytes. *Scientific reports*, *7*(1), p.44735.

Appendix A: Ethics waiver

UNIVERSITY OF THE WITWATERSRAND, JOHANNESBURG

HUMAN RESEARCH ETHICS COMMITTEE (MEDICAL)

Ref: W-CP-190708-1

08 July 2019

TO WHOM IT MAY CONCERN:

Waiver: This certifies that the following research does not require clearance from the Human Research Ethics Committee (Medical).

Investigator:	**Zanele Mangena (student no 1111927)**
Co-Investigators:	**Dr Carla Martins-Furness and Dr Armorel van Eyk**
Supervisor:	**Dr Leonie Harmse**
Faculty:	Health Sciences
School:	Therapeutic Sciences
Department:	Pharmacy and Pharmacology
Project title:	An evaluation of the effects of metal complexes on lung cancer cell lines
Reason:	In vitro lab study using the A549 commercially available lung cancer cell lines to evaluate cytotoxicity of novel metallo-compounds. No humans, human data and human tissues will be used in this study.

Dr Clement Penny

Chair: Human Research Ethics Committee (Medical)

Copy – HREC (Medical) Secretariat

Research Office Secretariat: Faculty of Health Sciences, Phillip Tobias Building, 3rd Floor, Office 301, 29 Princess of Wales Terrace, Parktown, 2193 Tel +27 (0)11-717-1252 /1234/2656/2700 Private Bag 3, Wits 2050, email: zanele.ndlovu@wits.ac.za Office email: hrec-medical.researchoffice@wits.ac.zaWebsite: www.wits.ac.za/research/about-our-research/ethics-and-research-integrity/

Appendix B: Supplier information

Table B1. Cell lines, reagents, and equipment used in this study along with their respective suppliers and locations

Category	Item	Supplier	Location
Cell Line	A549 pulmonary adenocarcinoma	Fox Chase Cancer Centre	Philadelphia, Pennsylvania, USA
Reagents	Ham's F-12 medium	Gibco	Massachusetts, USA
Reagents	Dulbecco's modified essential medium (DMEM)	Gibco	Massachusetts, USA
Reagents	Heat inactivated fetal bovine serum (FBS)	Gibco	Massachusetts, USA
Reagents	Non-essential amino acid	Lonza	Walkersville, USA
Reagents	Sodium pyruvate	Sigma-Aldrich	Munich, Germany
Reagents	Penicillin-streptomycin	Sigma-Aldrich	Munich, Germany
Reagents	Trypsin EDTA	Sigma-Aldrich	St Louis, USA
Reagents	Trypan blue dye	Sigma-Aldrich,	Johannesburg, South Africa
Reagents	L-glutamine	HyClone	Utah, USA
Reagents	Dimethyl sulfoxide (DMSO)	Applichem	Iowa, USA
Reagents	Test compounds	School of Chemistry, University of the Witwatersrand	Johannesburg, South Africa
Reagents	MTT	Duchefa Biochemie	Haarlem, Netherlands
Reagents	Propidium iodide	Sigma Aldrich	Johannesburg, South Africa
Reagents	Hoechst 33342	Sigma Aldrich	Johannesburg, South Africa
Reagents	Acridine orange	Thermo Fisher	Johannesburg, RSA
Reagents	NaCl; KCl; Na_2HPO_4; KH_2PO_4	Sigma Aldrich/ Merck,	Johannesburg South Africa

Reagents	Annexin-V-FLUOS Staining Kit	Roche	Basel, Switzerland
Reagents	CellEvent™ Caspase-3/7 Green Detection Reagent	Thermo Fisher Scientific	California, USA
Reagents	Abcam® Caspase-8 (active) Red staining kit (ab65618)	Biocom Africa	Pretoria, South Africa
Reagents	5,5‟,6,6‟-tetrachloro-1,1‟,3,3‟-tetraethylbenzimidazol-carbocyanine iodide (JC-1) dye	Sigma-Aldrich	Johannesburg, South Africa
Reagents	CellROX® Deep Red Reagent	Thermo Fisher Scientific	Massachusetts, United States
Reagents	Bradford protein assay	Bio-Rad Laboratories, Inc	California, United States
Reagents	Bovine serum albumin (BSA)	Fluka ™/Fischer Scientific	Massachusetts, USA.
Reagents	p21 Monoclonal Antibody (HJ21) (Catalog # AHZ0422)	Invitrogen/Life technologies	Massachusetts, USA.
Reagents	Phospho-p53 (Ser15) Recombinant Rabbit Monoclonal Antibody (14H61L24) (Cat #700439)	Invitrogen/Life technologies	Massachusetts, USA.
Reagents	Fluoromount	Sigma-Aldrich	Johannesburg, South Africa
Reagents	Proteome profiler human apoptosis array kit	R&D Systems	Minnesota, USA
Equipment	Heracell 150 CO_2 incubator	Thermo Fisher Scientific	Johannesburg South Africa
Equipment	CoolCell container	Corning	New York, USA
Equipment	Neubauer Haemocytometer	Sigma-Aldrich/Merch	Darmstadt, Germany
Equipment	96-well plate	Nest Biotech	Wuxi, China
Equipment	Six-well plate	Nest Biotech	Wuxi, China

Equipment	Coverslips	Sigma-Aldrich	Johannesburg, South Africa
Equipment	25 cm^3 and 75 cm^3 Greiner bio-one culture flasks	Lasec SA	Johannesburg South Africa
Equipment	Lab Systems Multiskan iEMS Plate reader	Thermo Fisher Scientific, located in Waltham	Massachusetts, USA
Equipment	Thermo Scientific TX-750 Rotor	Thermo Scientific	Massachusetts, USA
Equipment	Thermo Scientific™ Multiskan™ GO Microplate Spectrophotometer.	Thermo Scientific	Massachusetts, USA
Equipment	Olympus CKX41	Olympus Corporation	Tokyo, Japan
Equipment	Olympus BX41 fluorescence microscope	Olympus Corporation	Tokyo, Japan
Equipment	Olympus DP72 camera	Olympus Corporation	Tokyo, Japan
Equipment	Nikon Optiphot light microscope	Nikon Corporation	Tokyo, Japan
Equipment	BIO-RAD ChemiDoc ™ MP Imager	Bio-Rad Laboratories, Inc.	California, United States
Software	Microsoft Excel 2019	Microsoft Corporation	Washington, United States
Software	GraphPad Prism 5	GraphPad Software,	San Diego, California, USA, www.graphpad.com
Software	Image Lab Software Version 6	Bio-Rad Laboratories, Inc.	California, United States

Appendix C: Formulation of solutions

C.1 Phosphate-Buffered Saline (PBS)

Phosphate-buffered saline is a buffer solution that maintains a constant pH, typically used in biological research. PBS was prepared by adding 8 g of NaCl, 0.2 g of KCl, 1.44 g of Na_2HPO_4, and 0.24 g of KH_2PO_4 to 800 mL of distilled water. The pH was adjusted to 7.4 using HCl. The volume was then topped up to 1 litre with additional distilled water. The solution was sterilized by autoclaving and stored at room temperature.

C.2 Freezing Media

The freezing media was prepared using a mixture of DMEM and Ham's F-12 nutrient mixture in a 1:1 ratio. This base media was supplemented with 20% heat-inactivated foetal bovine serum (FBS) to nourish the cells, and 5% (v/v) dimethyl sulfoxide (DMSO) was added as a cryoprotectant to prevent cell damage during freezing. The final freezing media was filtered and stored at -20°C until use.

C.3 MTT

The MTT (3-(4,5-dimethylthiazol-2-yl)-2,5-diphenyl tetrazolium bromide) solution is used to assess cell metabolic activity as a measure of cell viability. MTT was prepared by dissolving 5 mg of MTT in 1 mL of PBS to make a 5 mg/mL solution. The solution was then filter-sterilized using a 0.22 μm filter to remove any undissolved particles. The MTT solution was stored in the dark at -20°C.

C.4 Trypan Blue

Trypan blue staining is a simple method to evaluate cell viability based on the principle that live cells possess intact cell membranes that exclude certain dyes, such as Trypan Blue. The Trypan blue solution was prepared by dissolving Trypan Blue powder to a final concentration of 0.2% (w/v) in PBS. The solution was then sterilized using a 0.22 μm filter and stored in a dark box at room temperature. For cell viability testing, a 1:1 mixture of Trypan Blue solution to cell suspension was prepared

Appendix D: Calibration and standard curves

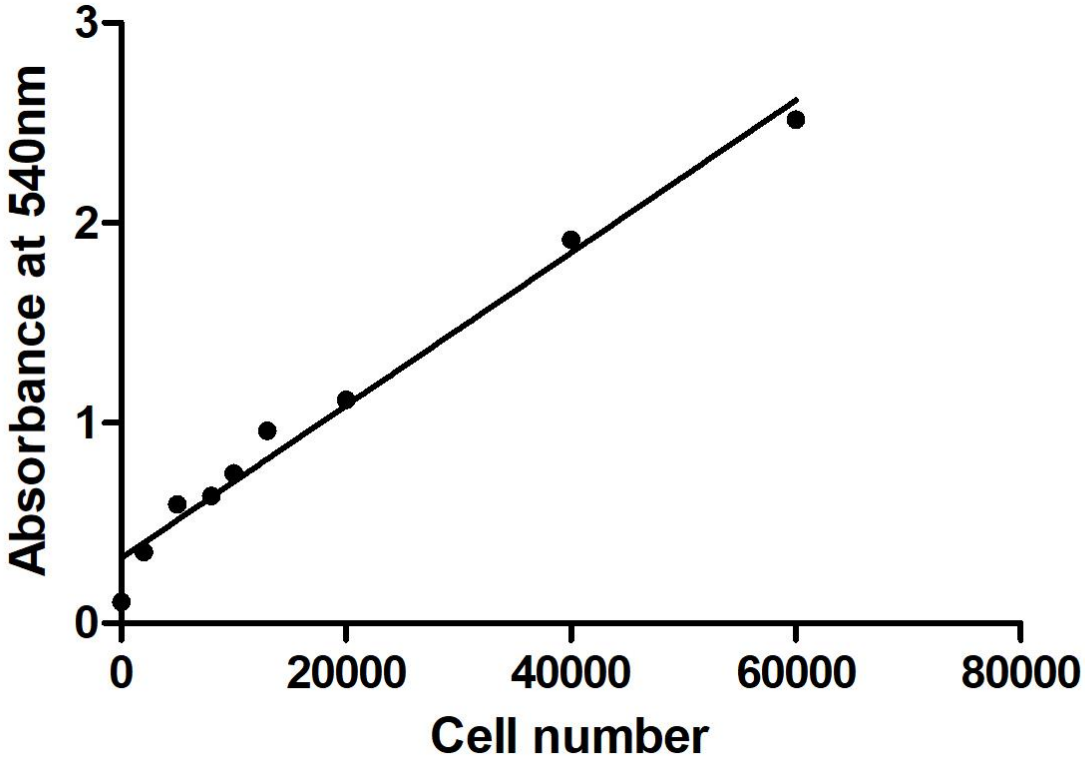

Figure D1 Calibration curve obtained from the MTT assay for A549 cells

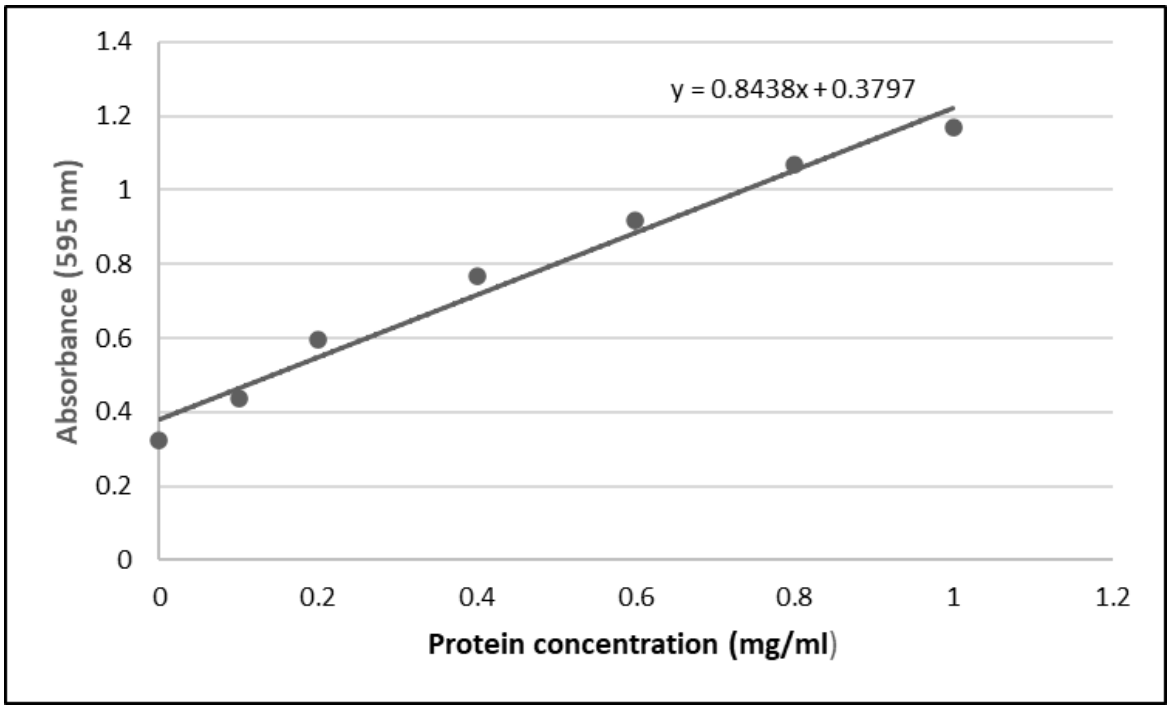

Figure D2 Standard curve for protein determination in the human apoptosis array for A549 cells

Appendix E: Statistcal analysis of IC_{50} values

Table E1: Statistical analysis was performed on these IC_{50} values in comparison to the positive control doxorubicin (IC_{50}: 6.25 ± 0.28 µM) using the two-sample Mann-Whitney U-test with a p-value less than <0.05 and a 95 % confidence interval

	Test Compounds							
	JD35	**JD46**	**JD47**	**JD88**	**OML**	**OM**	**AD3**	**JD49**
P value	0,02	0,02	0,02	0,02	0,06	0,03	0,63	0,11
P value summary	*	*	*	*	ns	*	ns	ns
P-value significance (P < 0.05)	Yes	Yes	Yes	Yes	No	Yes	No	No

Appendix F: Turnitin report

ZM Final MSc Disssertation TurnIn-1.docx

ORIGINALITY REPORT

14%	11%	13%	%
SIMILARITY INDEX	INTERNET SOURCES	PUBLICATIONS	STUDENT PAPERS

PRIMARY SOURCES

1	link.springer.com Internet Source	3%
2	Zeenat Ismail, Jean Dam, Clement Penny, Charles B. de Koning, Leonie Harmse. "Copper-imidazo[1,2-a]pyridines differentially modulate pro- and anti-apoptotic protein and gene expression in HL-60 and K562 leukaemic cells to cause apoptotic cell death", Biochimica et Biophysica Acta (BBA) - Molecular Cell Research, 2021 Publication	1%
3	www.idpublications.com Internet Source	1%
4	www.researchgate.net Internet Source	1%
5	www.science.gov Internet Source	1%
6	Leonie Harmse, Nadia Gangat, Carla Martins-Furness, Jean Dam, Charles B. de Koning. "Copper-imidazo[1,2-a]pyridines induce	<1%

intrinsic apoptosis and modulate the expression of mutated p53, haem-oxygenase-1 and apoptotic inhibitory proteins in HT-29 colorectal cancer cells", Apoptosis, 2019
Publication

7	Tebogo Peega, Rachael N Magwaza, Leonie Harmse, Izak A. Kotzé. "Synthesis and evaluation of the anticancer activity of [Pt(diimine)(N,N-dibutyl-N'-acylthiourea)]+ complexes", Dalton Transactions, 2021 Publication	<1 %
8	www.frontiersin.org Internet Source	<1 %
9	Linde Duprez, Ellen Wirawan, Tom Vanden Berghe, Peter Vandenabeele. "Major cell death pathways at a glance", Microbes and Infection, 2009 Publication	<1 %
10	www.nature.com Internet Source	<1 %
11	www.mdpi.com Internet Source	<1 %
12	Nahid Akhtar, Jeena Gupta Bansal. "Risk factors of Lung Cancer in nonsmoker", Current Problems in Cancer, 2017 Publication	<1 %

13	Internet Source	<1%
14	Leonie Harmse, Nurit Dahan-Farkas, Jenny-Lee Panayides, Willem van Otterlo, Clement Penny. "Aberrant Apoptotic Response of Colorectal Cancer Cells to Novel Nucleoside Analogues", PLOS ONE, 2015 Publication	<1%
15	Patricia de Groot, Reginald F. Munden. "Lung Cancer Epidemiology, Risk Factors, and Prevention", Radiologic Clinics of North America, 2012 Publication	<1%
16	hdl.handle.net Internet Source	<1%
17	Yin, Chia Yin. "Antioxidant and Antiproliferative Activities of Several Marine Organisms from the West Coast of Peninsular Malaysia", University of Malaya (Malaysia), 2023 Publication	<1%
18	Yin, Yuwen. "Novel Small Molecule Probes and Quantification of Binding to C1 Domains of Protein Kinase C in Living Cells", University of Kansas, 2022 Publication	<1%
19	pure.manchester.ac.uk	

Internet Source

<1%

---

20 Kohar, Yulia. "The Role of Microtubule-Associated Protein 1s (MAP1s) in Regulating Autophagy in the Heart.", The University of Manchester (United Kingdom), 2021

Publication

<1%

---

21 P Santos, D Murtinho, AS Pires Lourenço, J Araújo, R Martins, AM Abrantes, MF Botelho, MES Serra. "PO-416 Cytotoxicity of Ru (II) and Ru (III) salen complexes against breast and colorectal cancer cell lines", Poster Presentation: Experimental/Molecular Therapeutics, Pharmacogenomics, 2018

Publication

<1%

---

22 Hyuna Sung, Jacques Ferlay, Rebecca L. Siegel, Mathieu Laversanne, Isabelle Soerjomataram, Ahmedin Jemal, Freddie Bray. "Global cancer statistics 2020: GLOBOCAN estimates of incidence and mortality worldwide for 36 cancers in 185 countries", CA: A Cancer Journal for Clinicians, 2021

Publication

<1%

---

23 Nedzamba, Hulisani Theodorah. "The Relationship Between Human Papillomavirus (HPV) and Retinoblastoma Binding Protein 6 (RBBP6) in Cervical Cancer Progression",

<1%

	University of Johannesburg (South Africa), 2023 Publication	
24	insightsimaging.springeropen.com Internet Source	<1 %
25	patents.google.com Internet Source	<1 %
26	pdffox.com Internet Source	<1 %
27	www.ncbi.nlm.nih.gov Internet Source	<1 %
28	ndl.ethernet.edu.et Internet Source	<1 %
29	mural.maynoothuniversity.ie Internet Source	<1 %
30	Gyanajeet Yumnam, Ch. Ibohal Singh. "An Application of Bradford's Law of Scattering and Leimkuhler Model: Identification of the Core Journals of India Cancer Research Productivity", Science & Technology Libraries, 2023 Publication	<1 %
31	"Oxidative Stress and Toxicity in Reproductive Biology and Medicine", Springer Science and Business Media LLC, 2022 Publication	<1 %

32	Aiying Du, Shangli Zhang, Junying Miao, Baoxiang Zhao. "SAFROLE OXIDE INDUCES APOPTOSIS IN A549 HUMAN LUNG CANCER CELLS", Experimental Lung Research, 2009 Publication	<1 %
33	coek.info Internet Source	<1 %
34	www.hse.gov.uk Internet Source	<1 %
35	Linlin Wu, Chunfang Gao. "Comprehensive Overview the Role of Glycosylation of Extracellular Vesicles in Cancers", ACS Omega, 2023 Publication	<1 %
36	umu.diva-portal.org Internet Source	<1 %
37	www.cancer.org Internet Source	<1 %
38	I BOHM. "Apoptosis: The Complex Scenario for a Silent Cell Death", Molecular Imaging & Biology, 2003 Publication	<1 %
39	Zeenat Ismail, Jean Dam, Clement Penny, Charles B. de Koning, Leonie Harmse. "Copper-imidazo[1,2-a]pyridines differentially modulate pro- and anti-apoptotic protein and	<1 %

gene expression in HL-60 and K562 leukaemic cells to cause apoptotic cell death", Biochimica et Biophysica Acta (BBA) - Molecular Cell Research, 2022
Publication

40	academic.oup.com Internet Source	<1 %
41	core.ac.uk Internet Source	<1 %
42	John M. Pezzuto. "Resveratrol as an Inhibitor of Carcinogenesis", Pharmaceutical Biology, 2008 Publication	<1 %
43	Massarsky, Andrey, Vance L. Trudeau, and Thomas W. Moon. "Predicting the environmental impact of nanosilver", Environmental Toxicology and Pharmacology, 2014. Publication	<1 %
44	www.epgonline.org Internet Source	<1 %
45	www.lung-cancer.com Internet Source	<1 %
46	Amani A. Mahbub, Christine L. Le Maitre, Neil A. Cross, Nicola Jordan-Mahy. "The effect of apigenin and chemotherapy combination treatments on apoptosis-related genes and	<1 %

proteins in acute leukaemia cell lines", Scientific Reports, 2022
Publication

47	Annette Wunderlich, Tjadina Arndt, Melina Fischer, Silvia Roth et al. "Targeting the proteasome as a promising therapeutic strategy in thyroid cancer", Journal of Surgical Oncology, 2012 Publication	<1 %
48	Brian Leber, Fei Geng, Justin Kale, David W. Andrews. "Drugs targeting Bcl-2 family members as an emerging strategy in cancer", Expert Reviews in Molecular Medicine, 2010 Publication	<1 %
49	Tebogo Peega, Rachael N. Magwaza, Leonie Harmse, Izak A. Kotzé. " Synthesis and evaluation of the anticancer activity of [Pt(diimine)(, -dibutyl- ′-acylthiourea)] complexes ", Dalton Transactions, 2021 Publication	<1 %
50	Zulfiqar F. Cheema. "Ethanol Induces Fas/Apo [Apoptosis]-1 mRNA and Cell Suicide in the Developing Cerebral Cortex", Alcoholism Clinical and Experimental Research, 4/2000 Publication	<1 %
51	anatomy.org.tw Internet Source	<1 %

52	encyclopedia.pub Internet Source	<1 %
53	lib.dr.iastate.edu Internet Source	<1 %
54	www.tjpr.org Internet Source	<1 %
55	Darrin M. Beaupre, Jennifer McCafferty-Grad, Nizar J. Bahlis, Lawrence H. Boise, Mathias G. Lichtenheld. "Farnesyl Transferase Inhibitors Enhance Death Receptor Signals and Induce Apoptosis in Multiple Myeloma Cells", Leukemia & Lymphoma, 2009 Publication	<1 %
56	Mukosi, Muneiwa Christine. "Cannabis Sativa Extracts as a Potential Anticancer Treatment in Melanoma Cancer Cells", University of Johannesburg (South Africa), 2023 Publication	<1 %
57	Raman, Vishak. "Inhibition of Metabolism and Induction of Apoptosis in Triple Negative Breast Cancer Cells by Lippia Origanoides Plant Extracts", Purdue University, 2023 Publication	<1 %
58	Tricarico, Paola, Annalisa Marcuzzi, Elisa Piscianz, Lorenzo Monasta, Sergio Crovella, and Giulio Kleiner. "Mevalonate Kinase Deficiency and Neuroinflammation: Balance	<1 %

between Apoptosis and Pyroptosis", International Journal of Molecular Sciences, 2013.
Publication

59	eurjther.com Internet Source	<1 %
60	lorexplor.istex.fr Internet Source	<1 %
61	online.medunigraz.at Internet Source	<1 %
62	Gregory Kalemkerian. "Advances in the Treatment of Small-Cell Lung Cancer", Seminars in Respiratory and Critical Care Medicine, 2011 Publication	<1 %
63	Palaniyandi Ravanan, Renata Sano, Priti Talwar, Satoshi Ogasawara et al. "Synthetic Triterpenoid Cyano Enone of Methyl Boswellate Activates Intrinsic, Extrinsic, and Endoplasmic Reticulum Stress Cell Death Pathways in Tumor Cell Lines", Molecular Cancer Therapeutics, 2011 Publication	<1 %
64	Principles and Practice of Radiotherapy Techniques in Thoracic Malignancies, 2016. Publication	<1 %

65	Summya Rashid. "Cancer and Chemoprevention: An Overview", Springer Science and Business Media LLC, 2017 Publication	<1 %
66	Xin Lu. "A complex barcode underlies the heterogeneous response of p53 to stress", Nature Reviews Molecular Cell Biology, 09/2008 Publication	<1 %
67	YOSHIYA TANAKA. "Intercellular Adhesion Molecule 1 Discriminates Functionally Different Populations of Human Osteoblasts: Characteristic Involvement of Cell Cycle Regulators", Journal of Bone and Mineral Research, 10/2000 Publication	<1 %
68	open.library.ubc.ca Internet Source	<1 %
69	open.uct.ac.za Internet Source	<1 %
70	www.dovepress.com Internet Source	<1 %
71	9dok.net Internet Source	<1 %
72	A. Steimer. "Cell Culture Models of the Respiratory Tract Relevant to Pulmonary Drug	<1 %

Delivery", Journal of Aerosol Medicine, 06/2005
Publication

73	Linde Duprez. "Necrosis: Molecular Mechanisms and Physiological Roles", Essentials of Apoptosis, 2009 Publication	<1 %
74	Mohammad Moshfeghnia. "AI-Driven Insights into the complexities of Chinese hamster ovary cells death in order to optimize production processes.", Cold Spring Harbor Laboratory, 2023 Publication	<1 %
75	Tencho Tenev, Anna Zachariou, Rebecca Wilson, Angela Paul, Pascal Meier. "Jafrac2 is an IAP antagonist that promotes cell death by liberating Dronc from DIAP1", The EMBO Journal, 2002 Publication	<1 %
76	dora.dmu.ac.uk Internet Source	<1 %
77	journals.lww.com Internet Source	<1 %
78	radiologykey.com Internet Source	<1 %
79	s-space.snu.ac.kr Internet Source	<1 %

80	www.biorxiv.org Internet Source	<1%
81	Ankita Adhikary, Agradeep Mukherjee, Riddhi Banerjee, Shirisha Nagotu. "DRP1: At the Crossroads of Dysregulated Mitochondrial Dynamics and Altered Cell Signaling in Cancer Cells", ACS Omega, 2023 Publication	<1%
82	S. C. P. Costa, P. A. Girard, M. Brehelin, R. Zumbihl. "The Emerging Human Pathogen Photorhabdus asymbiotica Is a Facultative Intracellular Bacterium and Induces Apoptosis of Macrophage-Like Cells", Infection and Immunity, 2008 Publication	<1%
83	archive.org Internet Source	<1%
84	diyhpl.us Internet Source	<1%
85	pubmed.ncbi.nlm.nih.gov Internet Source	<1%
86	web.wpi.edu Internet Source	<1%
87	www.dailymail.co.uk Internet Source	<1%

88	Yoon, J.H.. "Death receptor-mediated apoptosis and the liver", Journal of Hepatology, 200209 Publication	<1 %
89	assets.researchsquare.com Internet Source	<1 %
90	c.coek.info Internet Source	<1 %
91	e-space.mmu.ac.uk Internet Source	<1 %
92	epdf.tips Internet Source	<1 %
93	theses.gla.ac.uk Internet Source	<1 %
94	www.intechopen.com Internet Source	<1 %
95	Markus Selzner. "Induction of Apoptosis in Liver Tumors", Malignant Liver Tumors, 01/12/2010 Publication	<1 %
96	Ru Li, Yongya Wu, Yan Li, Wen Shuai, Aoxue Wang, Yumeng Zhu, Xiuying Hu, Yong Xia, Liang Ouyang, Guan Wang. "Targeted regulated cell death with small molecule compounds in colorectal cancer: Current perspectives of targeted therapy and	<1 %

molecular mechanisms", European Journal of Medicinal Chemistry, 2023
Publication

97	Walsh, Catherine, Carl Luer, Jennifer Yordy, Theresa Cantu, Jodi Miedema, Stephanie Leggett, Brittany Leigh, Philip Adams, Marissa Ciesla, Courtney Bennett, and Ashby Bodine. "Epigonal Conditioned Media from Bonnethead Shark, Sphyrna tiburo, Induces Apoptosis in a T-Cell Leukemia Cell Line, Jurkat E6-1", Marine Drugs, 2013. Publication	<1 %
98	aranne5.bgu.ac.il Internet Source	<1 %
99	era.ed.ac.uk Internet Source	<1 %
100	m.moam.info Internet Source	<1 %
101	naac.msubaroda.ac.in Internet Source	<1 %
102	scholarbank.nus.edu.sg Internet Source	<1 %

Exclude quotes	On	Exclude matches	< 10 words
Exclude bibliography	On		